

The effect of molecular architecture on the properties of propylene impact copolymers

by

N. C. Basson

Thesis presented in partial fulfillment of the requirements for the degree of

Master of Science (Polymer Science)

at the

University of Stellenbosch



Study leader:
Prof. A. J. van Reenen

Stellenbosch
March 2010

Declaration

By submitting this thesis electronically, I declare that the entirety of the work contained therein is my own, original work, that I am the owner of the copyright thereof (unless to the extent explicitly otherwise stated) and that I have not previously in its entirety or in part submitted it for obtaining any qualification.

Signature

24 February 2010

Date

Abstract

Impact polypropylene copolymers (IPPC) are important commercial materials, but their morphology and molecular architecture are not yet fully understood. In this study the focus was on selectively removing specific fractions from the original IPPC, recombining the remaining fractions, and studying the properties of these recombined polymers.

It was found that some properties of the samples changed remarkably, depending on the fraction of material that was removed before recombination. For example, the degree of phase separation and the crystalline morphology of the recombined materials varied noticeably.

During the study an effective way of staining samples for transmission electron microscopy (TEM) was developed. Furthermore, a comparison of fourier transform infrared spectroscopy (FTIR), with TEM and scanning electron microscopy (SEM) results, revealed a hitherto unreported relationship between phase separation.

Absorption bands appeared at 1100 cm^{-1} and 1080 cm^{-1} in the FTIR spectra and appear to be an indication of phase separation. It was further established that specific copolymer fractions present in the original polymer affect not only the morphology of the final polymer, but also the hardness and impact resistance.

Opsomming

Impak polipropileen kopolimere (IPPK) is belangrike kommersiële materiale, maar die kennis met betrekking tot die morfologie en molekulere argitektuur van die materiale is nog gebrekkig. Tydens hierdie studie was die fokus op die selektiewe verwydering van spesifieke fraksies van die oorspronklike IPPK, herkombinering van die oorblywende fraksies, en die studie van die eienskappe van hierdie herkombineerde polimeriese materiale.

Daar is gevind dat sommige van die eienskappe van die herkombineerde materiale daadwerklik verskil van die oorspronklike materiaal, en dat die verskille direk verband hou met die spesifieke fraksie wat uit die oorspronklike materiaal verwyder is. Die mate van fase-skeiding asook die kristal-morfologie van die herkombineerde materiaal het opmerklik verskil van die oorspronklike.

Tydens die studie is 'n effektiewe manier ontwikkel om die materiale te vlek vir transmissie elektron-mikroskopie (TEM). Verder is daar 'n verband tussen die resultate verkry deur Fourier Transform infrarooi spektroskopie (FTIS) en die verkry met TEM en skandeer elektron mikroskopie (SEM) vasgestel. Die verwantskap tussen FTIS en fase-skeiding is tot dusver nie in die wetenskaplike literatuur vermeld nie. Meer spesifiek is daar gevind dat absorpsie-bande sigbaar by 1100 cm^{-1} en 1080 cm^{-1} in die FTIS spektra 'n aanduiding van fase skeiding kan wees. Dit was verder vasgestel dat spesifieke kopolimeer fraksies wat teenwoordig is in die oorspronklike IPPK, nie alleen die morfologie van die materiaal beïnvloed nie, maar ook die hardheid en impak-weerstand van die materiaal.

Dedicated to:

Jesus Christ

And

My father, Nico
and my mother, Christa.

Thank you for the guidance and love that I receive from You God and for my parents that You blessed me with and how You continually use them in my life.

Acknowledgements

I would firstly like to thank God, if it wasn't for Him I wouldn't have been able to do this, He helped me structure my thoughts and gave me insight and understanding and helped me make a new discovery that I can happily present in this work, and gave me strength in times I really needed it.

“Enter into His gates with thanksgiving, And into His courts with Praise. Be thankful to Him, and bless His name.” Psalm100:4(NKJV)

Secondly I would like to thank my promoter and study leader, Prof. Albert van Reenen, thank you for your support, financially and academically, your insight and leadership is exceptional and I appreciate the opportunity to be one of your students.

I would also like to thank my parents; you carried me through the years and helped making my studies at the University of Stellenbosch possible, through the grace of God, and your love and support, thank you, your son.

I would also like to thank the following people, for their contributions:

1. The Olefins research group
2. Dr. Gareth W. Harding (for the GPC run of my samples, and your extra support during this study)
3. Mr. Mohamed Jaffer (UCT, for your assistance on the TEM)
4. Ms. Heidi Assumption (NMR assistance)
5. Dr. D. J. Brand (NMR Lab., for your help with the NMR run of my samples)
6. Technical Assistants and Financial Staff at the Polymer Science Department
7. Mrs. M. R. Frazenburg (Geology Department, for your help on the SEM)
8. Rundicker Agencies (PAS-IR)
9. Mrs. Elbie van Wyk (Science Faculty Librarian)
10. Dr. M. J. Hurndall (Student Liaison Officer)
11. Dr. J. A. Gertenbach and Mr. Serge Opoubou-Lando (WAXD)
12. Dr. R. Bucher, iThemba Labs (WAXD)
13. Sasol for funding
14. Shofar Christian Church and my friends

Contents

List of Contents	I
List of Figures	VI
List of Tables	IX
List of Abbreviations	X

List of Contents

Chapter 1 Introduction and Objectives

1.1	Introduction	1
1.2	Objectives	2
1.3	Methodology	2
1.4	References	3

Chapter 2 Theoretical Background

2.1	The origin and first discovery of isotactic polypropylene	4
2.2	The history of heterogeneous catalyst development	5
2.2.1	First-generation catalysts	5
2.2.2	Second-generation catalysts	6
2.2.3	Third-generation catalysts	6
2.2.4	Fourth-generation catalysts	6
2.2.5	Fifth-generation catalysts	7
2.3	Polypropylene polymerization mechanism	7
2.4	Stereoregulation in α-olefin polymerization	8
2.5	Chain termination methods for polypropylene	9
2.6	Polymer morphology and catalyst morphology	9
2.6.1	Catalyst active site control	9
2.6.2	Catalyst particle and polymer morphology control	10

2.7	Production of polypropylene impact copolymers	11
2.7.1	Employing Ziegler-Natta catalysts	11
2.7.2	The gas phase manufacturing process for impact PP	12
2.8	Propylene-ethylene copolymer rubber particle morphology	13
2.9	Effect of chemical composition and processing conditions on the final impact polypropylene copolymer morphology	15
2.10	Crystalline forms of isotactic polypropylene	15
2.10.1	The α crystalline form	15
2.10.2	The β crystalline form	16
2.11	Important analytical techniques used in this study and the morphological and structural information revealed by them	16
2.11.1	Temperature rising elution fractionation	16
2.11.2	Microhardness testing	18
2.11.3	Differential scanning calorimetry	19
2.11.4	Dynamic mechanical analysis	19
2.11.5	Scanning electron microscopy	20
2.11.6	Transmission electron microscopy	20
2.11.7	Fourier transform infrared spectroscopy	22
2.12	Economic importance of impact polypropylene copolymers	23
2.13	Common uses of impact polypropylene copolymers today	23
2.14	References	23

Chapter 3 Experimental

3.1	Temperature rising elution fractionation	29
3.2	Carbon 13 (^{13}C) nuclear magnetic resonance spectroscopy	30
3.3	High temperature gel permeation chromatography	31

3.4	Fourier transform infrared spectroscopy	31
3.5	Transmission electron microscopy	31
3.5.1	Ruthenium oxide staining	32
3.5.2	Microtoming	32
3.6	Scanning electron microscopy	33
3.7	Dynamic mechanical analysis	33
3.8	Differential scanning calirometry	33
3.9	Microhardness testing	34
3.10	Hydraulic melt pressing	34
3.11	Injection moulding	34
3.12	Wide angle X-ray diffraction scattering	35
3.13	Isothermal differential scanning calirometry	35
3.14	References	36

Chapter 4 Results and Discussion

4.1	Fractionation and recombination of the impact PP copolymer	37
4.2	Characterization of the fractions	38
4.2.1	¹³ C NMR chemical shift predictions	38
4.2.2	¹³ C NMR chemical shift assignments	38
4.3	Characterization of the recombined material	43
4.3.1	¹³ C NMR	43
4.3.2	Molecular weight determination	48
4.3.3	Thermal properties of the recombined materials	49
4.3.4	Isothermal crystallization	54
4.3.5	Microhardness	55
4.3.6	Dynamic mechanical analysis	57
4.3.7	Scanning electron microscopy	60

4.3.8	Transmission electron microscopy	67
4.3.9	Fourier transform infrared spectroscopy	77
4.3.10	Wide angle X-ray diffraction spectroscopy	82
4.4	Summary	85
4.5	References	86

Chapter 5 Conclusions and Recommendations for Future Work

5.1	Conclusions	88
5.2	Recommendations for future work	90

APPENDIX A:	¹³C NMR spectra of the removed fractions at various temperatures of the IPPC (CMR 648)	91
APPENDIX B:	Differential scanning calirometry thermograms of the recombined samples of the IPPC (CMR 648)	93
APPENDIX C:	Differential scanning calirometry thermograms of the removed fractions at various temperatures of the IPPC (CMR 648)	99
APPENDIX D:	Dynamic mechanical analysis graphs of the recombined samples of the IPPC (CMR 648)	103
APPENDIX E:	Transmission electron microscopy images of the recombined samples of the IPPC (CMR 648)	117
APPENDIX F:	Wide angle X-ray diffraction scattering spectra of the recombined samples of the IPPC (CMR 648)	124

List of Figures

Chapter 2

- Figure 2.1: Tacticity types of polypropylene.
- Figure 2.2: A simplified mechanism for transition metal catalyzed propylene polymerization.
- Figure 2.3: Stereoregulation mechanisms in α -olefin polymerization.
- Figure 2.4: A schematic representation of the formation of IPPC.

Chapter 3

- Figure 3.1: Temperature rising elution fractionation column setup placed inside a modified GC oven.
- Figure 3.2: Trapezoidal shape required before microtoming.

Chapter 4

- Figure 4.1: Preparative TREF elution curves for propylene impact copolymer (CMR 648). [True weights per fraction and weight percentage difference per temperature interval difference.]
- Figure 4.2: Monomer sequences in the impact copolymer: (a) PPPP, (b) EEEE, (c) PEP sequence, (d) PPE sequence, and (e) PPEE sequence.
- Figure 4.3: DSC melt peak and crystallisation peak, thermograms, of fractions 60 °C, 80 °C and 90 °C.
- Figure 4.4: DSC melt peak and crystallisation peak, thermograms, of fractions 60 °C, 80 °C and 90 °C.
- Figure 4.5: Figure 4.5: ^{13}C NMR spectrum of sample “E-REF”.
- Figure 4.6: ^{13}C NMR spectrum of sample “Less25C”.
- Figure 4.7: ^{13}C NMR spectrum of sample “Less60C”.
- Figure 4.8: ^{13}C NMR spectra of sample “Less110C”.
- Figure 4.9: DSC thermogram (2nd heating) of sample series A.
- Figure 4.10: DSC thermogram (2nd heating) of sample series B.

- Figure 4.11: DSC thermogram (cooling) of sample series A.
- Figure 4.12: DSC thermogram (cooling) of sample series B.
- Figure 4.13: Microhardness averages of the hydraulic press system for the recombined polymers of sample series A and B.
- Figure 4.14: Microhardness trend of the recombined material, for the injection moulded and hydraulic press moulded samples for “E-REF”, “Less25C”, “Less60C” and “Less110C”.
- Figure 4.15: Dynamic mechanical analysis, $\tan \delta$, sample “E-REF A”.
- Figure 4.16: Dynamic mechanical analysis, $\tan \delta$, sample “Less80C A”.
- Figure 4.17: Three dimensional map of the dynamic mechanical analysis, $\tan \delta$, data.
- Figure 4.18: Projection map of the dynamic mechanical analysis, $\tan \delta$, data.
- Figure 4.19: SEM image of sample “E-REF A” at 2000 X magnification.
- Figure 4.20: SEM images of sample “Less25C B” (a) at 500 X magnification and (b) at 2000 X magnification.
- Figure 4.21: SEM images of sample “Less60C B” (a) at 500 X magnification and (b) at 2000 X magnification.
- Figure 4.22: SEM image of sample “Less80C B” at 500 X magnification.
- Figure 4.23: SEM images of sample “Less80C A” (a) at 500 X magnification and (b) at 2000 X magnification.
- Figure 4.24: SEM images of sample “Less60&80C B” (a) at 500 X magnification and (b) at 2000 X magnification.
- Figure 4.25: SEM images of sample “Less90C A” (a) at 500 X magnification and (b) at 2000 X magnification.
- Figure 4.26: SEM images of sample “Less100C A” (a) at 500 X magnification and (b) at 2000 X magnification.
- Figure 4.27: SEM images of sample “Less110C A” (a) at 500 X magnification and (b) at 2000 X magnification.

- Figure 4.28: SEM images of sample “Less120C A” (a) at 500 X magnification and (b) at 2000 X magnification.
- Figure 4.29: SEM images of sample “Less120C ½ A” (a) at 500 X magnification and (b) at 2000 X magnification.
- Figure 4.30: TEM image of sample “E-REF B” at 100 nm.
- Figure 4.31: TEM image of the recombined sample “Less25C B” at 200 nm.
- Figure 4.32: TEM images (a) and (b) of the recombined sample “Less60C B” at 200 nm.
- Figure 4.33: TEM image of the recombined sample “Less80C B” at 200 nm.
- Figure 4.34: TEM image of the recombined sample “Less60&80C B” at 200 nm.
- Figure 4.35: TEM image of the recombined sample “Less90C A” at 200 nm.
- Figure 4.36: TEM image of the recombined sample “Less100C A” at 200 nm.
- Figure 4.37: TEM image of the recombined sample “Less110C A” at 200 nm.
- Figure 4.38: TEM images of the recombined sample “Less110C A”, (a) left image at 100 nm and (b) right image at 50 nm.
- Figure 4.39: TEM image of the recombined sample “Less120C A” at 200 nm.
- Figure 4.40: PAS-FTIR spectrum for sample series A (block indicates the 1100 cm⁻¹ range).
- Figure 4.41: PAS-FTIR spectrum for sample series B (block indicates the 1100 cm⁻¹ range).
- Figure 4.42: WAXD spectra of sample series A and B.
- Figure 4.43: WAXD spectrum of the “Less60C” sample: deconvolution of the diffraction peak at 21.9 °.

List of Tables

Chapter 4

- Table 4.1: The integral values and chemical shifts of the sequence distributions of propylene and ethylene units in the ^{13}C NMR spectra of the three significant fractions removed from the polymer
- Table 4.2: Mole % Ethylene content in each removed fraction
- Table 4.3: High temperature GPC molecular weight averages of the TREF fractions
- Table 4.4: ^{13}C NMR chemical shift data and integral percentages of the main propylene and ethylene peaks, seen in Figures 4.5 to 4.8
- Table 4.5: The percentage integral values and chemical shifts of the sequence distributions of propylene and ethylene units in the ^{13}C NMR spectra of the recombined samples of the copolymer
- Table 4.6: Ethylene content (mole %) in each recombined sample
- Table 4.7: Molecular weight averages of the recombined samples
- Table 4.8: DSC analysis data of sample series A and B
- Table 4.9: PAS-FTIR peak ratios of PP, series A, relative to the PP content
- Table 4.10: PAS-FTIR peak ratios of PP, series B, relative to the PP content
- Table 4.11: Area ratios of the deconvoluted WAXD peaks at 21.9°

List of Abbreviations

AA	Aluminum reduced and activated
a-TREF	Analytical temperature rising elution fractionation
BLDPE	Branched low density polyethylene
CCD	Chemical composition distribution
DMA	Dynamic mechanical analysis
DSC	Differential scanning calorimetry
EP	Ethylene-propylene
EPR	Ethylene-propylene rubber
FTIR	Fourier transform infrared spectroscopy
GPC	Gel permeation chromatography
H	Microhardness
HDPE	High density polyethylene
IPPC	Impact polypropylene copolymer
iPP	Isotactic polypropylene
IR	Infrared
keV	Kilo electron volt
LLDPE	Linear low density polyethylene
M_n	Number average molecular weight
M_w	Weight average molecular weight
PAS FTIR	Photo acoustic fourier transform infrared spectroscopy
PE	Polyethylene
PE-PP	Polyethylene-polypropylene
PP	Polypropylene
p-TREF	Preparative temperature rising elution fractionation
SCBD	Short chain branching distribution
SEM	Scanning electron microscope
TEM	Transmission electron microscope
T_g	Glass transition temperature
TREF	Temperature rising elution fractionation
wt %	Weight percentage
WAXD	Wide angle X-ray diffraction scattering

CHAPTER 1 INTRODUCTION AND OBJECTIVES

1.1 INTRODUCTION

Isotactic polypropylene (iPP) polymer was first synthesized by Giulio Natta, at Montecatini, in 1954. This opened the way for commercial production of this polymer, and numerous improvements in catalyst technology followed.¹

However, it was soon discovered that iPP on its own is a rigid, hard material and the need arose to improve the polymer's impact properties in order to extend its usefulness to other applications. This led to the development of an impact polypropylene copolymer (IPPC). This copolymer is typically comprised of an iPP matrix, a rubbery amorphous ethylene-propylene (EPR) rubber phase, and a mixture of semi-crystalline ethylene-propylene copolymers.

The EPR phase imparts improved impact resistance and it is believed that the random copolymers have improved interaction between the iPP and EPR phases, acting as a compatibilizer between these phases.

IPPC materials are commercially important materials, with unique properties, but are still not fully understood. In our group, for example, we have previously fractionated some of these polymers and characterized them on molecular level.^{2,3}

The IPPC materials are extremely complex in nature, and this makes it extremely difficult to predict their expected properties based on subtle changes in molecular architecture. It is clear from our previous studies^{2,3} that simply being able to differentiate chemical composition differences in different copolymer is, by itself, not sufficient to explain property changes at a macroscopic level in these polymers. The effect of the various components on the overall morphology of the copolymer is also important.

The use of fourier transform infrared (FTIR) spectroscopy as a means to predict or explain the expected properties has been explored for homo-polymers like polypropylene and polyethylene systems^{4,5} and ethylene-propylene copolymer systems⁶. No information is available

(based on FTIR analyses) on the phase separation effects of the complex IPPC materials.

Attempts have been made to predict properties such as impact toughness, average melt flow index and flexural modulus properties from the IR spectra⁶. FTIR spectroscopy is a simple and rapid analysis technique, and it is possible that this technique could be applied to detecting subtle changes in phase morphology of the IPPC materials.

1.2 OBJECTIVES

As an overall objective, we want to understand the effect of the different molecular species present in the complex IPPC materials on the overall morphology of these polymers.

In order to achieve this objective, we will fractionate, by means of preparative temperature rising elution fractionation⁷ (TREF), a selected IPPC (CMR 648, Sasol Polymers). The fractions will be analyzed, and in a series of experiments we will selectively remove fractions and recombine the rest of the material before further analyses and testing.

This is the first time that this kind of study will be done and we believe this will give additional insight and understanding on the effect of the morphology on the properties of the polymer.

1.3 METHODOLOGY

- Carry out a series of preparative TREF (p-TREF) fractionation experiments to have enough material to selectively remove fractions and recombine material for further testing. Carry out full analyses (chemical composition, thermal properties, molecular weight and distribution) of the fractions.
- Analyze recombined materials
- Study the morphology of the recombined materials. This will be done by transmission electron microscopy (TEM) and scanning electron microscopy (SEM). Technique development for TEM will also be focused on, in order to obtain morphological information on the polymer and combined with other techniques, help broaden our

understanding of these complex polymers, WAXD will also be done to help confirm which crystalline phases are present in each polymer sample and to connect it with the observed phase morphology that TEM will reveal.

- Carry out FTIR analyses of the recombined materials to see if we can establish a relationship between the subtle changes in morphology with changes in the FTIR spectra of the polymers.

1.4 REFERENCES

1. Moore, E. P. Jr., Polypropylene Handbook, Hanser Publishers, New York, 1996, p 11.
2. Pretorius, M. S., Characterisation of molecular properties of propylene impact copolymers, MSc thesis, University of Stellenbosch, Stellenbosch, 2007.
3. Shebani, A. N., The correlation of the molecular structure of polyolefins with environmental stress cracking resistance, MSc thesis, University of Stellenbosch, Stellenbosch, 2006.
4. Geng, Y., Wang, G., Cong, Y., Bai, L., Li, L., Yang, C., Macromolecules, 42, 2009, p 4751.
5. Nielsen, J. R., Hathaway, C.E., Journal of Molecular Spectroscopy 10, 1963, p 366.
6. Pandey, G. C., Kumar, A., Garg, R. K., European Polymer Journal 38, 2002, p 745.
7. Rabie, A. J., Blends with low-density polyethylene (LDPE) and plastomers, MSc thesis, University of Stellenbosch, Stellenbosch, 2004.

CHAPTER 2 THEORETICAL BACKGROUND

2.1 *THE ORIGIN AND FIRST DISCOVERY OF ISOTACTIC POLYPROPYLENE*

Karl Ziegler was the first to publish and patent research on employing transition metal catalysts in the polymerization of ethylene to obtain a linear, high density polymer material.¹

The catalyst system developed by Ziegler was later licensed to Petrochemicals, Montecatini, Hoechst and Hercules.² Giulio Natta, employed at Montecatini at that time, was involved in the reaction kinetic study of ethylene polymerization and he started to use the catalyst system that Ziegler developed, to conduct his own research.³ This led to the first discovery of iPP,⁴ leading to the polymerization of other 1-alkenes to stereoregular polymers.⁵ This served as the basis for the subsequent discovery of improved catalyst systems by other groups, commonly referred to as the first-, second-, third-, fourth- and fifth- generation catalysts.^{6,7}

Due credit must also go to Karl Ziegler, who found that some transition metals had the ability to inhibit or improve the rate at which polymerization could take place. While Ziegler found that titanium halides worked well (when activated by a suitable cocatalyst) for the polymerization of ethylene, he concluded, after several failed attempts, that it could not be used to make PP. This was proved wrong by Natta, whose first successful polymerization of propylene yielded a polymer with an isotacticity of 40%. A short while later, in about 1955, other researchers made iPP with 80% isotacticity.⁶

Natta continued with his research and defined three major stereo conformations for PP,⁶ a simple illustration of which is shown in Figure 2.1.


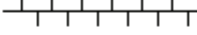
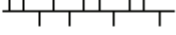
 Isotactic	 Syndiotactic	 Atactic
CH₃ on the same side of the backbone	CH₃ on alternating sides of the backbone	CH₃ has no order around the backbone

Figure 2.1: Tacticity types of polypropylene.

2.2 ***THE HISTORY OF HETEROGENEOUS CATALYST DEVELOPMENT***

Since Natta's first successes using a $\text{TiCl}_4/\text{AlR}_3$ catalyst system which produced PP with low isotacticity, and his subsequent discoveries of the importance of using different crystalline forms of TiCl_3 instead of the soluble TiCl_4 , isotactic PP has become a major industrial thermoplastic. A huge amount of effort has gone into developing more active and stereospecific catalysts. These are generally divided into "generations" of catalysts, the salient points of which are briefly discussed below.

2.2.1 **FIRST-GENERATION CATALYSTS**

The first catalyst system developed for PP synthesis is referred to as AA- TiCl_3 , which stands for aluminium-reduced and activated,⁶ it being a catalyst system that uses TiCl_3 as catalyst and AlEt_2Cl as a cocatalyst.⁶ This system had a few drawbacks though, as the activity and stereospecificity is low and catalyst removal is necessary,⁶ as is the removal of atactic material, which makes the production expensive and complex.⁸

Poor polymer morphology was also present, which called for further improvements to the process, this led to three approaches to improve the catalyst system by increasing the activity:⁶

- Size reduction of the catalyst micro-particles⁶
- Dispersion of Ti compounds on high surface carriers, such as MgCl_2 ⁶
- The use of soluble transition metal compounds⁶

2.2.2 SECOND-GENERATION CATALYST

Examples of second-generation Ziegler-Natta catalysts are the Solvay catalysts. These were developed to improve the surface area of the TiCl_3 catalyst, and increased the accessibility of the Ti atoms five times, according to literature.⁶ These catalysts had much better activity compared to the first generation catalysts and produced an iPP with a better isotacticity index.⁹ Diethyl aluminium chloride was still employed as cocatalyst, while the use of electron donors in these catalyst systems led to higher stereospecificity.⁹

2.2.3 THIRD-GENERATION CATALYST

With the third generation catalysts, improvements were focussed on using support systems for the catalysts (creating supported catalysts as they are called) in efforts to improve the activity of the catalyst system. The use of support materials (MgCl_2) to deposit the TiCl_3 catalyst onto, rewarded the advent of the third-generation catalysts, and while their activity was very high, initially only polymers with very low tacticity were obtained.^{10,11} The introduction of internal and external donors¹² lead to high-activity stereospecific catalysts. These catalysts were typically produced by co-milling the support material with the external donor, TiCl_4 , and a little of the cocatalyst. This pre-catalyst was then treated with cocatalyst (trialkyl aluminium) and an external donor to produce the active catalyst.⁶

2.2.4 FOURTH-GENERATION CATALYST

In an effort to remove all atactic PP from the reaction medium, much research into alternative electron donors lead to the advent of the fourth-generation catalysts. These catalysts are also known as the super high activity catalysts.^{6,13} These catalysts typically use a combination of dialkyl phthalates and alkoxy silanes as internal/external donor mixtures.

2.2.5 FIFTH-GENERATION CATALYST

The fifth generation catalysts employ 1,3-diethers as internal electron donors and give “extremely high activities and isotacticities”,¹ and excludes the need for external electron donors.

2.3 *POLYPROPYLENE POLYMERIZATION MECHANISM*

The mechanism of transition metal catalysed polymerization has received considerable attention, with the notable contributions initially coming from Ziegler et al.,¹⁴ Natta,¹⁵ Nenitzescu et al.,¹⁶ Friedlander and Oita.¹⁷ Subsequent to this the bimetallic mechanism of Natta and Mazzanti¹⁸ introduced the concept of a four-membered ring forming at the active site after monomer coordination and insertion, with the ring opening at the Ti-C bond when a new monomer coordinates. This was subsequently followed by Cossee’s monometallic mechanism, which became widely accepted.¹⁹ The basic concepts introduced by this mechanism were that the active complex must contain at least one metal-carbon or metal-hydride bond, and that an open coordination position or vacant orbital must be present for polymerization to occur.^{3,20}

Polymerization occurs after complexation of the monomer to the transition metal, followed by cis opening of the double bond and migratory insertion of the monomer into the metal-carbon bond. A general scheme for this polymerization is depicted in Figure 2.2. It can be seen that a vacant coordination site is formed at the position originally occupied by the polymer chain. To explain the formation of isotactic PP, the migration of the newly formed metal-carbon bond to the original position is required.

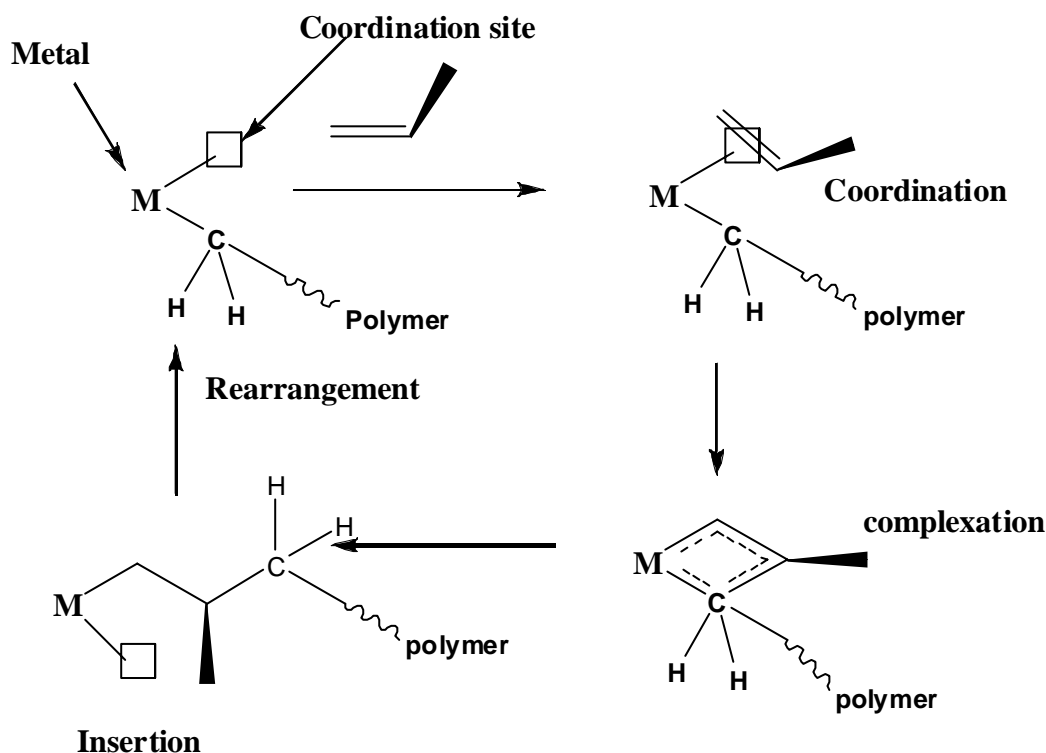


Figure 2.2: A simplified mechanism for transition metal catalyzed propylene polymerization.

2.4 STEREOREGULATION IN α -OLEFIN POLYMERIZATION

The driving force for the stereoregulation is a matter of energy. The stereospecificity of a catalyst is determined by the difference in activation energy of the two coordination positions (assuming that 1, 2 or primary coordination predominates) caused by steric interaction of the transition metal complex (mostly determined by the growing polymer chain) with the incoming monomer.²¹ Our understanding of the way stereoregulation occurs was greatly advanced by the advent of homogeneous or metallocene catalysts, an excellent discussion of which is given by Resconi et al.²²

Primarily, stereoregulation occurs by catalytic site control (also known as enantiomorphic site control) while chain end control (where the chirality of the last inserted monomer determines the way the next monomer coordinates) is theoretically possible, but is virtually never encountered.

These two types of stereoregulation with primary or 1, 2 insertions are shown in Figure 2.4:

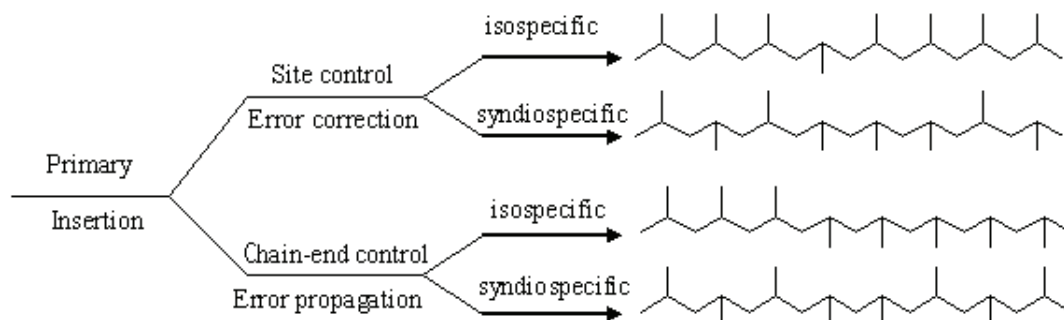
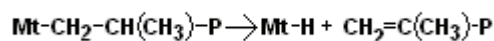


Figure 2.3: Stereoregulation mechanisms in α -olefin polymerization.

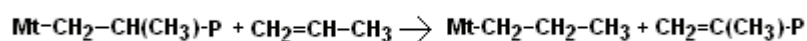
2.5 CHAIN TERMINATION METHODS FOR POLYPROPYLENE

There are four possible chain termination mechanisms for heterogeneous catalyst systems during PP polymerization, as shown below⁶ (Mt = transition metal, P = polymer chain):

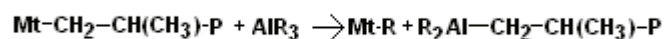
1. Beta-hydride elimination



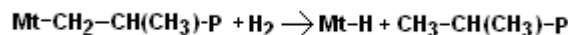
2. Monomer transfer



3. Cocatalyst transfer



4. Hydrogen transfer



2.6 POLYMER MORPHOLOGY AND CATALYST MORPHOLOGY

2.6.1 CATALYST ACTIVE SITE CONTROL

Over the years, scientists have started to understand the role that the catalyst morphology plays in the morphology of the polymer it is used to prepare. It was discovered that to increase the activity of isospecific polymerization, we need to increase the activity of the catalyst used towards that specific stereo arrangement. The polymer that is formed takes on the morphology, the “three

dimensional shape due to the physical and chemical structure of the active sites²² induced by the catalyst system being used. Research into third-generation catalyst systems revealed that there are some non-stereospecific sites present and, in order to change this, internal and external donors were used to help improve the activity of the catalyst system towards a specific stereo arrangement. Soga and Shiana et al.,²³ reports the following on the role of each of these donor types:

The internal donor has to prevent coagulation of $MgCl_2$ particles during the milling process, and it helps to improve the surface area of the catalyst system. The donor obviously also needs to adsorb onto those sites that will lead to non-isospecific sites after crystallization of $TiCl_3$ onto the support.

The external donor needs to coordinate onto or “poison” non-stereospecific sites selectively, and to convert these sites into highly isospecific sites, and to make “isospecific sites even more highly isospecific”. Together, the donors control the morphology of the support material and the final catalyst through selective adsorption onto certain sites.

2.6.2 CATALYST PARTICLE AND POLYMER MORPHOLOGY CONTROL

In order to understand how we make various polymers with the Ziegler-Natta catalyst system, such as iPP, and other polymers like IPPC, we need to focus on the catalyst particle we use to make the polymer with, as they clearly influence and determine the particle morphology of the polymer we finally prepare; as Karger-Kocsis, states, “the three dimensional shape can be duplicated by the polymer”.⁷

In order to achieve the best balance between the mechanical and chemical properties of the catalyst particles used, several requirements have to be met: a high surface area is necessary, the catalyst particles need to have a large number of evenly distributed pores/pathways, the porosity must be high, and the mechanical strength of the particles must be good enough to be handled and weak enough to allow polymerization to break up the particles. Last, the active centres need to be evenly distributed throughout the catalyst particle and the monomer must be able to penetrate into the smallest pores available.^{6,7}

If all the requirements are met, the polymer will replicate and assume the three dimensional shape of the catalyst particle, as shown by Karger-Kocsis.⁷ Very few papers on the morphology and kinetics of IPPC are available in the open literature, with the exceptions being those of Kakugo et al.,^{24, 25} Simonazzi et al.²⁶ and Galli.²⁷

2.7 PRODUCTION OF POLYPROPYLENE IMPACT COPOLYMERS

2.7.1 EMPLOYING ZIEGLER-NATTA CATALYSTS

Polypropylene on its own is a hard, strong material; it also has a high melt temperature, but with a low impact strength and low flexibility, which limits the applications. Thus the desire to improve its properties led to the creation of an impact PP.

Ziegler-Natta catalyst systems are used today to produce IPPC, as the catalyst particles provide a solid matrix for the polymer formation and the incorporation of comonomer, like ethylene, which is enclosed within the polymer-catalyst-particle matrix.^{6,7} Numerous research groups have studied the kinetics and morphological development of PP with these solid catalyst systems.²⁸⁻⁴² These studies are important, as the development of IPPC particles first requires a solid iPP matrix.

Ziegler-Natta catalysts provide several advantages for the production of IPPC. One advantage is that the catalyst can produce PP copolymers with low levels of co-monomer inclusion. Another advantage is that the solid polymer matrix obtained in the first stage of the polymerization prevents reactor build up during the copolymerization or second stage of the production. The sticky amorphous or partially crystalline copolymers that are produced in the second stage are contained within the porous iPP matrix produced in the first stage. The porosity of these catalysts also allows good penetration for two monomers, and thus allows the production of tailor-made copolymers. Mechanical limitations are also no longer a factor.^{6,7}

2.7.2 THE GAS PHASE MANUFACTURING PROCESS FOR IMPACT PP

Various processes to make heterophasic, high impact copolymers exist, but the most preferred way today is the gas phase process, of which an example is the Novolen system.²

The cascade polymerization system involves the initial polymerisation of propylene in the first reactor to produce the polymer matrix particles. The iPP particles are then transferred to a second reactor, to which ethylene is added. The combination of the ethylene introduced and the propylene trapped inside the iPP particles from the first stage produces a variety of random copolymers, ranging from crystalline ethylene or propylene rich copolymers to amorphous EPR. The ethylene content can be varied from 6-20%. Most of the rubbery material also tends to be closer to the outer surface of the polymer, as it grows inwards into the micro and macropores of the iPP particle,^{7,43} leaving the large pores and cracks in the particles intact.

Debling and Ray,⁴³ published an excellent paper on the morphological development during the gas phase production of IPPC. While they did use parameters reaching far beyond that of commercial production, several factors were highlighted in the study. It was clearly shown that the molecular weight of the copolymer phase was important and that the molecular weight of this phase tends to be higher than that of the iPP phase (due to the higher activity of the ethylene). The molecular weight of the copolymer phase affects the penetration of the rubbery phase into the polymer's micropores, and this affects monomer diffusion into the polymer particles during polymerization. Thus the molecular weight of the copolymer phase can affect the final chemical composition distribution of the material.⁴³

The amount of rubbery material also plays a role in the final morphology, as illustrated by Debling and Ray.⁴³ If the rubbery content gets too high, the interior of the iPP particles remains unfilled, due to the blocking effect of the rubbery layer. The copolymerization temperature also has an interesting effect on the properties, with Debling and Ray reporting that at "low temperature distinct elastomeric domains are visible", but at "90 °C the copolymer fused the polymer together".

2.8 **PROPYLENE-ETHYLENE COPOLYMER RUBBER PARTICLE MORPHOLOGY**

Yong Chen et al.^{44,45} reported the structure of an iPP particle to be made up of a series of sub particles; an iPP particle consists of an agglomeration of sub globules, and each sub globule consists of an agglomeration of primary particles which are the smallest particles present in the iPP particle.

Macropores exist between the sub globules, and micropores between the primary globules, and this constitutes an iPP particle in the first stage of polymerization before the copolymerization or second stage takes place.^{44,45}

Figure 2.4, illustrates the formation of impact copolymers.⁴³

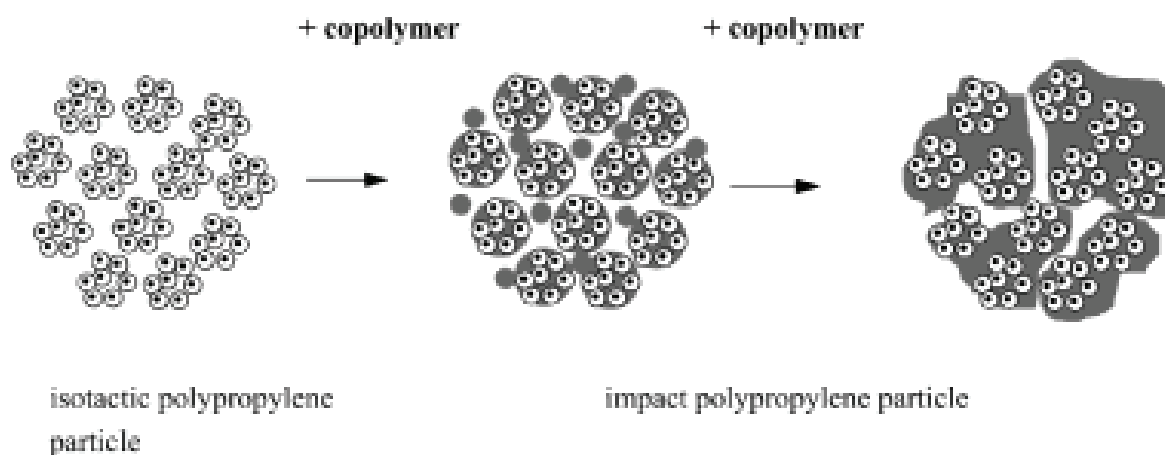


Figure 2.4: A schematic representation of the formation of IPPC.⁴³

During the second stage of the polymerization of iPP particles, the comonomer (ethylene) is able to diffuse through the macro and micropores to the active centres still present in these pores, as is the propylene still trapped within these particles. Polymerization takes place and is confined to the inner diameter of the iPP particles. SEM images revealed the outer surface of the particles to be smoother after the second stage of co-polymerisation, but the contours of the sub globules are still clearly visible, an indication that the EPR copolymer is contained inside the particles. This proves why reactor fouling normally does not occur. SEM images of particles revealed some macropores were still visible, but no micropores. TEM images, after staining with RuO_4 , showed the distribution and inclusion of the EPR phase in the micropores.^{44,45}

TEM analysis also showed that the EPR phase is preferentially located on the outside surface of the sub globules and the outer edges of the micro pores of the primary globules, with little to no penetration of the EPR into the inner micropores.

Tong et al.⁴⁶ argued that the reason why the EPR phase does not readily penetrate deeper into the micropores is because some atactic PP is present, formed during the first polymerization stage, and is contained inside these pores to some extent. They were able to extract a small amount of atactic PP with xylene, but they did admit that their findings were not completely conclusive, as other factors could also have had an influence.⁴⁶

Tong et al.⁴⁶ also found that upon cutting an impactPP particle, lightly coloured protrusions were visible on the cut surface in SEM images. This they attributed to EPR, reasoning that since these domains were under high strain inside the pores of the iPP particle, upon cutting, these EPR domains were able to release the strain, causing the protrusions observed..

Chen et al.^{44,45} also revealed that upon thermal treatment of the impactPP particles, slight changes occurred, a darker boundary region appeared between the iPP and EPR phases on the edges of the sub globules, and crystalline PE structures were clearly visible, and seemed to become more visible depending on the thermal treatment and time. They also reported a core-shell particle structure inside the EPR phase, with some EP copolymer on the boundary of the sub globules and the EPR phase.

The inside of the core-shell particles revealed a crystalline structure, which is believed to be due to both PE and PP chains.

The rubber phase viscosity (or mobility) also plays a large role in the final morphology of the IPPC particle. The factors that have an impact on this are the following:

- High reaction temperature, enhancing flow.
- Low crystallinity, enhancing flow.
- Low molecular weight, enhancing flow.

2.9 EFFECT OF CHEMICAL COMPOSITION AND PROCESSING CONDITIONS ON THE FINAL IMPACT POLYPROPYLENE COPOLYMER MORPHOLOGY

The chemical composition of the copolymer phase, i.e. random or block copolymer chains, will affect the morphology and resultant properties of the IPPC copolymer, but the nature of the rubbery phase will also play a role, i.e. its molecular weight and molecular weight distribution, and thus the chemical composition will determine the degree of compatibilization.^{47,48} Much has been reported on the structure-property relationships of IPPC.⁴⁹⁻⁶⁴ There is also evidence that the non-crystalline part of the polymer does hinder the crystallization of the rest of the polymer to some extent.⁴⁸

It has been proven that the processing conditions can also influence the final morphology of the IPPC. Tochacek et al.⁶⁵ observed an increase in the size of the rubbery domains at elevated temperatures. Chen et al.⁴⁴ have reported that thermal treatment does affect the phase morphology of the IPPC.

Hence, the chemical composition distribution, the molecular weight, the processing conditions and nature and distribution of the copolymer phase all greatly influence the final morphology of the IPPC.

2.10 CRYSTALLINE FORMS OF ISOTACTIC POLYPROPYLENE

2.10.1 THE α CRYSTALLINE FORM

The α -iPP crystalline form is identified by its unique “cross-hatched” lamellae structure. The spherulites comprise long radial lamellae with tangential, smaller lamellae in between them. These smaller lamellae grow almost orthogonal to the radial, parent lamellae, and occasionally overlap or interrupt the radial lamellae.⁶

The tangential lamellae also grow into one another or overlap, and will appear thicker in the regions where this happens. This type of crystalline form is the most common type for iPP, and forms under almost any type of thermal conditioning; but it is predominant in fast cooled and quenched cooled

samples. It also the crystalline form that gives iPP the highest impact toughness compared to the other crystalline forms.⁶ The melt temperature of this crystalline form is also strongly dependent on the tacticity and thermal history.

2.10.2 THE β CRYSTALLINE FORM

The β -iPP crystalline phase can be formed under isothermal crystallization conditions and/or a slow cooling rate from the melt. This crystalline morphology is also referred to as the hexagonal crystalline structure in iPP, the reason being that it has a hexagonal unit cell arrangement.⁶

The morphology of this crystalline form is comprised of long, uninterrupted, and parallel stacked thick lamellae. Lamellae are stacked closer together than in the α -phase crystals, and have a slightly higher density. The spherulite boundaries between β -phase crystals have characteristic zig-zag patterns. The β -iPP crystals are unstable at high temperatures and easily convert to α -iPP crystals upon reheating.⁶

2.11 IMPORTANT ANALYTICAL TECHNIQUES USED IN THIS STUDY AND THE MORPHOLOGICAL AND STRUCTURAL FORMATION REVEALED BY THEM

2.11.1 TEMPERATURE RISING ELUTION FRACTIONATION

There are two types of temperature rising elution fractionation (TREF), preparative TREF (p-TREF) and analytical TREF (a-TREF). During p-TREF, fractions of the polymer are collected at predetermined temperatures during elution from a support and can be analyzed off-line by (GPC, NMR and FTIR, etc.). This allows us to gain a great deal of information about the molecular composition of the material being analyzed. During analytical TREF an in-line detector measures the change in concentration of polymer in solution during the elution step. This method only supplies information on the distribution of crystallizable species in the polymer.⁶⁶

A review article by Xu and Feng⁶⁷ discusses how the fractionation during a TREF experiment takes place. A support material such as silica, beads or sea

sand can be used. The size of the support particles is important. Generally the support material is preheated to the same temperature at which the polymer is dissolved. The polymer is dissolved at elevated temperature in a suitable solvent (e. g. 130 °C in xylene for iPP). The dissolved polymer is then added to the preheated support and slow cooled to room temperature.

During the cooling step the polymer crystallizes onto the support. The most crystallizable chains crystallize first, followed by the rest of the material in order of decreasing crystallizability, with the least crystalline material crystallizing at the lowest temperature. We thus fractionate the polymer based on crystallinity. This will only happen if the rate of cooling is slow enough. During the elution step, the column is heated while solvent is passed through the support material. The reverse of the crystallization step occurs, with the least crystalline materials dissolving first, etc.⁶⁷

TREF fractionation in the case of iPP also takes place on the basis of crystallizability, and is thus strongly influenced by the tacticity of the polymer chains. Disruption of the tacticity of the polymer chains will lead to a less crystallizable polymer. In the case of copolymers, introduction of the comonomer further disrupts the symmetry of the chain, leading to still lower crystallizability.⁶⁶⁻⁶⁹

Anantawaraskul et al.⁷⁰ studied the importance of the operation parameters such as cooling rate, heating rate and solvent flow rate, during the TREF process, and carried out some concentration dependency studies.

A slow cooling rate such as 1-1.5 °C/ hour is generally preferred, as the slower the cooling rate the better the fractionation that will take place.⁷⁰

The heating rate and flow rate during elution is also very important, and a ratio of 1 between these two is found to be the most appropriate.⁷⁰

According to Soares and Hamielec,⁶⁶ Mirabella^{71,72} was the first to fractionate impact PP using TREF. Mirabella used analytical TREF coupled with an IR detector during the elution stage and reported three zones during elution.

The first zone eluted at room temperature and comprised the rubbery ethylene-propylene random copolymer. The second zone was due to the ethylene-propylene copolymer range, which is semicrystalline, and contains

sequences of both PP and PE, long enough to crystallize. The third zone was the iPP fraction.⁷¹⁻⁷³

2.11.2 MICROHARDNESS TESTING

The generally accepted equation for microhardness (H) determination is:⁷⁴

$$H = k \times \left(\frac{P}{d^2} \right)$$

where:

- P is the applied load.
- d is the diagonal of the impression in m.
- k is the geometric factor, equal to 1.854.

Hardness testing involves making a permanent indentation on a sample, by using a square shaped indenter. A specific load is applied, which can be changed if needed, and the speed of the penetration and the dwell time can also be changed as needed.¹⁶ Typically, at least 10 measurements are performed using the same load, penetration speed and dwell time, in order to obtain an average value for the hardness..

In semi-crystalline polymers and copolymers the hardness is strongly affected by the crystallinity of the sample, the size of the crystals present, the phase of crystal and the perfection of the crystal phase.¹⁷ Some studies focussed on the effect of strain induction on iPP polymers and how hardness properties can be related to crystal phase transitions from β - to α - phase crystals, and the influence of annealing temperatures on the microhardness properties.^{75,76} Other studies focussed on the influence of the amorphous domains between the crystal lamella in PE samples and its influence on the microhardness value.⁷⁷

Since hardness values (or microhardness, as values obtained at low loads used for soft polymers are referred to) are localised measurements, a series of values to obtain an average value is necessary in order to be more representative of the whole sample, since the microhardness value is strongly influenced by the morphology of the polymer, i.e. crystal phase (α -phase crystals and the β -phase crystals could have different effects on the microhardness value due to their difference in morphology), perfection of the

crystal phase, and how the amorphous phase is spread between the crystalline lamellae of the polymer.⁷⁵⁻⁷⁷

2.11.3 DIFFERENTIAL SCANNING CALORIMETRY

The results of preparative TREF fractionation experiments of IPPC materials have been evaluated by DSC, for example by Tan et al.⁷⁸

According to them, DSC results revealed that the fraction they obtained by eluting at 30 °C to be mostly non-crystalline propylene-ethylene copolymer, while those materials eluted between 70 °C to 90 °C, showing small melt peaks in the DSC melting curves, indicating partially crystalline copolymer materials. They also concluded that a melt peak similar to that of homopolymeric PE was visible in the fraction obtained by elution between 90 °C and 108 °C, while the material eluted at 110 °C revealed crystalline material with PP sequences believed to be long enough to crystallize, probably because they were propylene-rich copolymers. Finally the material that was obtained, by elution in the 120 °C-140 °C temperature range, revealed a broad melting peak in the DSC curve, similar to that of isotactic PP.

The peaks of the DSC traces can also reveal the type of crystal structures present, for example the polymorphic forms of iPP such as α - and β -forms.⁷⁹ Similarly, we can also distinguish the crystallizable PP and PE block sequences in copolymer systems. The melting and crystallization transitions observed with DSC analysis allows us, therefore, to distinguish to some extent the different polymer constituents from one another.^{79, 80}

2.11.4 DYNAMIC MECHANICAL ANALYSIS

Hongjun et al.⁸⁰ studied two impact copolymer PP samples that differed on the basis of ethylene content distribution. The DMA results revealed two T_g transitions: one at -40 °C, which they attributed to the EPR copolymer phase and segmented EP copolymer, and the other at 20 °C, which they attributed to PP.

Depending on how well the EPR rubber phase is dispersed in the matrix of the polymer, the two T_g transitions become more or less distinct. It appears that increased compatibility leads to less distinct T_g transitions.

2.11.5 SCANNING ELECTRON MICROSCOPY

Scanning electron microscopy reveals the surface morphology of samples, and can also be used to obtain information on the bulk morphology of a sample when combined with a depth profiling system. In order to obtain an image in SEM, the surface that is being studied needs to be coated with a thin layer of gold in order to give reflective properties to the surface, as electrons are being bounced/reflected off the surface and then detected.

SEM studies on IPPC have been carried out by Zacur et al.⁸¹ In order to obtain some information on the distribution of the amorphous materials (and phase separation), the amorphous material was first removed by etching with an acid and washing with toluene, prior to gold coating the samples.

Since the crystalline copolymer segments act as a compatibilizer between the EPR phase and the PP matrix,^{81,82} the way in which the EPR phase is dispersed through the matrix determines its properties and is an indication of the compatibility between the phases.^{81,82} Studies revealed the EPR phase to be distributed relatively homogeneously within the matrix of the sample. It was found that the amount of EPR phase was dependent on the ethylene content present,⁵ while the average size of the spherical EPR domains was dependent on how well the different phases could interact. The better the compatibility between the phases the smaller the spherical EPR domains become.⁸¹ The same study concluded that the crystalline copolymer fractions were at the interface of the iPP matrix, since only the EPR rubber was removed by etching with toluene. SEM can only give indirect information regarding the dispersion of the EPR phase in the iPP, it cannot give information regarding crystalline structure.^{78,81}

2.11.6 TRANSMISSION ELECTRON MICROSCOPY

Transmission electron microscopy (TEM) is able to reveal a great deal of morphological information about a sample. Using the correct staining agent one can, with TEM, distinguish between amorphous domains and crystalline domains. The staining agent normally used is RuO₄. The staining agent will primarily allow the amorphous areas to be stained, thus resulting in darker

amorphous domains and lighter crystalline domains. The stained sections looked at should also be very thin to enable one to view the crystalline structure. Samples that are too thick appear too dark to distinguish any contrast differences clearly.⁸³

The crystalline structure can also be clearly seen with TEM analysis, and the technique is able to reveal different crystalline morphologies due to differences in staining as the α - and β -phase crystalline lamellae have different densities, and as a result the stain will penetrate them to different degrees, and thus provide a contrast difference between them. Differences in contrast between PE and PP lamellae can also be seen. TEM therefore provides a very rich source of morphological information of the polymer being observed.⁸³

Lamellar morphologies can also only give a contrast difference that can be viewed if the lamellae are in the same direction as the plane of the section or slice taken, otherwise no contrast difference will be seen and the image will appear opaque and unclear.⁸²

Three in-depth studies have been carried out on PE, PP and EP copolymers⁸³⁻⁸⁵ and the results were very useful in explaining the morphology seen in the IPPC, including the α - and β -crystalline forms of iPP.

The morphology of high molecular weight samples of different types of PE (LLDPE, LDPE and HDPE) were studied by TEM, and this study revealed that the higher the molecular weight of the sample, the more twisting lamellae are visible for the same type of ethylene polymer, and the HDPE and LDPE in turn had thicker and longer lamellae than the LLDPE.⁸³

For the EP copolymers (including IPPC), the ethylene rich domains were shown to have inner core-shell particle morphology present. These core-shell particles have an EPR-rich outer layer, while an ethylene-rich crystalline structure exists in the interior of these core-shell particle (revealed by X-ray diffraction analysis).⁸⁴

TEM analysis of iPP revealed that iPP had both α - and β -phase iPP crystals present, as their morphologies could clearly be distinguished from one another. The α -phase has a characteristic cross-hatched lamellar morphology, consisting of long radial lamellae with tangential lamellae in between them,

sometimes overlapping or interrupting the radial lamellae, and the β -phase lamellae morphology revealed long, thick uninterrupted parallel lamellae. The difference in contrast between these two phases is believed to be due to the parallel stacked lamellae of the β -phase crystals that is less penetrable to the stain used than for the α -phase. The study of the iPP revealed that the boundaries between the α -phase spherulites comprise parallel oriented lamellae and the boundaries between β -phase spherulites have a zig-zag pattern.⁸⁵ Although TEM studies have also been carried out in an effort to obtain more morphological information,^{79,86-91} no clear TEM images have as yet been obtained for IPPC.

2.11.7 FOURIER TRANSFORM INFRARED SPECTROSCOPY

FTIR spectroscopy is a well-known technique and one of the easiest, fastest and most inexpensive methods to obtain chemical and structural information on a polymer. The vibrational bands observed in the infrared region of the spectrum can give information on both crystalline and amorphous structures within a polymer. For iPP the degree of isotacticity of a sample can also be estimated, as the helical bands seen by infrared spectroscopy are sensitive to the isotacticity of polymer, and since these helices are affected by the conformational environment around them, such as the type of chain packing, unit cells and defects, it is also possible to determine what crystal structures/phases are present, such as the mesomorphic phases of iPP, α , β , and γ .⁹²

The IR spectrum has been used to view differences in structure and ethylene content of different IPPC,⁹³ and also to predict the expected mechanical properties of a polymer, such as PP, in a simple, non-destructive way.⁹⁴

Infrared studies have also been performed to determine the effect of shear-induced strain on the vibrational bands of an iPP sample instead of temperature effects to see how they change and to obtain a relationship between the length of monomer sequences in a helical arrangement, and the change in the corresponding IR bands of the different vibrational modes.⁹⁵

An interesting study on the orthorhombic and hexagonal crystal phase of normal paraffins has been done by Nielsen and Hathaway⁹⁶ where the band adsorption at 1100 cm^{-1} is of very significant importance.

2.12 ECONOMIC IMPORTANCE OF IMPACT POLYPROPYLENE COPOLYMERS

The main reason behind the creation of IPPC is improved impact strength at a low temperature.⁶ IPPC does not only have improved low temperature impact strength, but the partial incorporation of crystalline core-shell particles (PE crystals) in the EPR phase also helps strengthen the rubber phase and gives it unique properties, such as the prevention of void formation inside the rubber phase when the polymer is stretched, due to formation of shish-kebab structures, and provides improved toughness. IPPC is a superior polymer compared to the homopolymer in many ways, and the applications for this polymer much more versatile.⁶

2.13 COMMON USES OF IMPACT POLYPROPYLENE COPOLYMERS TODAY

The important applications of IPPC are due to the fact that it can be processed into films with the air-quenched bubble process or callendering,⁶ which is not possible with normal PP.

Some of the most common uses of IPPC are the following: biohazard bags, diaper backing films, industrial bags, roof sheeting, geomembranes, medical tubing and bags, and car bumpers.⁶

2.14 REFERENCES

1. Ziegler, K., Holzkamp, E., Breil, K., and Martin, H., German patent 973, 626, 1960.
2. Sailors, H. R., Hogan, J. P., Journal of Macromolecular Science, Chemistry, A 15, 1981, p 1375.
3. Boor, J., Ziegler-Natta Catalysts and Polymerization, New York, Academic Press, 1979.
4. Natta, G., Pino, P., Farina, M., Ricerca Science Supplementary, 25, 120, 1955, p 120.
5. Natta, G., Journal of Polymer Science, 16, 1955, p 143.
6. Edward P. M. Jr., Polypropylene Handbook, Hanser Publishers, Munich, 1996, p 12.

7. Karger-Kocsis, J., Polypropylene Structure, Blends and Composites, Copolymers and blends, 2, Chapman & Hall, London, 1995, p 1.
8. Welch, M. B., Hsieh, H. L., Vasile, C., Seymour, R. B., Handbook of Polyolefins, Marcel Dekker, New York, 1993.
9. Solvay, German Patent 2, 213, 086, 1972.
10. Montedison, British Patent 1, 286, 867, 1968.
11. Pasquon, I., Giannini, U., Anderson, J. R., Boudart, J. R., M., Springer Verlag, Berlin, 1984.
12. Montedison, Belgian Patent, 785,332, 1972.
13. Galli, P., Barbe, P. C., Noristi, L., Angewandte Makromolekulare Chemie, 120, 1984, p 73.
14. Ziegler, K., Gellert, H., Holzkamp, E., Wilke, G., Duck, E., Kroll, W., Annalen, 629, 1960, p 172.
15. Natta, G., Macromolecular Chemistry, 16, 1955, p 213.
16. Nenitzescu, C. D., Huch, C., Huch, A., Angewandte Chemie, 68, 1956, p 438.
17. Friedlander, H. N., Oita, K., Journal of Industrial and Engineering Chemistry, 49, 1957, p 1885.
18. Natta, G., Mazzanti, G., Tetrahedron, 8, 1960, p 86.
19. Cossee, P., Tetrahedron Letters, 17, 1960, p 12.
20. Sinn, H., Kaminsky, W., Advances in Organometallic Chemistry, 18, 1980, p 99.
21. Huang, J., Rempel, G. L., Progress in Polymer Science, 20, 1995, p 467.
22. Resconi, L., Cavallo, L., Fait, A., Piemontesi, F, Chemical Reviews, 100, 2000, p 1.
23. Soga, K., Shiono, T., Progress in Polymer Science, 22, 2007, p 1503.
24. Kakugo, M., Hashimoto, M., Isobata, J., Paper presented at the AIChE Annual Meeting, New York, 1987.
25. Kakugo, M., Sadatoshi, H., Sakai, J., Keii, T., Soga, K., Elsevier, New York, 1990, p 345.
26. Simonazzi, T., Cecchin, G., Mazzullo, S., Progress in Polymer Science, 16, 1991, p 303.

27. Galli, P., Paper presented at the 6th International Workshop on Polymer Reaction Engineering, Berlin, 1998.
28. Chen, C., PhD thesis, University of Wisconsin–Madison, 1993.
29. Hutchinson, R. A., PhD thesis, University of Wisconsin–Madison, 1990.
30. Rincon-Rubio, L. M., Wilen, C. E., Lindfors, L. E., *European Polymer Journal*, 26, 1990, p 171.
31. Rotzinger, B., PhD thesis, Eidgenossischen Technischen Hochschule-Zurich, 1984.
32. Tait, P., Jaber, I., Loontjens, A., Keii, T., Soga, K., in *Proceedings of the International Symposium on Recent Developments in Olefin Polymerization Catalysts*, Tokyo, Oct. 23–25, 1990.
33. Bukatov, G. D., Zaikovskii, V. I., Zakharov, V. A., Kryukova, G. N., Fenelonov, V. B., Zagrafskaya, R. V., *Polymer Science U.S.S.R.*, 23(3), 1982, p 599.
34. Ferrero, M., Sommer, R., Spanne, P., Jones, K. W., Conner, W. C. J., *Polymer Science*, 31, 1993, p 2507.
35. Galli, P., Haylock, J. C., *Progress in Polymer Science*, 16, 1991, p 443.
36. Hock, C., *Journal of Polymer Science: Part A-1*, 4, 1966, p 3055.
37. Kakugo, M., Sadatoshi, H., Yokoyama, M., Kojima, K., *Macromolecules*, 22, 1989, p 547.
38. Kakugo, M., Sadatoshi, H., Sakai, J., Yokoyama, M., *Macromolecules*, 22, 1989, p 3172.
39. Noristi, L., Marchetti, E., Baruzzi, G., Sgarzi, P., *Journal of Polymer Science, Polymer Chemistry Edition*, 32, 1994, p 3047.
40. Vermel, E. E., Zakharov, V. A., Fenelonov, V. B., Zaikovskii, V. I., Zagrafskaya, R. V., Moroz, E. M., Bukatov, G. D., *Kinetika i Kataliz*, 22, 1981, p 480.
41. Wristers, J., *Journal of Polymer Science: Polymer Physics Edition*, 11, 1973, p 1601.
42. Wristers, J., *Journal of Polymer Science: Polymer Physics Edition*, 11, 1973, p 1619.
43. Debling, J. A., Ray, H. W., *Journal of Applied Polymer Science*, 81, 2001, p 3085.

44. Chen, Y., Chen, Y., Chen, W., Yang, D., *Polymer*, 47, 2006, p 6808.
45. Chen, Y.; Chen, Y., Chen, W., Yang, D., *European Polymer Journal*, 43, 2007, p 2999.
46. Tong, C., Chen, Y., Chen, Y., Zhang, X., Yang, D., Zhang, J., *Polymer*, 49, 2008, p 2974.
47. Fan, Z., Zhang, Y., Xu, J., Wang, H., Feng, L., *Polymer*, 42, 2001, p 5559.
48. Cai, H., Luo, X., Chen, X., Ma, D., Wang, J., Tan, H., *Journal of Applied Polymer Science*, 71, 1999, p 103.
49. Yang, D., Zhang, B., Yang, Y., Fang, Z., Sun, G., Feng, Z., *Polymer Engineering and Science*, 24, 1984, p 612.
50. Jang, B. Z., Uhlmann, D. R., Van der Sande, J. B., *Journal of Applied Polymer Science*, 30, 1985, p 2485.
51. Van Gisbergen, J. G. M., Hoeben, W. F. L. M., Meijer, H. E. H., *Polymer Engineering and Science*, 31, 1991, p 1539.
52. Van Gisbergen, J. G. M., Meijer, H. E. H., Lemstra, P. J., *Polymer*, 30, 1989, p 2153.
53. Choudhary, V., Varma, H. S., Varma, I. K., *Polymer*, 32, 1991, p 2534.
54. Choudhary, V., Varma, H. S., Varma, I. K., *Polymer*, 32, 1991, p 2541.
55. D'Orazio, L., Mancarella, C., Martuscelli, E., Sticotti, G., Massari, P., *Polymer*, 34, 1993, p 3671.
56. Chiang, W. Y., Yang, W. D., Pukanszky, B., *Polymer Engineering and Science*, 32, 1992, p 641.
57. Manson, J. A., Sperling, L. H., *Polymer Blends and Composites*, Plenum Press, New York, 1976.
58. Bucknall, C. B., *Toughened Plastics*, Applied Science Publishers, London, UK, 1977.
59. Prentice, P., *Polymer*, 23, 1982, p 1189.
60. Yeh, P. L., Birley, A. W., Hemsley, D. A., *Polymer*, 26, 1985, p 1155.
61. Sun, Z., Yu, F., Qi, Y., *Polymer*, 32, 1991, p 1059.
62. Wang, L., Huang, B., *Journal of Polymer Science: Part B Polymer Physics*, 28, 1990, p 937.
63. Besomles, M., Menguel, J. F., Delmas, G., *Journal of Polymer Science: Part B Polymer Physics*, 26, 1988, p 1881.

64. Karger-Kocsis, J., Kissin, L., Kuleznev, V. N., *Polymer Communications*, 25, 1984, p 122.
65. Tochacek, J., Jancar, J., Kalfus, J., Zborilova, P., Buran, Z., *Polymer Degradation and Stability*, 93, 2008, p 770.
66. Soares, J. B. P., Hamielec, A. E., *Polymer*, 36, 1996, p 1639.
67. Xu, J., Feng, L., *European Polymer Journal*, 36, 2000, p 867.
68. Xu, J., Feng, L., Yang, S., Yang, Y., Kong, X., *European Polymer Journal*, 34, 1998, p 431.
69. Rabie, A. J., *Blends with low-density polyethylene (LDPE) and plastomers*, MSc thesis, University of Stellenbosch, Stellenbosch, 2004.
70. Anantawaraskul, S., Soares, J. B. P., Wood-Adams, P. M., *Polymer Physics*, 41, 2003, p 1762.
71. Mirabella, F. M. Jr., *Journal of Applied Polymer Science*, 51, 1992, p 117.
72. Mirabella, F. M. Jr., *Polymer*, 34, 1993, p 1729.
73. Pretorius, M. S., *Characterization of molecular properties of propylene impact copolymers*, MSc thesis, University of Stellenbosch, Stellenbosch, 2007.
74. Balta-Calleja, F. J., Cagliaio, M. E., Adhikari, R., Michler, G. H., *Polymer*, 45, 2004, p 247.
75. Krumova, M., Karger-Kocsis, J., Balta Calleja, F. J., Fakirov, S., *Journal of Materials Science*, 34, 1999, p 2371.
76. Satoshi, O., Porter, R. S., *Polymer*, 37, 1996, p 2095.
77. Balta Calleja, F.J., Giri, L., *Polymer*, 38, 1997, p 5769.
78. Tan, H., Li, L., Chen, Z., Song, Y., Zheng, Q., *Polymer*, 46, 2005, p 3522.
79. Alamo, R. G., Brown, G. M., Mandelkern, L., Lehtinen, A., Paukkeri, R., *Polymer*, 40, 1999, p 3933.
80. Hongjun, C., Xiaolie, L., Xiangxu, C., Dezhu, MA, Jianmin, W., Tan, H., *Journal of Applied Polymer Science*, 71, 1999, p 103.
81. Zacur, R., Goizueta, G., Capiati, N., *Polymer Engineering and Science*, 40, 2000, p 1921.

82. Rongbo, L., Zhang, X., Zhao, Y., Hu, X., Zhao, X., Wang, D., *Polymer*, 50, 2009, p 5124.
83. Sano, H., Usami, T., Nakagawa, H., *Polymer*, 27, 1986, p 1497.
84. Chen, Y., Chen, Y., Chen, W., Yang, D., *Journal of Applied Polymer Science*, 108, 2008, p 2379.
85. LI, J. X., Cheung, W. L., *Journal of Applied Polymer Science*, 72, 1999, p 1529.
86. Svoboda, P., Svobodova, D., Slobodian, P., Ougizawa, T., Inoue, T., *European Polymer Journal*, 45, 2009, p 1485.
87. Tortorella, N., Beatty, C. L., *Polymer Engineering and Science*, 48, 2008, p 1476.
88. Cieslinski, R. C., Silvis, H. C., Murray, D. J., *Polymer*, 36, 1995, p 1827.
89. Schurmann, B.L., Niebergall, U., Severin, N., Burger, C., Stocker, W., Rabe, J. P., *Polymer*, 39, 1998, p 5283.
90. Hong, S., Bushelman A. A., MacKnight, W. J., Gido, S. P., Lohse, D. J., Fetters, L. J., *Polymer*, 42, 2001, p 5909.
91. Brown, G. M., Butler, J. H., *Polymer*, 38, 1997, p 3937.
92. Karger-Kocsis, J., *Polypropylene. An A-Z Reference*, Kluwer Academic Publishers, 1999, p 320.
93. Hongjun, C., Xiaolie, L., Dezhu, M., Jianmin, W., Hongsheng, T., *Journal of Applied Polymer Science*, 71, 1999, p 93.
94. Pandey, G. C., Kumar, A., Garg, R. K., *European Polymer Journal*, 38, 2002, p 745.
95. Geng, Y., Wang, G., Cong, Y., Bai, L., Li, L., Yang, C., *Macromolecules*, 42, 2009, p 4751.
96. Nielsen, J. R., Hathaway, C. E., *Journal of Molecular Spectroscopy*, 10, 1963, p 366.

CHAPTER 3 EXPERIMENTAL

3.1 TEMPERATURE RISING ELUTION FRACTIONATION

The equipment used for the preparative TREF experiments was designed and built in-house.^{1,2} The polymer (propylene impact copolymer CMR 648, Sasol Polymers, ethylene content 14.87%) was dissolved in 300 ml xylene (KIMIX Chemicals), in 3 g quantities, at 135 °C. Stabilizer (2% w/w mixture of Irganox1010 and Irgafos168) was added to prevent degradation. After complete dissolution, the solution was added to pre-heated sand (-50 to +70 mesh grade Silica Sand, Sigma Aldrich) in a 1 L reactor. The amount of sand was such that it covered the solution completely.

The reactor with the polymer and the sand support was then transferred to an oil bath preheated to 130 °C and held at that temperature for 2 hours, after which it was slow cooled, from 130 °C to 25 °C, at a rate of 1 °C/ hour. This is referred to as the cooling stage.

During the process of cooling the polymer crystallizes onto the support in layers of decreasing crystallizability.

The polymer-coated sand was then transferred a column (see Figure 3.1) and placed in a modified GC oven.¹ Fractionation of the polymer was then achieved by elution of fractions with xylene at a range of (increasing) temperatures through the column. The elution volume per sample was typically 400 ml. The first sample involved removing the amorphous fraction from the original material; this was done by eluting with a portion of xylene at room temperature. This fraction was called the 25 °C fraction. When the elution temperature finally reached 140 °C the column was washed with two portions of xylene to remove all remaining polymer from the column.

The eluents of the various extracted fractions were allowed to cool, and the excess xylene was removed on a rotary evaporator. Thereafter, the polymer was further precipitated and washed with acetone, then dried to constant weight in a vacuum oven at 30 °C.

For the recombination experiments, the selected fraction was omitted, but the rest of the fractions were recombined and mixed in xylene, stabilizer was added, and the polymer dissolved at elevated temperature. The mixture was cooled, excess xylene removed by rotary evaporation, precipitated with acetone, washed, and dried to constant weight at 30 °C under vacuum.

The following recombined materials were prepared in this fashion:

1. E-REF: Entire polymer recombined after the TREF fractionation
2. Less25C: Room temperature or 25 °C fraction was removed
3. Less60C: Fraction that elutes from 40 °C to 60 °C was removed
4. Less80C: Fraction that elutes between 61 °C to 80 °C was removed
5. Less90C: Fraction that elutes between 81 °C to 90 °C was removed
6. Less100C: Fraction that elutes between 91 °C to 100 °C was removed
7. Less110C: Fraction that elutes between 101 °C to 110 °C was removed
8. Less120C: Fraction that elutes between 111 °C to 120 °C was removed

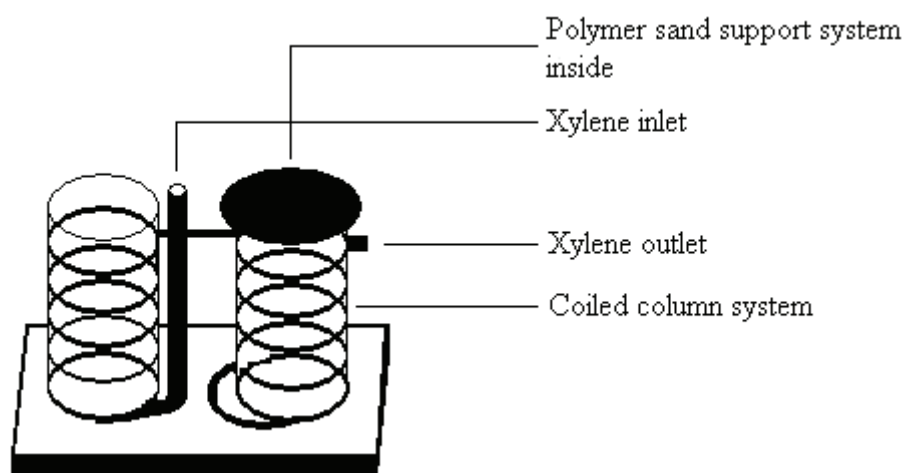


Figure 3.1: Temperature rising elution fractionation (TREF) column setup placed inside a modified GC oven.

3.2 **CARBON 13 (^{13}C) NUCLEAR MAGNETIC RESONANCE SPECTROSCOPY**

A Varian Unity Inova, 600 MHz NMR spectrometer was used to analyze the recombined samples and the excluded fractions. Deuterated 1,1,2,2-tetrachloroethane- d_2 (95.5 +atom % D, Sigma Aldrich) was used as solvent for NMR analyses.

Analyses were carried out at 130 °C in an argon atmosphere, with an acquisition time of 1.8 seconds, and a pre-acquisition delay time of 30 seconds. A signal to noise ratio of $1300 \leq S/N \leq 5000$ was achieved for all samples. This led to analysis times of 3 to 10 hours per sample.³

3.3 HIGH TEMPERATURE GEL PERMEATION CHROMATOGRAPHY

Molecular weight determination was carried out with a PL-GPC 220 high-temperature chromatograph from Polymer Laboratories. Measurements were performed at 160 °C, using a flow rate of 1 ml/ min⁻¹, and 1,2,4-trichlorobenzene as solvent (stabilized with 0.0125% 2,6-di-tert-butyl-4-methylphenol (BHT)²). Columns were packed with a polystyrene/divinyl benzene copolymer (PL gel MIXED-B [9003-53-6]) from Polymer Laboratories.

3.4 FOURIER TRANSFORM INFRARED SPECTROSCOPY

A Perkin Elmer Paragon 1000PC FTIR spectrometer, equipped with a photo-acoustic MTEC 300 cell, was used to perform the FTIR analyses of the samples. The instrument was calibrated with carbon black for a minimum of 8 hours. Each sample was then placed inside a sample holder and inside a sealed chamber. The chamber was flushed with inert helium gas. An instrument resolution of 8 cm⁻¹, 128 scans, and a mirror speed of 0.15 cm/s were used to perform the analysis of each sample.

3.5 TRANSMISSION ELECTRON MICROSCOPY

Polymer samples were prepared by isothermal crystallization in DSC pans (see Section 3.13). Samples were then stained, embedded in resin and cut, into thin slices using a Reichert UltracutS microtome. A LEO 912 EM TEM was used to record TEM images of the stained and microtomed samples. Ruthenium (III) chloride hydrate powder (Merck Chemicals) was used to prepare a Ruthenium (VIII) oxide (RuO₄) vapour with which to stain these samples.

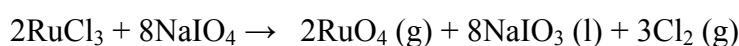
The samples were cut into small strips, 0.05 to 1 mm wide, then stained for 90 minutes, and then left to equilibrate. The stained samples were embedded in an Agar low viscosity resin and cured at 60 °C for 24 hours.

In order to obtain the morphological information on the sample under the electron microscope one needs to see a contrast between the different amorphous and crystalline areas present. This can be achieved by staining the samples with RuO₄.

The contrast difference is achieved because the amorphous areas are less dense and the stain can penetrate these more easily. The crystalline areas in the polymer sample will appear white or grey, compared to the darker amorphous areas. Care needs to be taken however to prevent over-staining and degrading the sample.

3.5.1 Ruthenium oxide staining

RuO₄ can be prepared by reacting RuCl₃ or RuO₂·xH₂O with a periodate such as NaIO₄. In this study RuCl₃ was reacted with NaIO₄ to produce RuO₄ (see reaction below):



RuCl₃ (0.2 g) was reacted with 10 ml of 5% NaIO₄ solution to produce 9.64 x 10⁻⁴ mol RuO₄ vapour.

3.5.2 Microtoming

The samples were cut to remove most of the resin until a trapezoidal shape was obtained, see Figure 3.2.

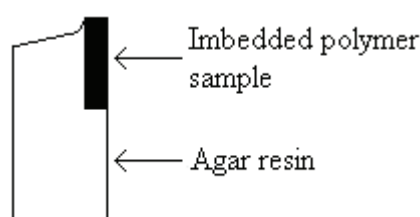


Figure 3.2: Trapezoidal shape required before microtoming.

Once the trapezoidal shape was obtained, a diamond blade was used to cut the sample into thin sheets of 0.11 μm to 0.13 μm thickness. A cutting speed of 0.4 mm/s was used. The thin sheets were collected on water and then transferred onto copper grids for viewing under the electron microscope. An

exposure time of 1000 ms was used, and images were taken at 10 000 X, 25 000 X and 50 000 X magnifications.

This gave a resolution (measurement bar), 500 nm, 200 nm and 100 nm. Selected images of the Less110C sample were recorded at 50 nm resolution.

3.6 SCANNING ELECTRON MICROSCOPY

A Leo® 1430VP Scanning Electron Microscope was used to for the SEM analyses. Each sample disc prepared by the hydraulic press method (see Section 3.10) was placed on a stub with double-sided carbon tape and mounted on the SEM stage. Each sample was coated with a thin layer of gold.

The SEM stage was then placed in a chamber under high vacuum (6 to 10 Pa) and the energy beam switched on (7 keV to 10 keV). Each sample was identified with secondary electron images (SE), where the electron beam can be focused to produce a sharp image and the magnification of the image can be set. In this case magnifications at 500 X and 2000 X were taken of each sample.

3.7 DYNAMIC MECHANICAL ANALYSIS

A Perkin Elmer DMA 7e was used to perform DMA analyses of the samples. Samples were cooled to -80 °C and then heated to 140 °C, during which period the data acquisition took place. The heating rate was 5 °C/ min and a nitrogen purge gas with a flow rate of 28.0 ml/min was used. The static force used was 110 mN, with a static force tension of 120%. The dynamic force was 100 mN, the amplitude 10.0 µm, and the frequency 1.00 Hz.

3.8 DIFFERENTIAL SCANNING CALORIMETRY

A DSC Q100 (TA Instruments) was used to perform the DSC analyses. Standard aluminium pans were used. A N₂ gas flow rate of 2 ml/min was used. The initial equilibrating temperature was 25 °C. The sample was heated at 10 °C/min to 220 °C and held there isothermally for 5 min, then cooled down to -40 °C at a rate 10 °C/min, while recording the crystallization exotherm. It was then left to equilibrate at -40 °C. For the second heating run the temperature was raised to 200 °C at 10 °C/min and the melt endotherm recorded.

3.9 MICROHARDNESS TESTING

A UHL VMH-002 Microhardness tester was used to perform the microhardness testing of the polymer samples. Analyses were performed at 25 °C, using an indentation load of 10 gf (0.01 N), an indentation speed of 25 um/s and a dwell time of 15 seconds for each sample. Twenty hardness values were recorded for each sample.

3.10 HYDRAULIC MELT PRESSING

An hydraulic melt press (APEX Construction Ltd.) was used to heat the mould and press a disc of each sample. Hardness tests and SEM analyses were carried out.

Sample preparation before using the melt press involved freezing the polymer in liquid nitrogen and grinding it to a powder with a mortar and pestle, to improve the rate of melting. Typically, 200 mg of sample was used, with 2% (w/w) stabilizer, dissolved in acetone, added to the polymer. The acetone was allowed to evaporate, leaving the stabilizer homogeneously distributed throughout the sample. Samples were then dried under reduced pressure for an additional 6 hours before melt pressing the disks.

Disks were pressed by heating the sample at 190 °C for 7 minutes, applying a pressure of 1 MPa for 3 minutes, and then removing the sample and cooling in an ice bath for 3 minutes.

3.11 INJECTION MOULDING

A HAAKE Mini Jet II bench top injection moulder (Thermo Scientific) was used with injection mould sample discs (20 mm diameter). Polymer material was prepared in a similar fashion to the material used in the melt press, with 1.0 g of each sample (3% w/w stabiliser) was used in each case.

The cylinder temperature was set to 250 °C and the mould temperature to 60 °C and samples injection moulded (30 seconds of preheating) at an initial injection pressure of 250 bar. After moulding, the pressure was maintained at 250 bar for another 30 seconds, after which the sample was removed from the mould and allowed to cool to ambient temperature.

3.12 WIDE ANGLE X-RAY DIFFRACTION SCATTERING

A Bruker AXS D8 advanced diffractometer with a filtered Cu-K α radiation, and a PSD Vantec-1 gas detector with up to 1600 channels, was used to perform analyses of the crystal phases present in each sample. The samples were all scanned at 2 θ angles between 10 ° and 35 °, with a step size of 0.014 °. The samples were flattened before they were placed in the sample chamber.

3.13 ISOTHERMAL DIFFERENTIAL SCANNING CALIROMETRY

In order to perform TEM analysis successfully on each of the samples and to be able to view an image with significant differences, such as the morphological changes across the samples, it was necessary to perform a controlled isothermal sample preparation step, to allow enough time for phase separation to take place during the melt stage of each polymer sample and allowing enough time for the different phases to develop. Isothermal crystallization was carried out in the DSC.

Hermetic aluminium pans were used. A N₂ gas flow rate of 2 ml/min was used. The initial equilibrating temperature was 25 °C. Samples were then heated at a rate of 50 °C/min to a temperature of 220 °C and held there for 2 minutes, then cooled to 110 °C at a rate of 50 °C/min. The temperature was then maintained at 110 °C for 30 minutes, followed by cooling to 100 °C at a rate of 50 °C/min, then held there for 30 minutes. Finally the sample was cooled to 25 °C at a rate of 50 °C/min.

This isothermal DSC procedure was used as a sample preparation method, to induce a controlled isothermal history on each sample in an effort to subsequently obtain improved TEM analyses.

3.14 REFERENCES

1. Rabie, A.J., Blends with low-density polyethylene (LDPE) and plastomers, MSc thesis, University of Stellenbosch, 2004.
2. Harding, G.W., van Reenen, A.J., *Macromolecular Chemistry and Physics* 207, 2006, p 1680.
3. Assumption, H., Sasol Polymers, private communication.

CHAPTER 4 RESULTS AND DISCUSSION

4.1 FRACTIONATION AND RECOMBINATION OF THE IMPACT PP COPOLYMER

The objective of this study was to study the effect of the subsequent removal of fractions on the properties and morphology of the IPPC. Preparative TREF (p-TREF) was used to fractionate a selected propylene impact copolymer (CMR 648 from Sasol Polymers). This fractionation proceeded on the basis of crystallizability. After the p-TREF experiments, fractions were removed and the remainder of the material recombined. The properties and morphology of the remaining material was studied and conclusions drawn with respect to the effect of the removal of the fractions.

Sample were analysed with respect to physical and mechanical properties such as the microhardness of the material, changes in crystallinity, glass transition(s), chemical composition and morphology. The p-TREF elution curves, with the true weights per fraction and weight percentage difference per temperature interval difference for the polymer, are shown in Figure 4.1. Based on the curve, and analysis of the individual fractions, I selected material to be removed prior to recombination and analysis.

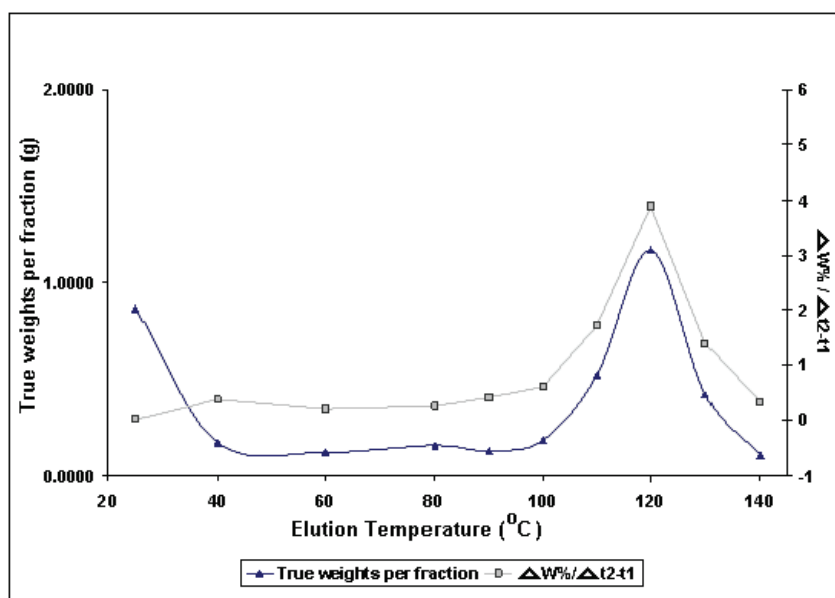


Figure 4.1: Preparative TREF elution curves for propylene impact copolymer (CMR 648). [True weights per fraction and weight percentage difference per temperature interval difference.]

It is clear that about 20% of the material remains soluble at room temperature, and this is denoted the 25 °C fraction. By the same token, about half the polymer sample elutes at 110 °C and 120 °C. The soluble part of the polymer is normally assumed to be rubbery and non-crystalline in nature, while the fractions eluting at the higher temperatures are more highly crystalline. The fractions of the material that elute in the range 40 °C to 80 °C are less crystalline than those that elute at higher temperatures, and are regarded as being propylene/ethylene copolymers of limited crystallinity.¹

The overall contribution of the so-called copolymer fractions to the total weight of the polymer is between 20% and 30%; 50% by weight is crystalline iPP and 20% is soluble, rubbery material, possibly non-crystallisable PP-PE copolymers, or low molecular weight isotactic PP and EPR rubber.

The fractions that were to be removed were the 25 °C fraction, the copolymer fractions at 60 °C and 80 °C, the 90 °C fraction that contains very long PP sequences with partial ethylene inclusions, and the 100 °C, 110 °C and 120 °C fractions, which comprise mostly the iPP matrix of the impact copolymer.

4.2 CHARACTERIZATION OF THE FRACTIONS

4.2.1 ¹³C NMR CHEMICAL SHIFT PREDICTIONS

¹³C chemical shift predictions were made using Grand and Paul² additivity rules to help assign the peaks obtained during the experimental analysis of each sample. This enables determination of specific monomer sequence distributions that could be present within the polymer sample. The additivity parameters and correction factors are presented in Appendix A.²⁻⁴

4.2.2 ¹³C NMR CHEMICAL SHIFT ASSIGNMENTS

Figure 4.2 shows some of the expected monomer arrangements that could be present within each of the polymer samples. The Grant and Paul parameters were used to predict the ¹³C NMR chemical shifts for these sequences.

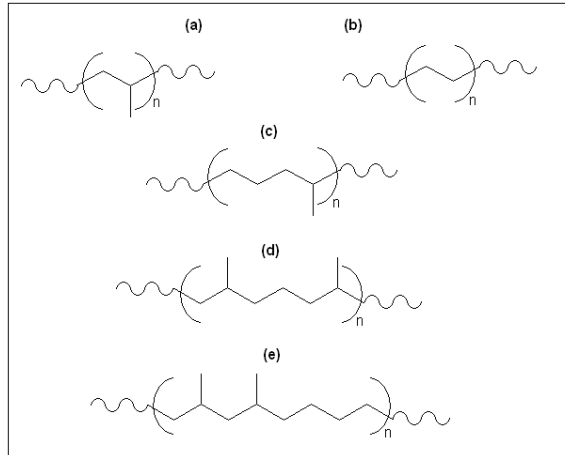


Figure 4.2: Monomer sequences in the impact copolymer: (a) PPPP, (b) EEEE, (c) PEP sequence, (d) PPE sequence, and (e) PPEE sequence.

The ethylene content (mole %) was also calculated for each sample using the method developed by Joubert.⁵ The subscript names are related to the different sequence types which are presented in Table 4.5. The subscript $\alpha\alpha$ refers to two propylene units next to each other, and might be found in PPPP, PPPE and EPPE sequences. The subscript $\alpha\gamma$ refers to two propylene units separated by one ethylene unit, and might be found in EPEPE and PPEP_{P/E}, $\alpha\sigma$ refers to two propylene units separated by two ethylene units, possibly found in PPEE_{n>1} and EPEE_{n>1}. It is important to note here that $\alpha\gamma$ and $\alpha\sigma$ both contribute toward propylene and ethylene units, so only half of each is taken for propylene determination. In the same manner the subscripts $\beta\beta$ (EPEPE, PPEPE, PPEPP), $\beta\sigma$ (EPEE_{n>1}, PPEE_{n>1}), $\gamma\gamma$ (PEEP), $\gamma\sigma$ (PEEE), and $\sigma\sigma$ (PEEE) refer to the ethylene content, as indicated, with n referring to any number larger than one, of that specific distribution that is present.

$$P = I_{\alpha\alpha} + \frac{1}{2}(I_{\alpha\gamma} + I_{\alpha\delta}) \quad (1)$$

$$E = \frac{1}{2}[I_{\beta\beta} + I_{\beta\delta} + I_{\gamma\gamma} + I_{\gamma\delta} + I_{\delta\delta} + \frac{1}{2}(I_{\alpha\gamma} + I_{\alpha\delta})] \quad (2)$$

$$C = \frac{100E}{P + E} \quad (3)$$

Equation (1) represents the propylene content (P), equation (2) the ethylene content (E) and equation (3) the ethylene content (C) as a mole %. The symbol I is defined as the integral value for a specific carbon type, calculated as a percentage of the total integral value of all the backbone carbons of the polymer represented in the spectra.

The individual fractions were characterized in terms of comonomer content (where enough sample was present for ^{13}C NMR analysis), molecular weight and thermal properties. The results are shown in Tables 4.1, 4.2, and 4.3. Figure 4.3 presents an example of the ^{13}C NMR spectra of a fraction removed. In this case it was the 60 °C fraction from the TREF experiment. The ^{13}C NMR analyses were only done for the 60 °C, 80 °C and 90 °C fractions, as these are the fractions that play a significant role in the morphology of the polymer.

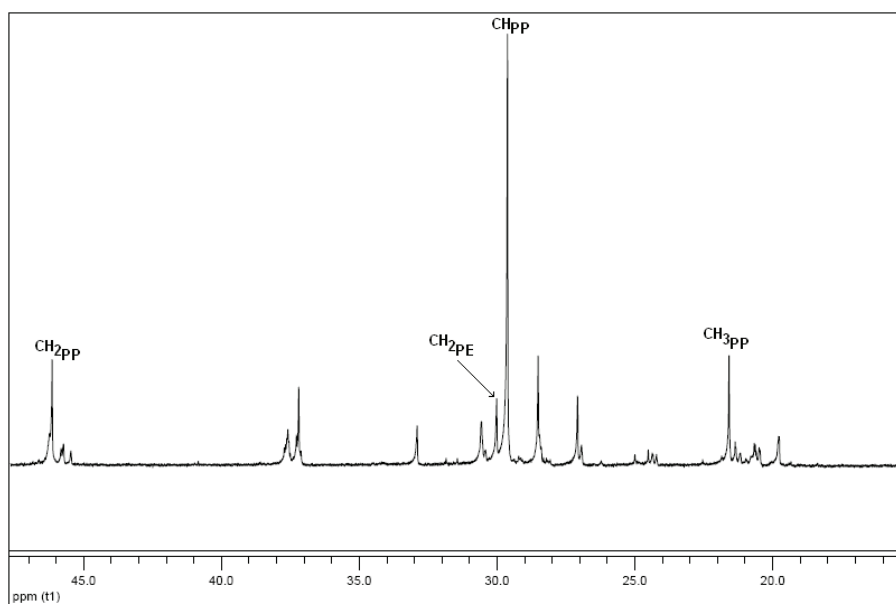


Figure 4.3: ^{13}C NMR spectrum of the 60 °C fraction.

The other ^{13}C NMR spectra can be seen in Appendix A.

Table 4.1: The integral values and chemical shifts of the sequence distributions of propylene and ethylene units in the ^{13}C NMR spectra of the three significant fractions removed from the polymer

Carbon type	Sequence type	Predicted shift(ppm) ref.TCE 75.0 ppm	Integral % fraction 60C	Integral % fraction 80C	Integral % fraction 90C
$\alpha\alpha$	PPPP	47.51	47.59	40.80	120.04
	PPPE	47.14	13.44		
	EPPE	46.77	4.65	4.20	
$\alpha\gamma$	EPEPE	38.76	27.05		6.35
	PPEPP	39.13	33.30		
$\alpha\sigma$	PPEE _{n>1}	38.82		15.53	
	EPEE _{n>1}	38.45		19.84	
$\gamma\gamma$	PEEP	30.75	27.64	15.27	4.01
$\gamma\sigma$	PEEE	30.44	25.37	11.49	
$\sigma\sigma$	PEEE	30.13			
$\beta\sigma$	EPEE _{n>1}	27.19			
	PPEE _{n>1}	27.25			
$\beta\beta$	EPEPE	24.25	0.40	23.55	
	PPEPE	24.31			
	PPEPP	24.37			

Table 4.2: Mole % Ethylene content in each removed fraction

Sample ID of the removed fractions	Ethylene content (mole %)
60C	30.36
80C	35.16
90C	2.83

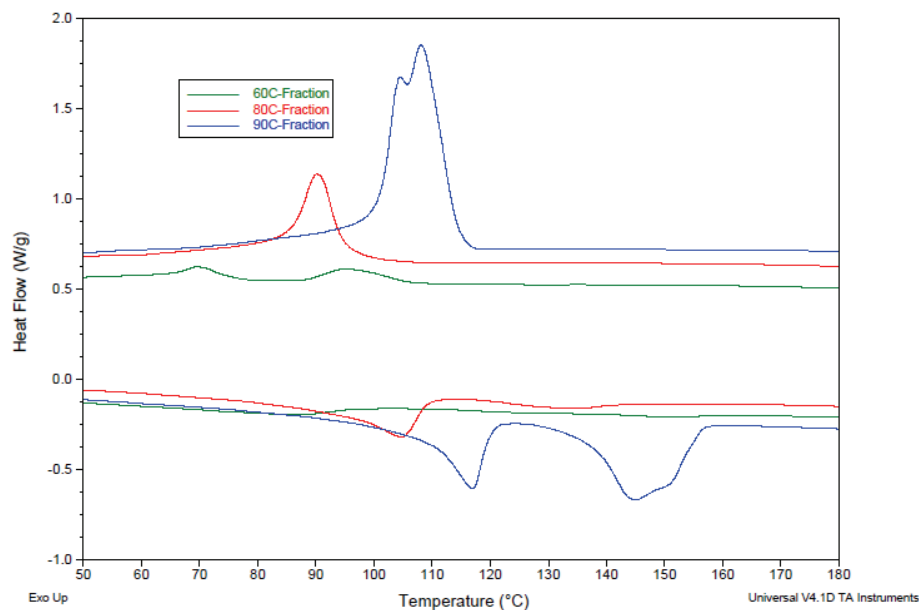


Figure 4.4: DSC melt peak and crystallisation peak, thermograms, of fractions 60 °C, 80 °C and 90 °C.

Figure 4.4 shows the crystallization and melt peak thermograms of the 60 °C, 80 °C and 90 °C fractions. The 90 °C fraction obtained from the p-TREF experiment is quite complex in nature. The crystallization peak exhibits a distinct double peak, and there are also two separate, well-defined melting peaks present at 104.6 °C and 144.6 °C. The higher temperature peak also seems to have a bimodal nature. It therefore appears as if this fraction does contain both isotactic PP as well as copolymer material, possibly both ethylene rich and propylene rich types. The single, broad melting peak at about 104 °C for the 80 °C fraction indicates that this is mostly an ethylene-rich copolymer fraction, while the 60 °C fraction shows two weak crystallization peaks at 70 °C and 95 °C, and little or no melting peak in the region of 89 °C, indicating that this fraction has limited crystallinity and that the crystallinity is probably due to some copolymer present.

Table 4.3: High temperature GPC molecular weight averages of the TREF fractions

Sample ID	Mw	Mn	PD
25C	123902	66822	1.85
60C	73914	43283	1.70
80C	112201	25877	4.33
90C	211376	21131	10.00
100C	168959	23612	7.15
110C	93841	43900	2.13
120C	246752	87833	2.81

It is extremely interesting to note that the polydispersities of the 80 °C, 90 °C and 100 °C fractions are quite wide. This is a clear indication that the fraction of material that eluted at these temperatures comprises possibly short chains of isotactic PP as well as longer copolymer chains. It is very apparent in the 90 °C fraction, which once again leads us to believe, in conjunction with the DSC and NMR data, that this fraction contains both low molecular weight iPP as well as higher molecular weight copolymer material. This is supported by the large polydispersity value of the 90 °C fraction (see Table 4.3).

4.3 CHARACTERIZATION OF THE RECOMBINED MATERIAL

4.3.1 ¹³C NMR

Tables 4.4 and 4.5 tabulates the integral percentages and chemical shifts of the chemical composition and sequence distributions present in copolymers of propylene and ethylene. These vary only slightly from the predicted values.^{4,6,7}

Table 4.4: ¹³C NMR chemical shift data and integral percentages of the main propylene and ethylene peaks, seen in Figures 4.5 to 4.8

Peaks	CH ₃ PP	CH ₂ PE	CH _{PP}	CH ₂ PP
Predicted shifts ppm	21.59	29.80	28.64	46.32
Experimental shifts				
E-REF ppm	21.60	29.75	28.60	46.20
Integral percentages	94.88	22.28	100.00	96.03
Less25C ppm	21.74	29.62	28.50	46.66
Integral percentages	103.94	16.06	100.00	100.04
Less60C ppm	21.60	29.62	28.50	46.15
Integral percentages	98.38	19.24	100.00	98.04
Less110C ppm	21.55	29.63	28.47	46.65
Integral intensities	95.95	35.82	100.00	96.23

The ^{13}C NMR spectra of the reference material and some of the recombined materials are presented in Figures 4.5 to 4.8. More spectra are shown in Appendix A.

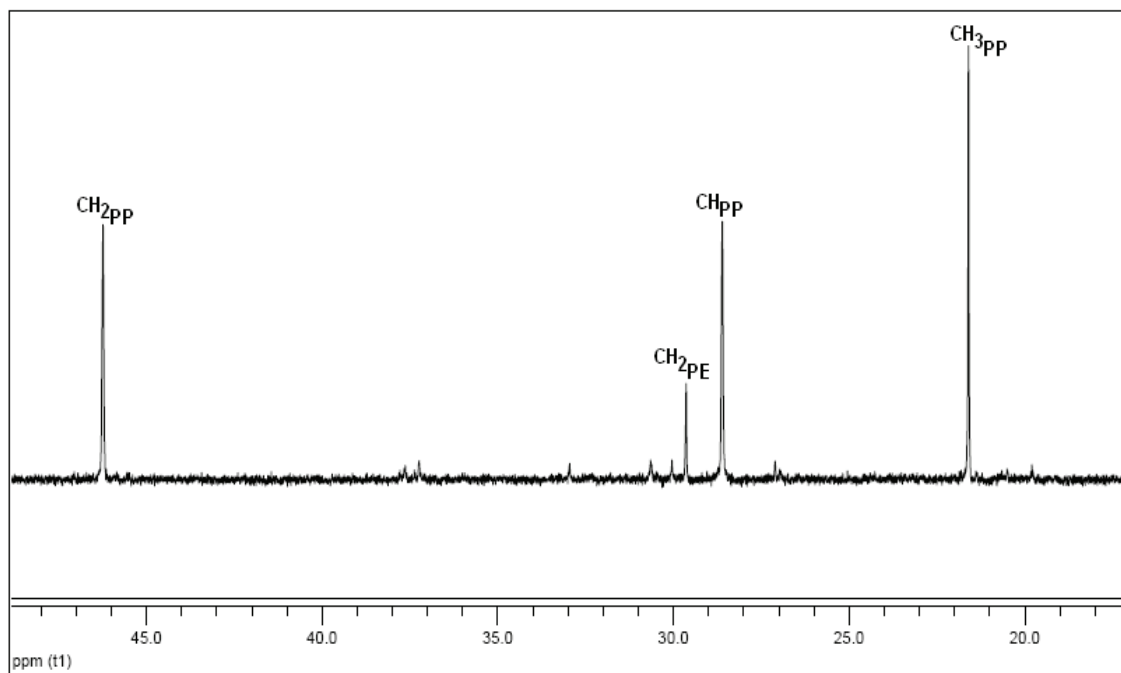


Figure 4.5: ^{13}C NMR spectrum of sample "E-REF".

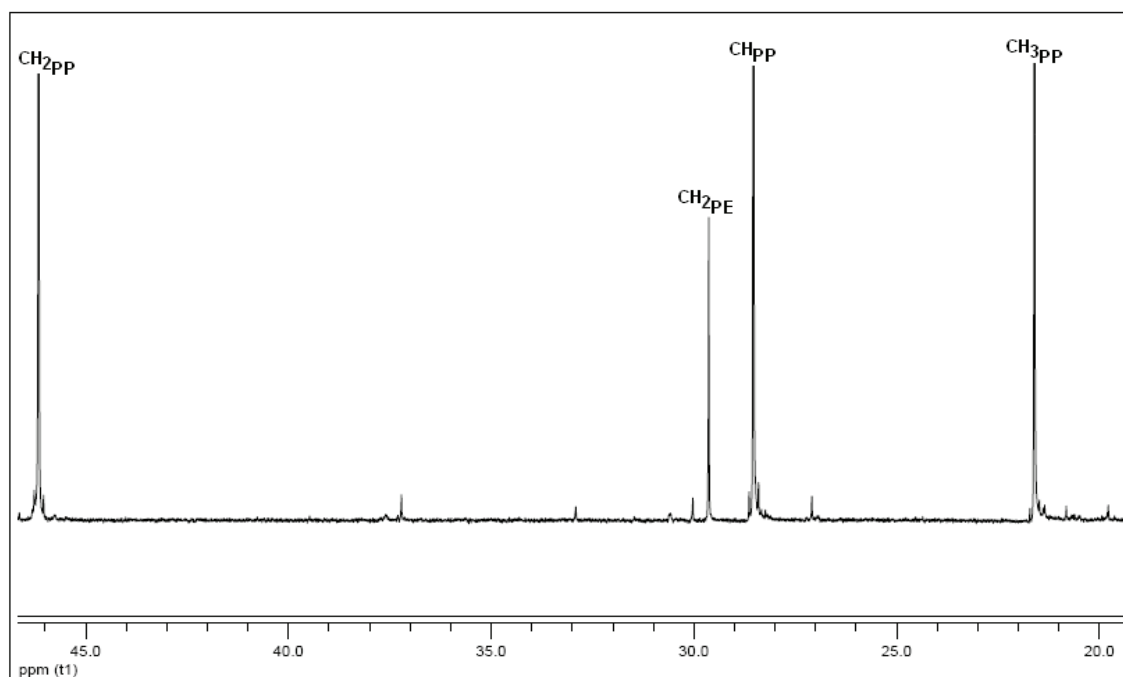


Figure 4.6: ^{13}C NMR spectrum of sample "Less25C".

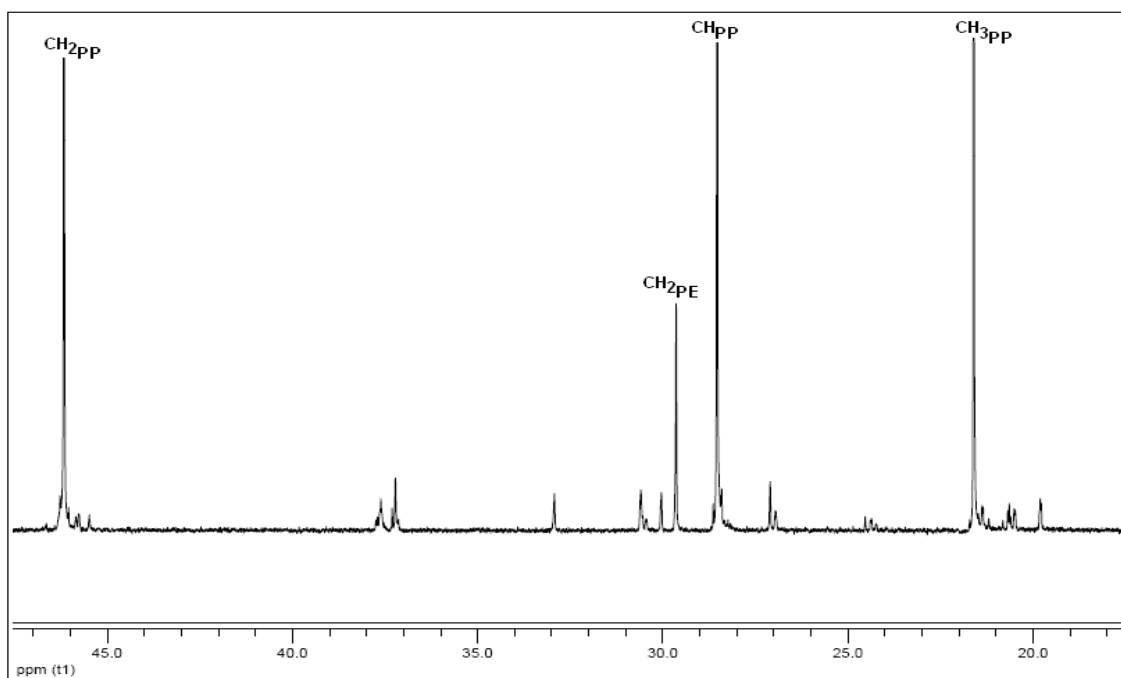


Figure 4.7: ^{13}C NMR spectrum of sample "Less60C".

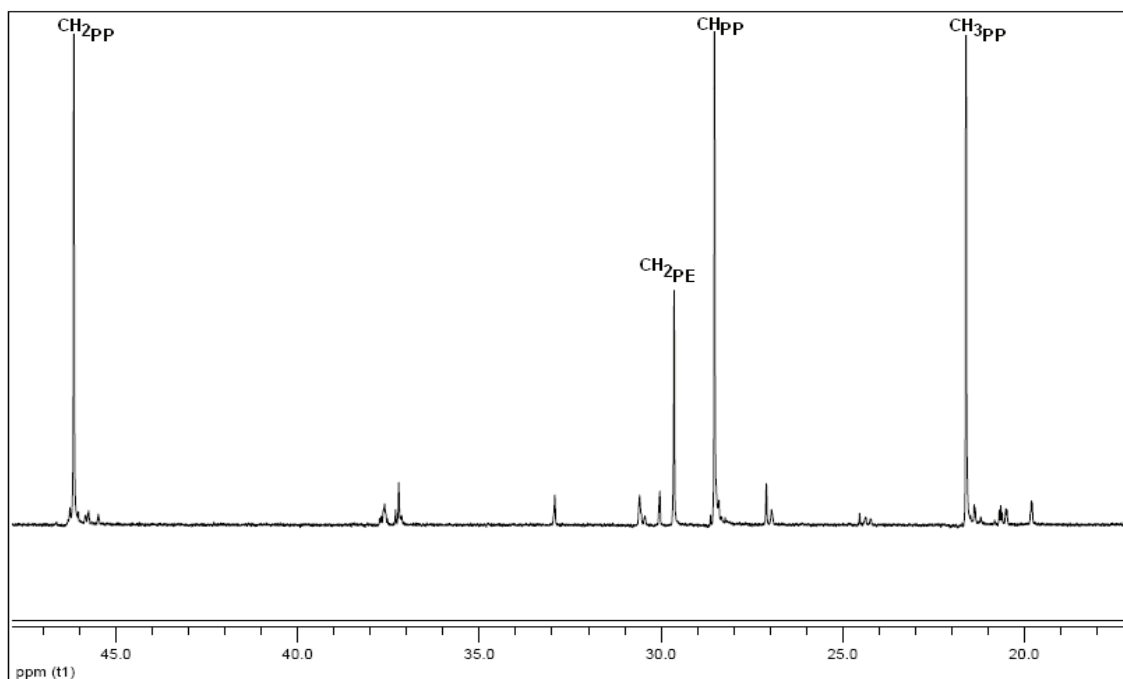


Figure 4.8: ^{13}C NMR spectra of sample "Less110C".

Table 4.5: The percentage integral values and chemical shifts of the sequence distributions of propylene and ethylene units in the ^{13}C NMR spectra of the recombined samples of the copolymer

Carbon type	Sequence type	Predicted shift (ppm)	Integral % sample E-REF	Integral % sample Less25C	Integral % sample Less60C	Integral % sample Less110C
$\alpha\alpha$	PPPP	46.30	96.03	100.04	98.04	96.23
	PPPE	45.80		0.73	3.53	5.77
	EPPE	45.60		0.47	1.50	2.28
$\alpha\gamma$	EPEPE	37.90				
	PPEP _{P/E}	37.80	6.49			
$\alpha\sigma$	PPEE _{n>1}	37.50			7.09	9.92
	EPEE _{n>1}	37.40	5.79	1.60	7.16	11.62
$\gamma\gamma$	PEEP	30.60	7.08	0.96	7.52	10.85
$\gamma\sigma$	PEEE	30.10	5.07	1.31	3.89	6.52
$\sigma\sigma$	PEEE	29.80	22.28	16.06	19.24	35.82
$\beta\sigma$	EPEE _{n>1}	25.60				
	PPEE _{n>1}	25.50				
$\beta\beta$	EPEPE	24.70				
	PPEPE	24.60			0.73	
	PPEPP	24.40			1.39	4.89

Table 4.6: Ethylene content (mole %) in each recombined sample

Sample ID	Ethylene content (mole %)
E-REF	16.57
Less25C	8.57
Less60C	15.33
Less110C	23.03

The peaks due to PP sequences in Figures 4.5 to 4.8, are visible at about 21.59 ppm, 28.64 ppm and 46.32 ppm, and correspond to the methyl, methine and methylene carbons. The peak at about 29.80 ppm is due to long ethylene sequences present. These values are tabulated in Table 4.4.

In all four of the samples the $\alpha\alpha$ distributions have the highest relative integral percentages, as expected, since the matrix of each sample consists mainly of iPP.

It's interesting to notice the slight differences in the $\alpha\alpha$ sequence distributions of each of the samples in Table 4.5. It appears that upon removal of the 60 °C and 110 °C fractions respectively, peaks that correspond to single ethylene inclusions in long propylene chains become visible. Although the relative integral percentages are quite small, they are clearly visible and resolved from the PP $\alpha\alpha$ sequence distributions. These sequences are probably present in all the samples, but are hidden or swamped by the presence of the fractions mentioned above.

In all four of the samples a variety of different sequence distributions of longer ethylene inclusions can be seen, and these vary slightly, depending on the fraction of polymer that was removed. The largest difference can be seen for the samples "Less25C" and "Less60C".

The integral percentages are considerably decreased for the "Less25C B" sample. The longer the ethylene inclusions present in each of the different sequence distributions, the lower the integral percentage is, which is to be expected, since removal of the 25 °C fraction is essentially removal of the rubbery material of the polymer, which consists mostly of longer ethylene units.

Table 4.6, which shows the mol % ethylene content of each sample, shows that it decreases considerably (compared to the reference material) when the 25 °C fraction of material is removed, it changes slightly when the 60 °C fraction is removed, and seems to increase when the 110 °C fraction of polymer material is removed. This is to be expected, if we look at the ethylene present in all of the fractions that were removed.

It is clear from the NMR results that changing the composition by removing fractions from the material has a significant effect on the average monomer sequence distribution present in the material.

4.3.2 MOLECULAR WEIGHT DETERMINATION

The results for the molecular weight determination of the recombined material are given in Table 4.7.

Table 4.7: Molecular weight averages of the recombined samples

Sample ID	Mw	Mn	PD
E-REF	252971	62335	4.06
Less25C	140850	57545	2.45
Less60C	173536	65877	2.63
Less80C	157116	63127	2.49
Less90C	165685	71146	2.33
Less100C	163587	64546	2.53
Less110C	117200	50843	2.31
Less120C	202950	68066	2.98
Less120C $\frac{1}{2}$	217994	68425	3.19

Sample “Less120C” is made up of all the material between 25 °C to 140 °C excluding half of the 120 °C fraction by weight.

If we look at Tables 4.3 and 4.7, the following is worth comment. Upon removal of the 25 °C fraction we see that the average molecular weight decreases by more than 100 000. Such a large decrease is quite surprising, since the 25 °C fraction makes up 20% of the overall weight of the original polymer and had a molecular weight of only around 120 000. The decrease in the polydispersity of the recombined material from “E-REF” to “Less25C” by almost 2 also appears strange, as the fraction has quite a narrow molecular weight distribution, but if we consider that the fraction comprises mostly low molecular weight material, this will in effect mean that the amount of low molecular weight material decreases, which should lead to a narrower molecular weight distribution.

Overall, the polydispersity of all of the remaining recombined materials are quite narrow. Referring back to Table 4.3, it is noticeable that the polydispersity values of the 80 °C, 90 °C and 100 °C fractions were quite wide, so it is to be expected that the recombined materials without these fractions would have a narrower molecular weight distribution. One must bear in mind that the values given were determined using linear polystyrene

materials as standards. As the fractions are removed, and the material recombined, we are in effect changing the chemical composition of these complex materials and therefore, quite possibly, the hydrodynamic volume in the solvent used for the HT GPC experiment.

While the polydispersity values are of some interest, one should however not place too much emphasis on the actual molecular weight values determined by these experiments.

The wide polydispersity values of the 80 °C, 90 °C and 100 °C fractions, combined with the chemical compositions of these fractions, appear to be quite important. This will be borne out later when we look at phase morphology as determined by the SEM and TEM results. We observed large phase separation for the recombined materials, “Less80C” and “Less90C”. The 80 °C, 90 °C and 100 °C fractions have a significant contribution to the compatibility between the amorphous and crystalline phases in the polymer and, combined with these results, it would suggest that the contributing factor to increased compatibility with the presence of these fractions in the polymer, are also due to their broad distribution in chains lengths.

4.3.3 THERMAL PROPERTIES OF THE RECOMBINED MATERIALS

Table 4.8: DSC analysis data of sample series A and B

Sample ID – DSC	Peak T_{melt} (°C)	Onset of the crystallization (°C)	Peak T_{cryst} (°C)	Crystallinity relative to PP 209J/g (%)
E-REF A	164.13	127.10	124.15	49.55
Less80C A	159.79	119.64	113.36	43.28
Less90C A	148.68	109.75	106.54	35.17
Less100C A	156.17	115.36	112.65	40.62
Less110C A1	149.31	110.14	105.59	37.41
Less120C A	149.28	111.59	107.05	23.05
Less120C ½ A	162.26	119.46	113.54	61.78
E-REF B	160.54	121.97	116.26	49.89
Less25C B	159.33	119.04	114.92	54.85
Less60C B	159.60	119.21	114.90	54.79
Less80C B	153.13	116.20	110.44	46.26
Less60C&80C B	157.09	117.92	113.25	42.82

The first initial series of experiments involved removal of the more crystalline fractions of the polymer that are present from 80 °C till 140 °C (Sample series A). The thermal characterization results of the recombined materials are given in Table 4.8. The DSC thermograms for crystallization and melting are given in Figures 4.9 to 4.12.

Series A

The removal of the 120 °C fraction, is the major fraction of the polymer, and causes the overall crystallinity and melting temperature to decrease markedly. This is hardly surprising, as this fraction is the major part of the polymer, and reportedly comprises mostly iPP.

This is also borne out by the characterization of the fractions resulting from work previously done in our group.^{3,8} Similarly, removal of the other fractions gives a similar, expected change in thermal properties, with the exception of the recombined material, after removal of the 100 °C fraction. The molecular weight of the recombined material is somewhat lower than that of the other samples, and this might play a role in the crystallizability of the polymer chains, as we have frequently observed reducing the molecular weight enhances crystallization in the solid phase.

Of interest is the effect of removing only half of the 120 °C fraction, which results in only a slight decrease in melting temperature, but a significant increase in overall crystallinity. The trend is illustrated in Table 4.8 for all the polymers. We see that the crystallinity decreases when we remove more crystalline material (which is to be expected).

Of more interest is the actual shape of the DSC melting and crystallization curves of the reference and recombined materials. We see a broadening of the peaks, with a shoulder appearing on the melting peaks for the materials with various fractions removed. Noticeably, removing the 90 °C fraction results in a very broad peak with three discernable maxima. There are clear indications that removing crystalline material results in a change in crystalline morphology of these complex materials. From these results we can deduce that removing most of the crystalline material (the 110°C and 120 °C fractions) obviously affects the crystallinity and melting significantly.

However, as these fractions represent more than 50% of the mass of the material, the change is not unexpected, and, in practical terms, not really significant. The changes brought about by removing the 90 °C fraction, however, seem to be significant. We see a change in the peak melting temperature, as well as a distinct second maximum on the melt peak. All of this indicates a change in crystalline morphology.

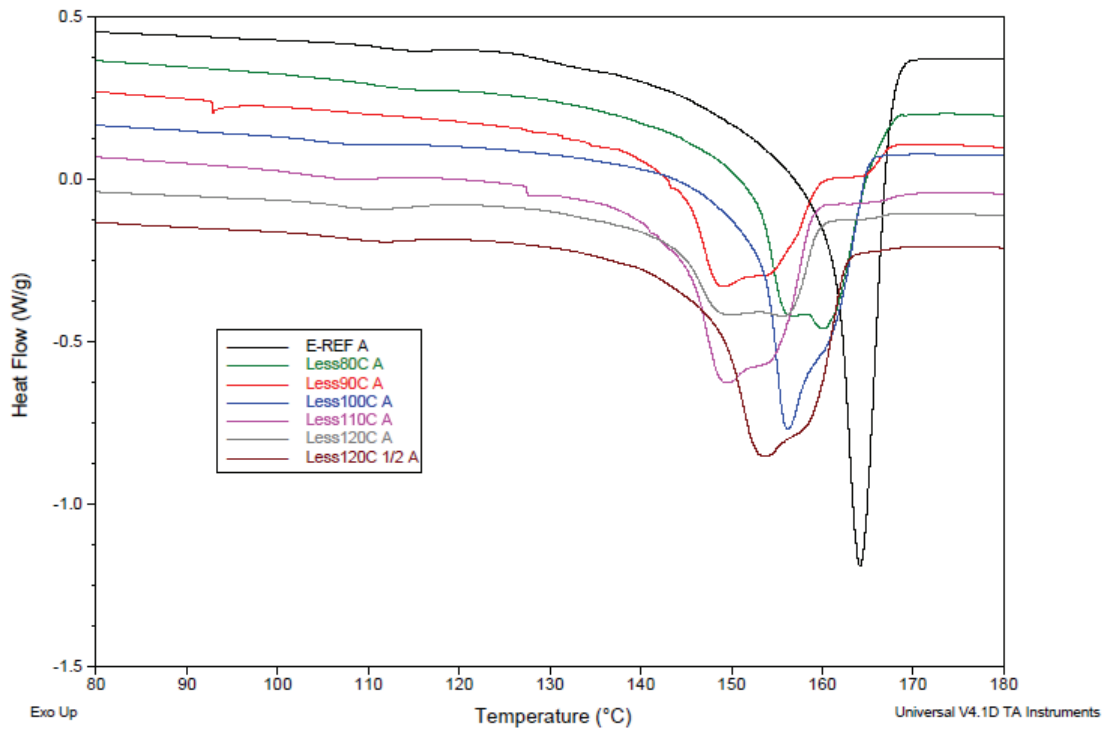


Figure 4.9: DSC thermogram (2nd heating) of sample series A.

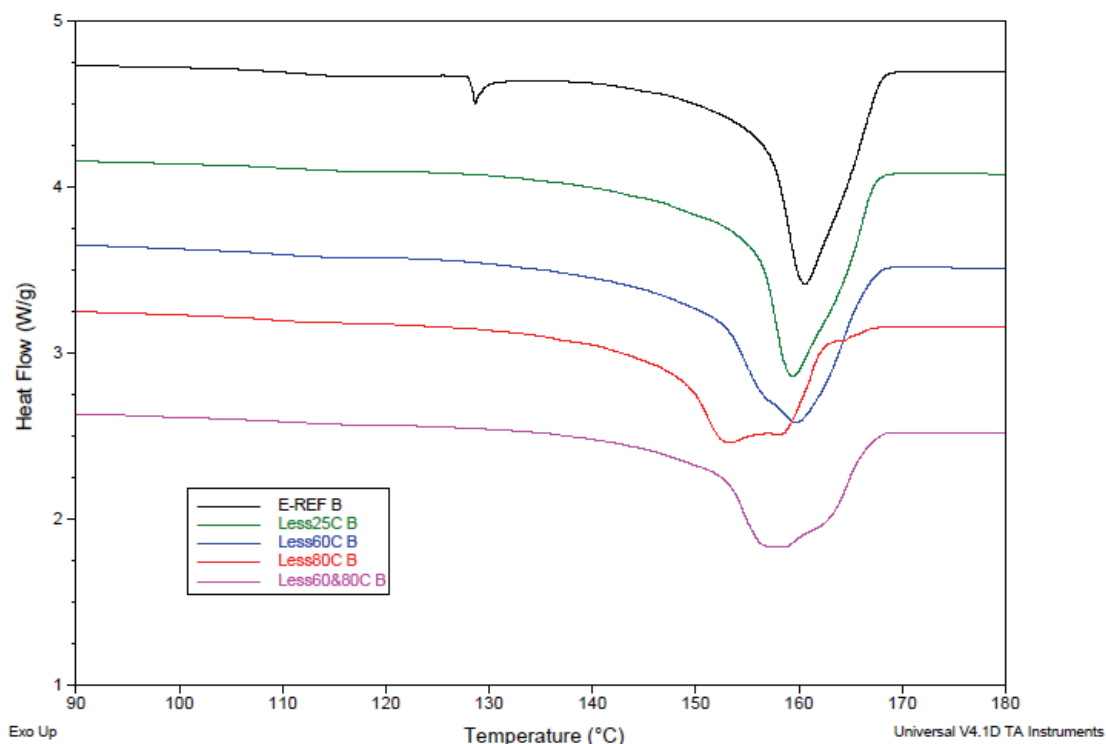


Figure 4.10: DSC thermogram (2nd heating) of sample series B.

Figure 4.10 shows the melt peaks of sample series B. In this group of samples we specifically investigated the effect of fraction removal focussing on the less crystalline materials. Removing the room temperature soluble (rubbery) fraction does little to change the melt peak, as would be expected. However, removing the 60 °C and 80 °C fractions (and a combination of the two) does change the shape of the melt peak, with a distinct second maximum developing and the peak melting temperature decreasing a little. As in the case of the 90°C fraction, this indicates that these fractions are quite important with regards to the development of the final morphology of the material.

The crystallizations, as determined by DSC, are shown in Figure 4.11 and Figure 4.12.

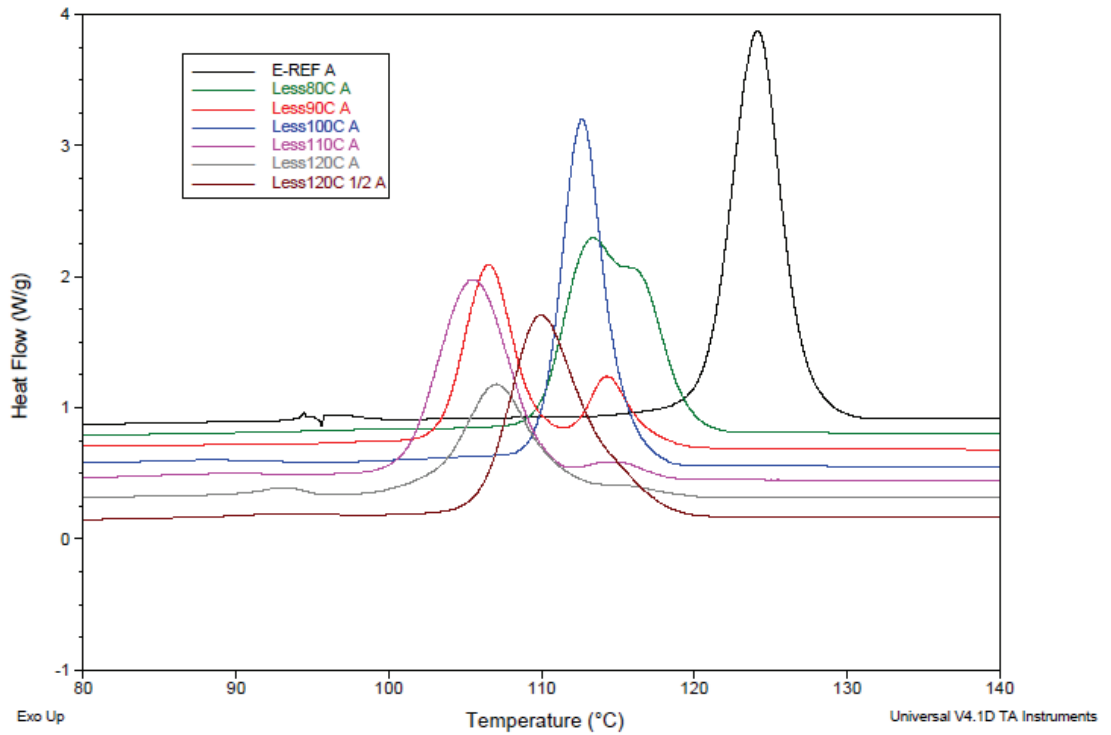


Figure 4.11: DSC thermogram (cooling) of sample series A.

For both sample series A and B the crystallization thermograms reveal much the same trend as the melting thermograms. Removal of the highly crystalline material brings about a distinct decrease in crystallization temperature and removal of the 90 °C fraction results in a decreased peak crystallization temperature as well as two distinct crystallization peaks.

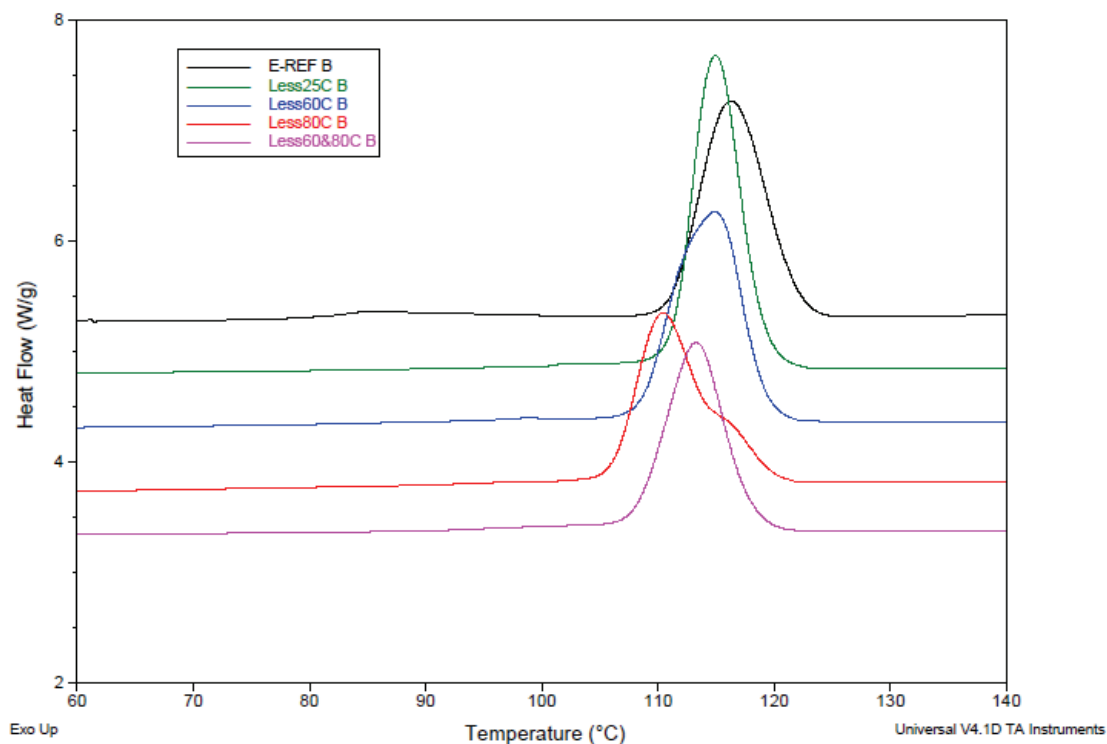


Figure 4.12: DSC thermogram (cooling) of sample series B.

The results shown in Figure 4.12 show that the removal of the 25 °C, 60 °C and 80 °C fractions can have the expected results, with only the 80 °C fraction's removal resulting in a broadening of the peak, with a possible shoulder developing. This is in agreement with the trend noted for the 90 °C fraction.

4.3.4 ISOTHERMAL CRYSTALLIZATION

The idea behind the isothermal crystallization was to see if we could force phase separation and crystallization events to occur to the extent that we could easily detect this via techniques like SEM and TEM. It was quite clear from the thermal analyses that we are seeing changes in the type and distribution of crystalline species.

The procedure here involved isothermal crystallization at 110 °C and 100 °C. It was thought that allowing crystallization to occur at 110 °C we would allow for the formation of the β -phase crystals, while the 100 °C crystallization would allow the α -phase crystallization.⁹

Isothermal crystallization of the samples was done to allow enough time for crystallization to take place so that clear differences between the crystal phases and amorphous phases in polymer samples could be seen with TEM, so that it will be possible to distinguish recombined samples from each other, because the samples each had a different fraction removed before recombination, one would expect to see different morphologies with TEM after doing isothermal crystallization.

It is important to note that the discussion of TEM results (Section, 4.3.8), is about the morphological differences seen in the samples after isothermal crystallization had been performed on them.

4.3.5 MICROHARDNESS

Initially, recombined fractions were prepared for microhardness tests by pressing samples in a hydraulic press and quench cooling the resultant samples. The results of the microhardness analysis are shown in Figure 4.13.

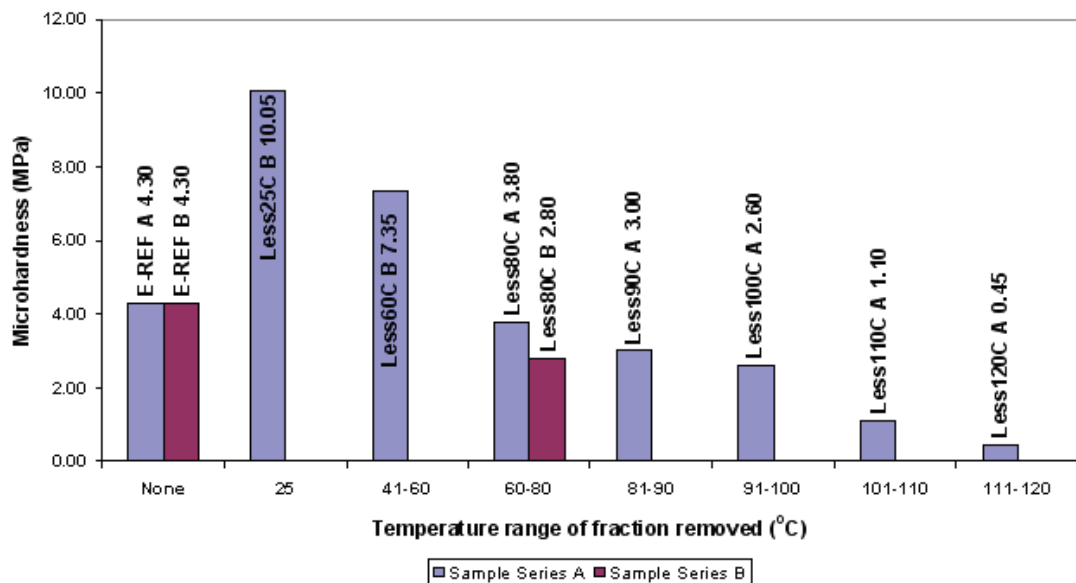


Figure 4.13: Microhardness averages of the hydraulic press system for the recombined polymers of sample series A and B.

The reference sample has a hardness value of 4.3 MPa. On removal of the amorphous fraction the hardness value reaches a value of 10.5 MPa, which is significantly larger than the reference samples' value. The changes is not surprising because the rubbery material was removed.

Similarly, when the majority of the sample was removed (110 °C and 120 °C fractions) it is not surprising that the hardness value falls to an extremely low value, as these fractions contain most of the hard, crystalline material.

As you start removing the copolymer fractions of the polymer, the recombined material shows a decreasing trend in the hardness values as you remove a higher order copolymer fraction, i.e. one that has a higher TREF elution temperature. It is interesting to note, however, that removal of the barely crystalline 60 °C fraction still results in a higher hardness value than the original IPPC sample, even though the rubbery material is all still present. This suggests that the partially crystalline 60 °C fraction does contribute significantly to the softness of the polymer. In addition, removal of the 80°C, 90°C and 100 °C fractions has little or no difference in effect on the hardness values. While initial results indicate that these fractions do play a significant role in determining the overall morphology of the material, they have no real effect on the hardness. As the hardness-impact strength balance of polyolefins are of some importance, this could be a significant indication of how to adjust this balance, particularly if we could show that removal of these fractions could influence the impact properties of these polymers.

When both copolymer fractions 60 °C and 80 °C were removed, we see a far greater effect on the hardness of the recombined material than we would expect based on the effect of removal of the individual fractions. This could be due to the role that these materials together play in acting as compatibilizer between the EPR, PE and iPP phases. This could result in less homogenous distribution of crystalline material and an apparently lower hardness value. However, to prove this statement we will have to show it in the TEM results obtained.

As a second set of experiments, we selectively prepared disks by injection moulding materials using the Haake bench top (Mini jet) injection mould. It is expected that these samples should be more uniform. Results of a few microhardness tests are shown in Figure 4.14. Although the values differ, the trends are the same, for both series of samples prepared.

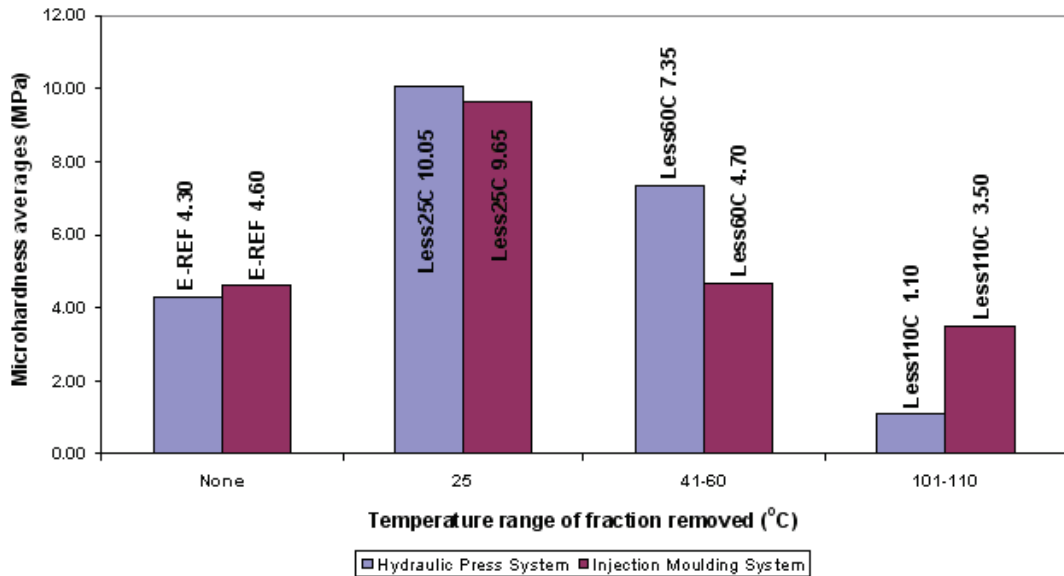


Figure 4.14: Microhardness trend of the recombined material, for the injection moulded and hydraulic press moulded samples for “E-REF”, “Less25C”, “Less60C” and “Less110C”.

The differences result from the sample preparation methods used in each system: the hydraulic press uses a different melting and cooling profile to the injection moulding system, and the time that each sample was subjected to the heating profile of each system used is also different. The procedure used for each system is described in (section 3.10 and 3.11).

4.3.6 DYNAMIC MECHANICAL ANALYSIS

The $\tan \delta$ curves for each of the recombined samples were recorded. The $\tan \delta$ curves for the reference material and for one of the recombined materials are shown in Figures 4.15 and 4.16. Other curves are presented in Appendix D.

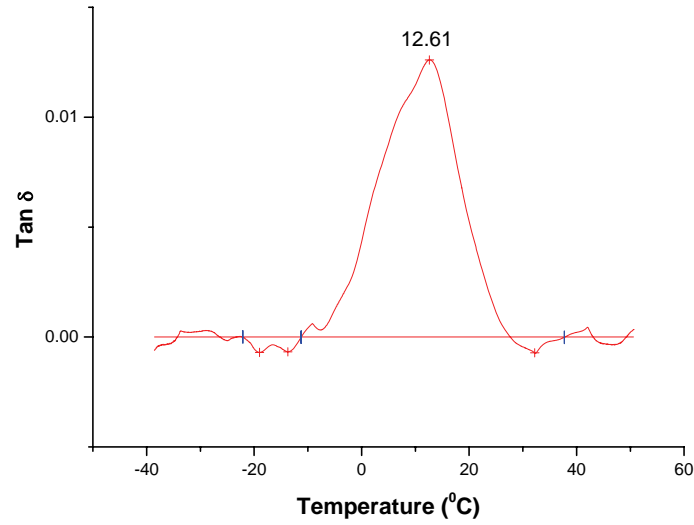


Figure 4.15: Dynamic mechanical analysis, $\text{tan } \delta$, sample "E-REF A".

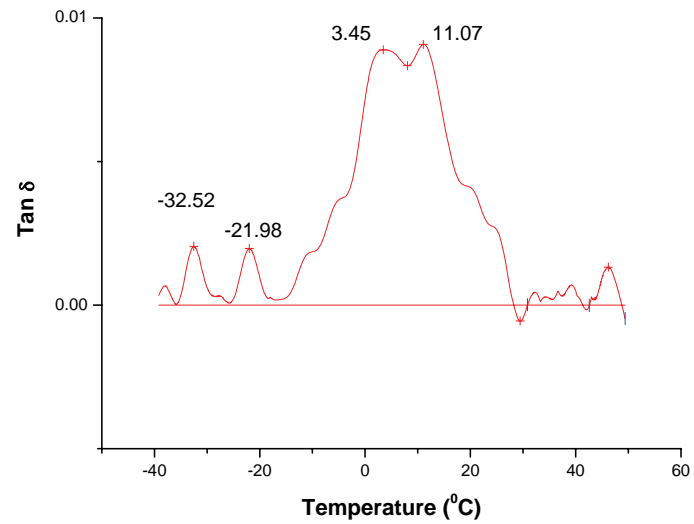


Figure 4.16: Dynamic mechanical analysis, $\text{tan } \delta$, sample "Less80C A".

In order to compare the effect of the changes in $\text{tan } \delta$ peak position, as well as the broadness and intensity of these peaks, were plotted, the data as (a) a three-dimensional and (b) a projection map. See Figures 4.17 and 4.18.

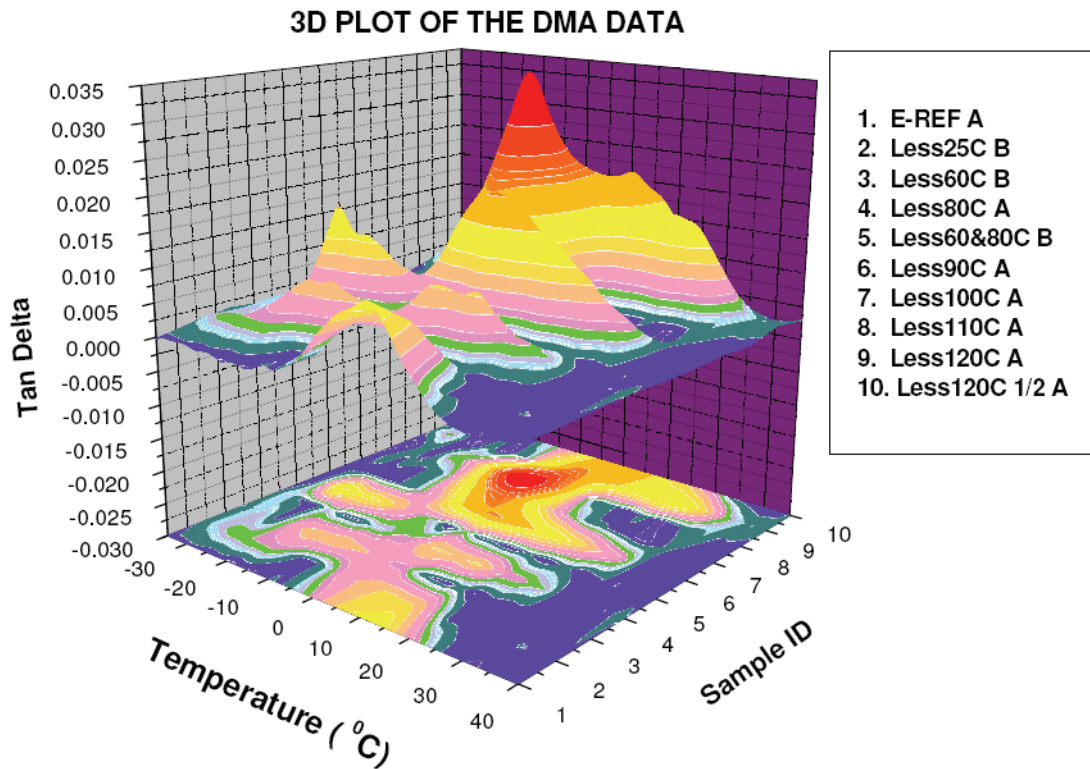


Figure 4.17: Three dimensional map of the dynamic mechanical analysis, $\tan \delta$, data.

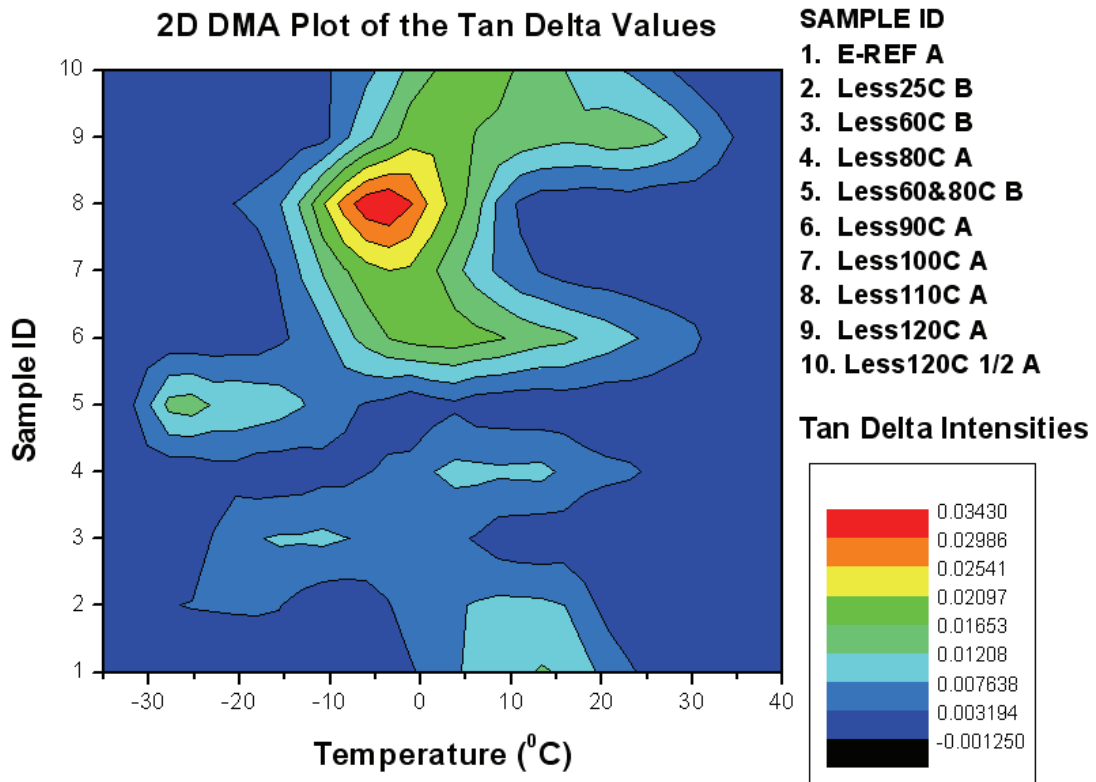


Figure 4.18: Projection map of the dynamic mechanical analysis, $\tan \delta$, data.

Figure 4.15 and Figure 4.16 (E-REF and Less80C) clearly show that the “E-REF” sample shows only a single $\tan \delta$ transition (maximum at 12.61 °C), which indicates good interaction between the different phases of the polymer, and well-dispersed, small rubber domains. This clearly is not the case for the “Less80C A” sample. The $\tan \delta$ plot of the “Less80C A” sample shows multiple peaks, indicating multiple T_g transitions present, each due to a different phase. The two peaks in the negative temperature range are possibly due to variations in the ethylene content of the EPR copolymer chains, and the two higher temperature peaks are possibly due to longer propylene and ethylene sequences. The presence of multiple T_g peaks serves as a general indication that phase separation is present, and the increased broadness and intensity in the “Less80C A” sample’s $\tan \delta$ plot is an indication of increased mobility of the chains. The picture becomes really interesting when we look at the 3D and projection plots.

Figures 4.17 and 4.18 clearly show how the T_g transition regions shift from the one sample to the next, and also clearly maps the broadness and separation of the samples. From the top down of the map in Figure 4.18 we can see that removing the crystalline materials leads to an increase in the intensity of the $\tan \delta$ transition, without significantly altering the position of the transition. This is to be expected, as removing the crystalline material should have that effect. Removing most of the polymer is, however, of little practical significance, and in this regard we find the effect of removing the 60 °C to 90 °C fractions (sample ID 3-6) very clear. We can see real changes in the position and number of $\tan \delta$ peaks, which indicates that these fractions play a significant role in the final morphology of the polymer in question.

4.3.7 SCANNING ELECTRON MICROSCOPY

In order to gain some visual information on the morphology of the recombined materials we used both SEM and TEM. The SEM analyses were done on samples that were pressure moulded and then quench cooled.

The following images were obtained of the surface of each of the different recombined polymer samples (Figures 4.19 to 4.29):

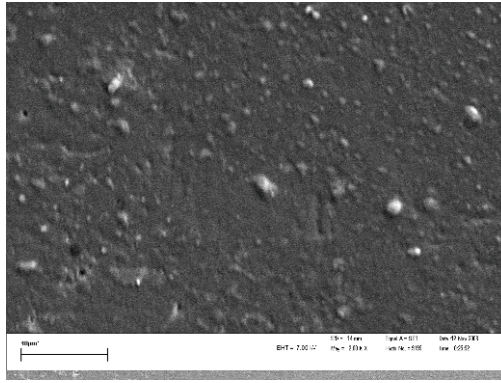


Figure 4.19: SEM image of sample “E-REF A” at 2000 X magnification.

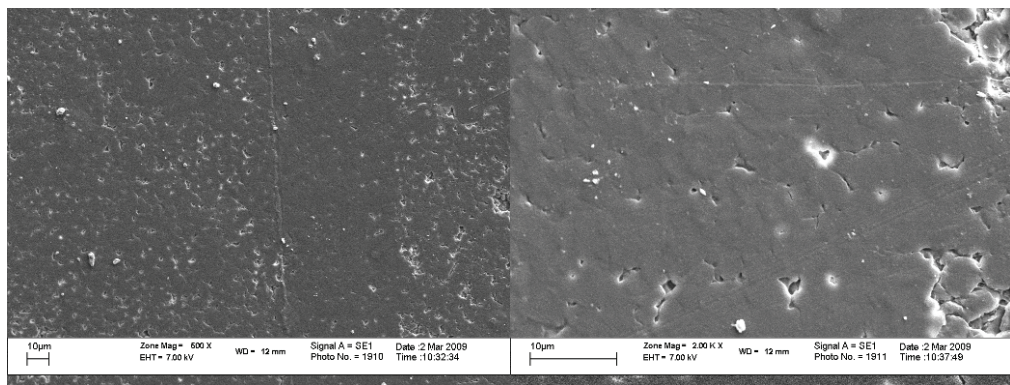


Figure 4.20: SEM images of sample “Less25C B” (a) at 500 X magnification and (b) at 2000 X magnification.

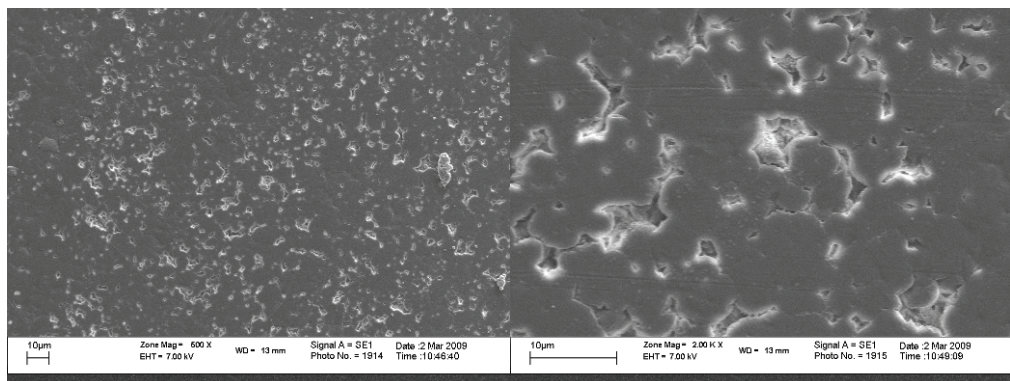


Figure 4.21: SEM images of sample “Less60C B” (a) at 500 X magnification and (b) at 2000 X magnification.

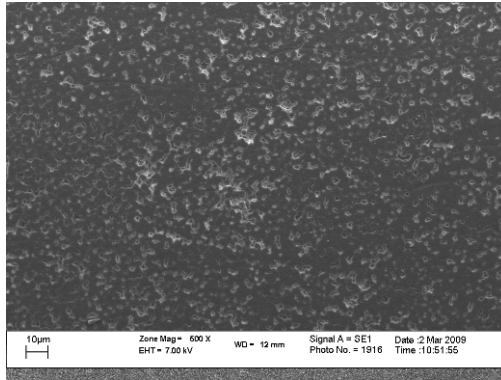


Figure 4.22: SEM image of sample “Less80C B” at 500 X magnification.

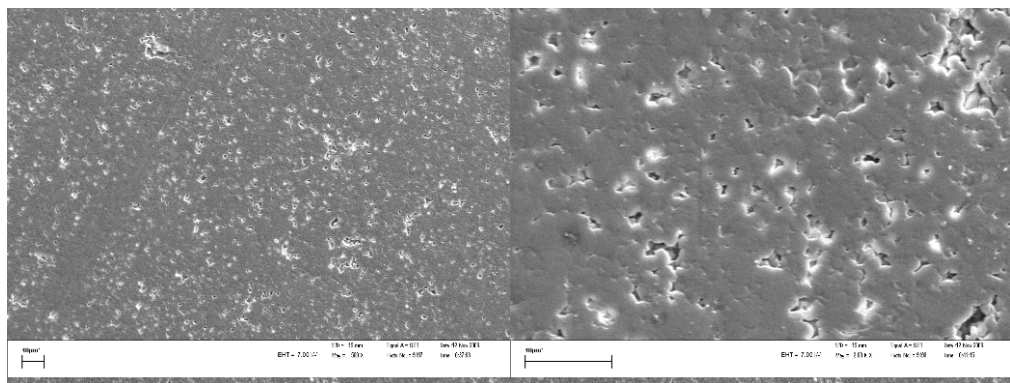


Figure 4.23: SEM images of sample “Less80C A” (a) at 500 X magnification and (b) at 2000 X magnification.

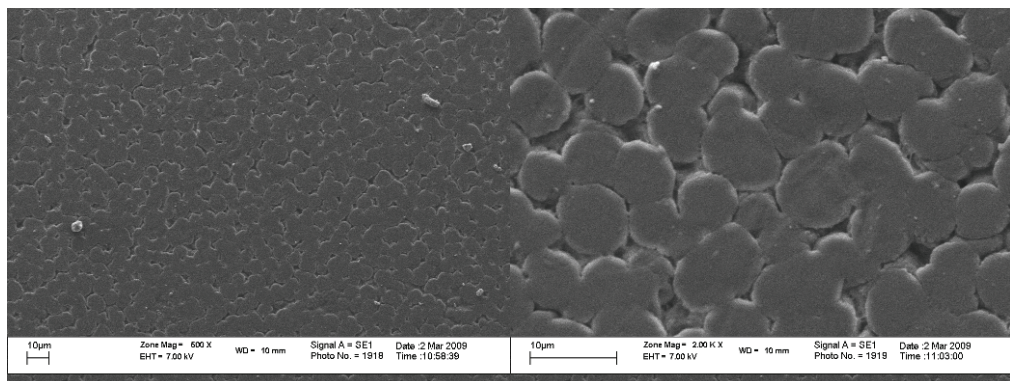


Figure 4.24: SEM images of sample “Less60&80C B” (a) at 500 X magnification and (b) at 2000 X magnification.

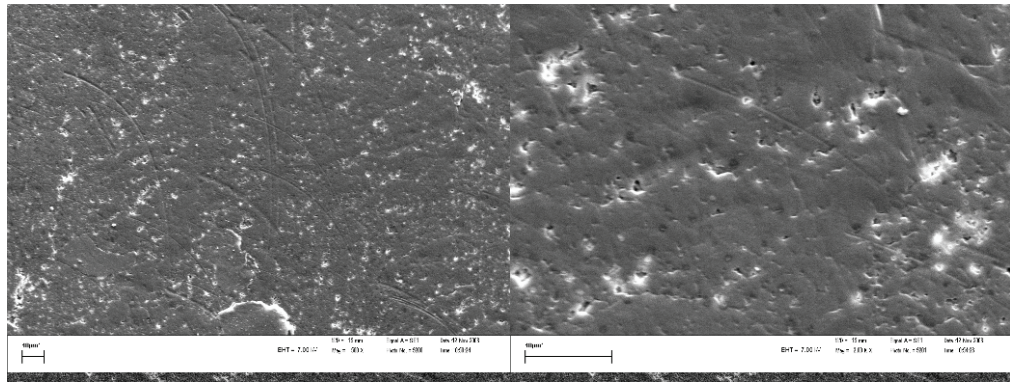


Figure 4.25: SEM images of sample “Less90C A” (a) at 500 X magnification and (b) at 2000 X magnification.

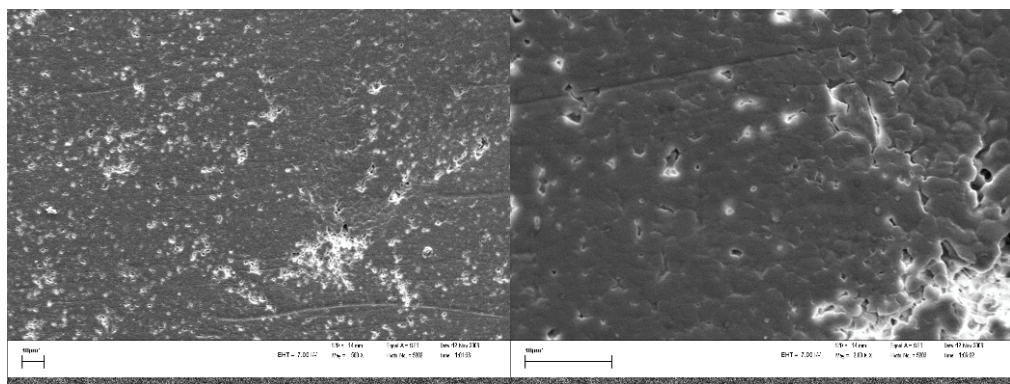


Figure 4.26: SEM images of sample “Less100C A” (a) at 500 X magnification and (b) at 2000 X magnification.

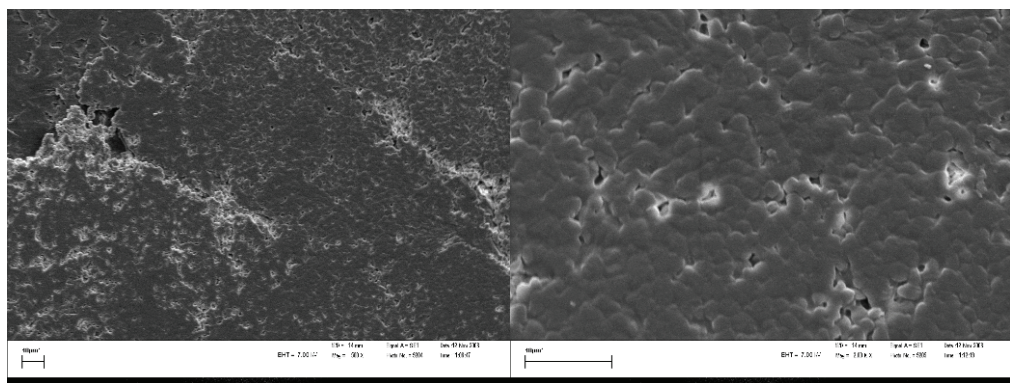


Figure 4.27: SEM images of sample “Less110C A” (a) at 500 X magnification and (b) at 2000 X magnification.

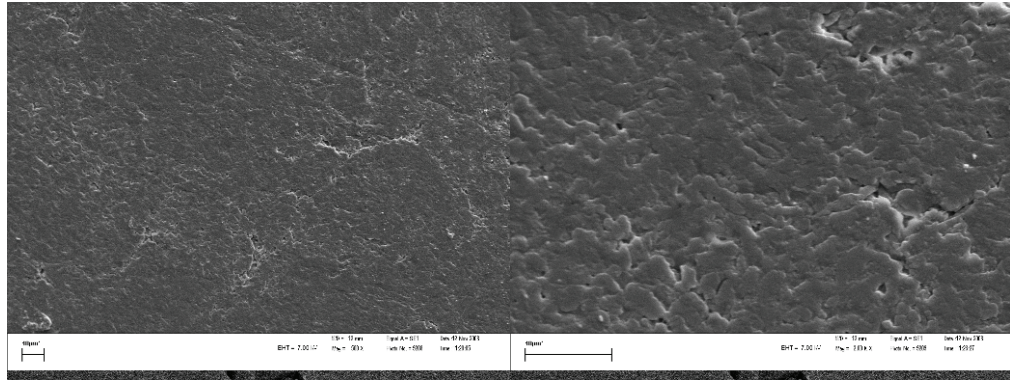


Figure 4.28: SEM images of sample “Less120C A” (a) at 500 X magnification and (b) at 2000 X magnification.

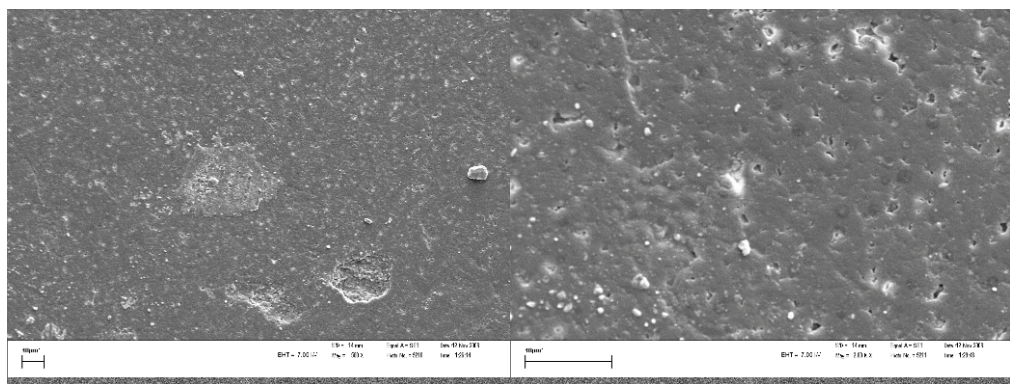


Figure 4.29: SEM images of sample “Less120C ½ A” (a) at 500 X magnification and (b) at 2000 X magnification.

Scanning electron micrographs reflect changes in the surface morphology and height differences of the surface reflected electrons. The darker areas are typically the more crystalline areas, and the lighter areas the more amorphous ones.

Figure 4.19 shows that the reference material appears to be homogenous with no defects visible on the surface. Particles appear to protrude from the surface of the sample, and these appear to be rubberlike particles, since they are lightly coloured, in fact almost white compared to the rest of the sample surface. These particles are evenly distributed. In the case of the “Less25C B” material (Figure 4.20), the surface appears to be relatively homogenous and smooth, with very small defects or crevices visible.

These defects are evenly distributed across the sample surface. There also appear to be rubber-like particles protruding from the surface, as is the case for

the reference sample, but they are smaller in size than that of the reference sample.

Clear crevices are visible on the surface of the “Less60C B” sample (Figure 4.21), and they are well defined. TEM (Section 4.3.8) and SEM results show that the crevices appear to be an indication of phase separation. The phase separation visible in this sample is distinct and this proves that the removal of the 60 °C fraction has a significant influence on the morphology of the recombined polymer.

For the “Less80C B” material we can see that defects or crevices are distributed evenly across the surface of this polymer sample, but that the dimensions of the crevices are not as large in the “Less60C B” sample. Some evidence of phase separation is present and no protruding rubber-like particles are visible on the surface of this sample. When both the 60 °C and 80 °C fractions are removed, we can see large, interconnected, crevices. Thus a very distinct phase separation took place on the surface of the sample, much larger than when removing just the 60 °C or 80 °C fractions.

Now interconnected crevices are visible, and the phase separated areas are well defined, large spherical like domains, and some appearing too agglomerate. A few rubber-like particles are also visible on the surface. This is the same sample that had a very low hardness value. As hardness measurements are based on the penetration of the tip into the sample surface, it is clear why removal of both the 60 °C and 80 °C fraction resulted in such a drastic lowering of the microhardness values (Section 4.3.6).

Removal of the 90 °C fraction resulted in a sample where the surface appears to have a large number of widely spread crevices, and appears to be the result of phase separation. The phase separated areas are not as well defined as in the Less60C B sample, they appear smoother, and no discernable spherical morphology is visible.

Small rubber-like particles are also visible on the surface of this sample, but there are also darker, spherical core-shell-like particles visible and widely spread across the surface. The important feature to notice is that they appear to be relatively close to the crevices on the surface, i.e. close to rubbery domains.

It is to be noted that the lines visible on the surface of the samples are due to the mould surface and not the sample morphology.

With removal of the more crystalline materials we would expect to see more clearly defined rubbery domains appearing. Removing the 100 °C fraction results in a crevice-like morphology visible here, and much more distinct than for the “Less90C A” sample, and appears to indicate a larger degree of phase separation than the “Less90C A” sample, yet less than the “Less60C B” and “Less80C A & B” samples. No rubber-like particles are visible on the surface, but the darker core-shell particles are even more visible here than was the case in the “Less90C A” sample.

When we remove the large fractions, like the 110 °C fraction we get very large interconnected crevices that are clearly visible on the surface, indicating large phase separation. The important difference here is that this phase separation is due to the removal of a large amount of crystalline PP material. The morphology of these areas appears to comprise spherical objects; the morphology is smaller and smoother than that of the “Less60C B” and “Less80C A & B” samples. The strange thing visible here is that there are no core-shell particles visible on the surface of this sample: Particles were however seen in the TEM images, but in the 50 nm diameter size range.

For the material with the most crystalline (and largest) fraction removed, the Less120C A material, we see a surface morphology that contains large crevices and clearly visible rubber-like particles. This is hardly surprising, as most of the crystalline matrix has been removed. This feature is not visible in any of the other samples. Large, well-defined phase separated domains are visible.

For the sample with only half the 120 °C fraction removed (Less120C ½ A) the surface also shows a crevice-like morphology, but less so than the “Less110C A” sample, and the degree of phase separation is also less than in the “Less110C A” sample.

The interesting feature to note here is that the darker, core-shell particles are present and clearly visible in the surface of this sample, but appear to be two to three times the size in the “Less90C A” sample.

4.3.8 TRANSMISSION ELECTRON MICROSCOPY

TEM images were obtained of samples that were isothermally crystallized. The best images in terms of the contrast differences (making it possible to see the morphology of the recombined polymer samples) were obtained at a magnification resulting in 200 nm resolution. Selected images are included here and others can be seen in Appendix E.

The following images are presented to illustrate the morphological differences between the recombined samples, and will be the main focus of the TEM discussion. RuO₄ was used as the staining agent according to Tortella and Beatty.¹⁰ The darker areas are the amorphous and low density domains in the polymer, whilst the lighter areas are the more dense crystalline domains. The reason for this is that the amorphous, less dense domains will scatter more electrons as they pass through the sample, creating a darker image.

It is to be noted that while the TEM images are objective, they show the morphology present in the sample analyzed, but may not be representative of the whole sample.

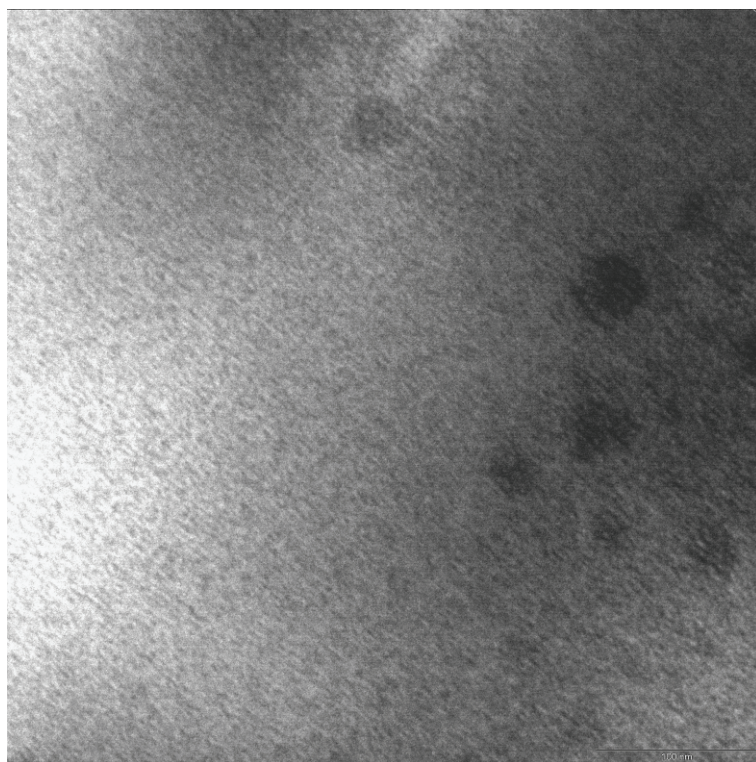


Figure 4.30: TEM image of sample “E-REF B” at 100 nm.

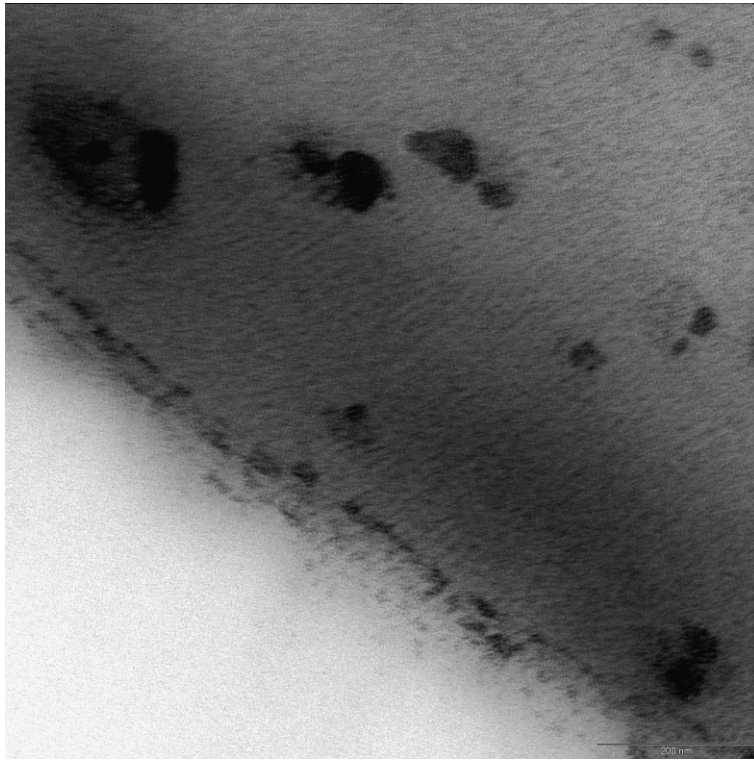


Figure 4.31: TEM image of the recombined sample “Less25C B” at 200 nm.

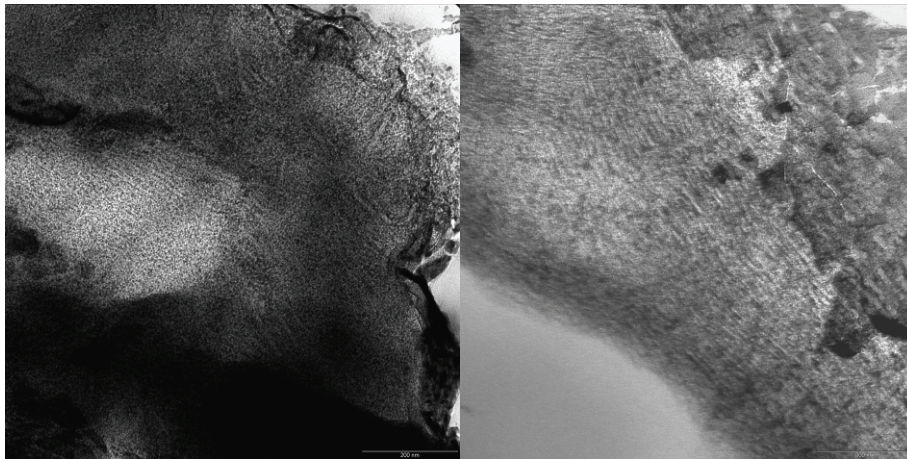


Figure 4.32: TEM images (a) and (b) of the recombined sample “Less60C B” at 200 nm.

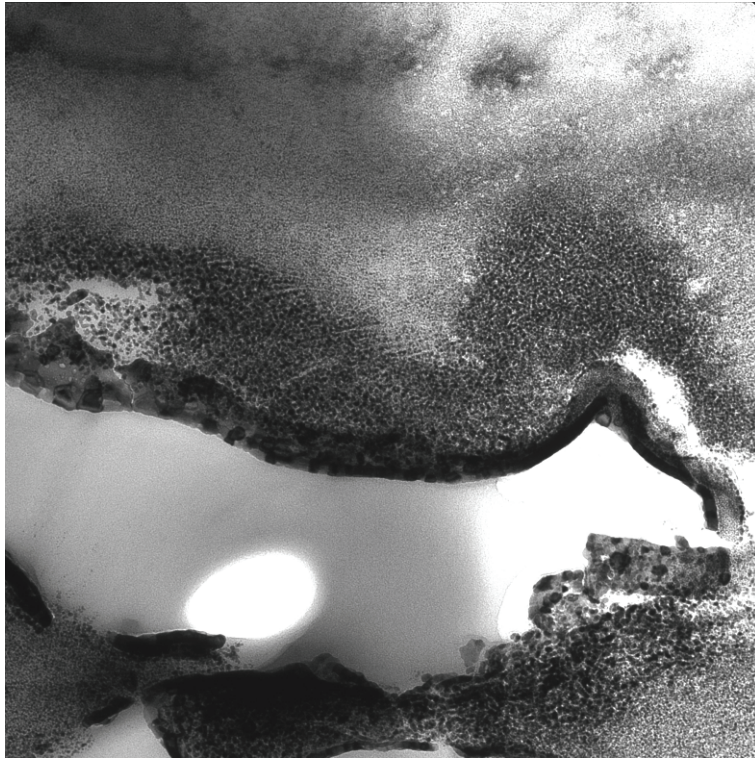


Figure 4.33: TEM image of the recombined sample “Less80C B” at 200 nm.

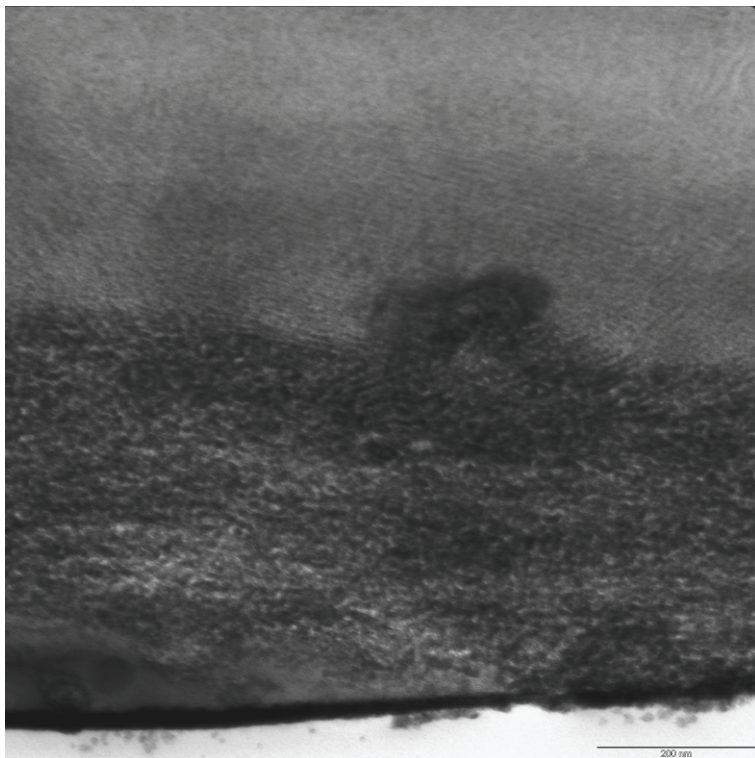


Figure 4.34: TEM image of the recombined sample “Less60&80C B” at 200 nm.

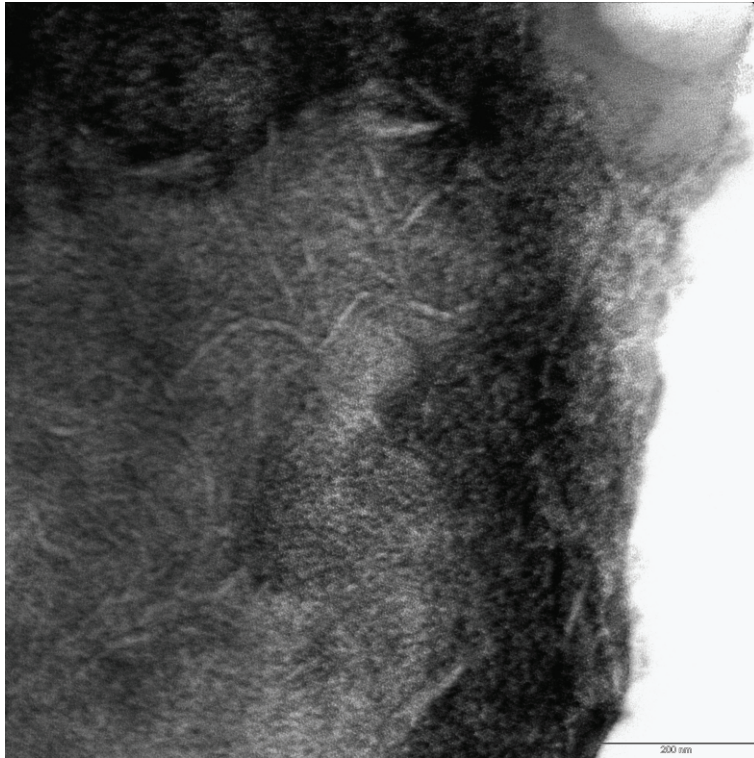


Figure 4.35: TEM image of the recombined sample “Less90C A” at 200 nm.

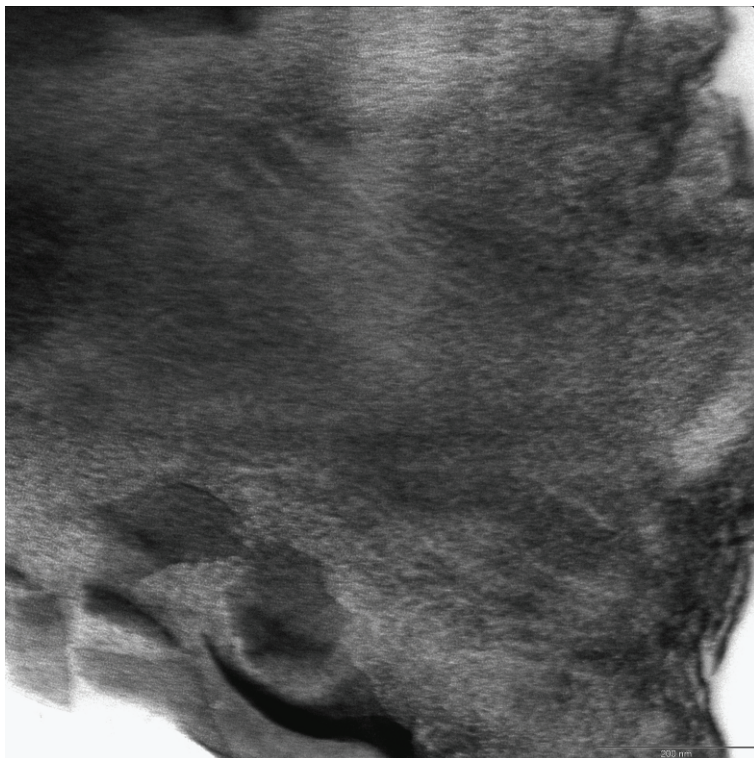


Figure 4.36: TEM image of the recombined sample “Less100C A” at 200 nm.

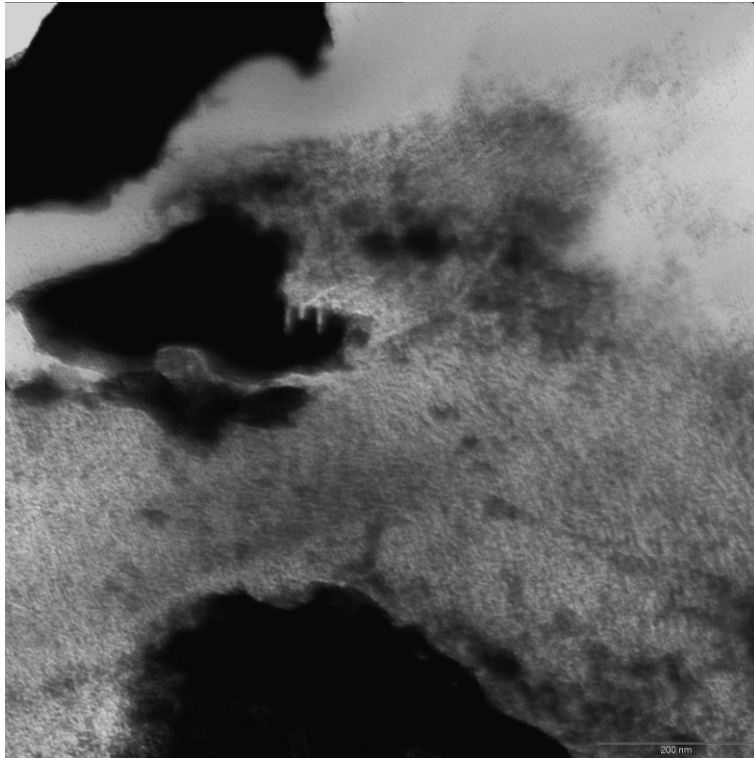


Figure 4.37: TEM image of the recombined sample “Less110C A” at 200 nm.

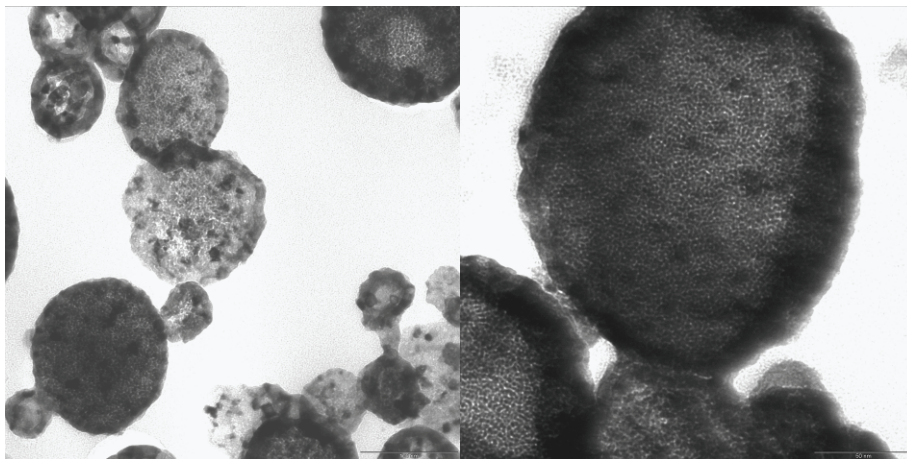


Figure 4.38: TEM images of the recombined sample “Less110C A”, (a) left image at 100 nm and (b) right image at 50 nm.

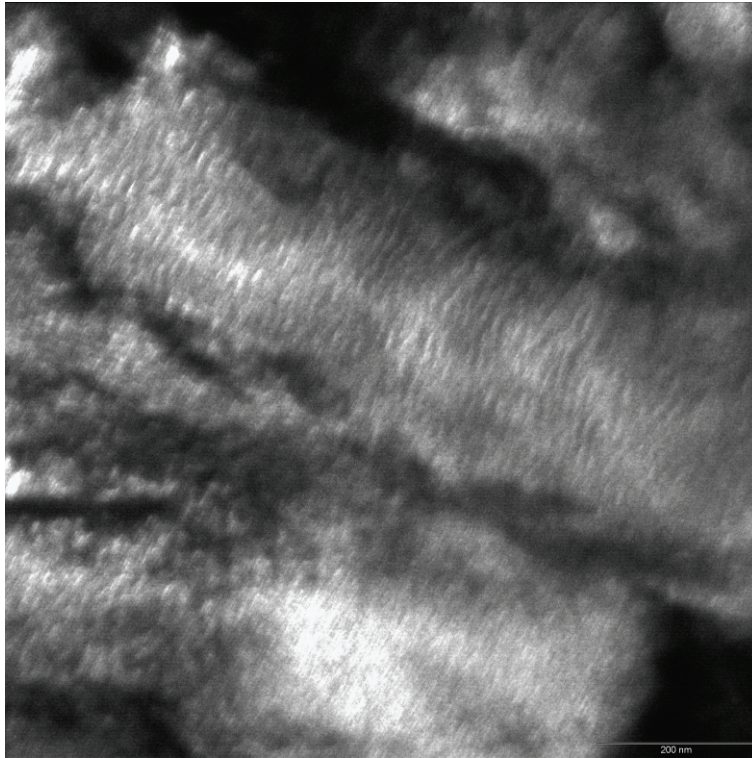


Figure 4.39: TEM image of the recombined sample “Less120C A” at 200 nm.

Figure 4.30 shows that the reference sample is to be relatively homogenous. The darker domains are spread evenly through the polymer lamellar morphology. A few larger darker domains are also visible and appear to be in close proximity to one another. They appear to range from 30-50 nm in diameter.

An enlarged view of Figure 4.30 (refer to Appendix E, Figure E1) reveals that there are multiple long lamellae structures, stacked parallel and closely together with a relative thickness of 10 nm. They appear to have a growth direction from the top left to the bottom right of the image.

The reason why these images are presented at 50 nm and not 200 nm, as the other sample images are, is that there was no discernable morphology visible at 200 nm.

In Figure 4.31 sample “Less25C”, we can see darker domains of the order of approximately 34 nm to 100 nm in diameter. They are not perfectly spherical; they seem to group together relatively close to one another, yet are still widely

spread across the image. The figure reveals the crystalline morphology of the sample to some degree. Although the contrast achieved here was not very good, one can still discern the darker domains from the lighter matrix, and a parallel stacked lamellar morphology is visible. The crystalline growth direction appears to be from the bottom left to the top right of the image. The thickness of the lamellae appears to be larger than observed for the reference sample, namely between 10 nm to 30 nm.

In Figure 4.32 the “Less60C B” sample reveals the presence of crystalline morphology. The lightly coloured domain appears to have specific growth direction towards the bottom right of the image. The lamellar morphology in this domain is rather difficult to ascertain. They lamellae appear to be stacked parallel to each other, with a thickness that is less than in the darker crystalline domain. Upon careful observation it also appears that there is crystalline material in between the lamellar structure within this domain.

Figure 4.32 (a) shows that the lightly coloured crystalline morphology appears to have α phase crystal morphology,¹⁰ and seems to be growing into the darker crystalline domain. The darker domain has thicker crystals, two to three times that of the lighter domain. The crystals appear to be very long, but randomly ordered, with no specific growth direction clearly visible. It is believed to be a β phase crystal morphology.¹⁰ Very dark domains are also visible in the TEM image, and seem to be confined to the outskirts of these crystalline domains.

Figure 4.32 (b) shows different types of crystalline morphology present. The lamellae are stacked parallel to one another. They have a growth direction from the top left to the bottom right of the image and appear to be segmented along the growth direction. They give the illusion of depth, i.e. three-dimensional, possibly due to lamellae stacking on one another. These lamellae have a relative thickness of 10 nm.

The far right of the image shows a darker stained crystalline morphology with a clear boundary between this domain and the one on the left of the image. This darker domain appears to have the same growth direction and segmented crystalline morphology, but the lamellae are thicker (about 20 nm).

Another crystalline domain is also visible, to the top left of the image, with the lamellae appearing to grow in a direction from left to right on the image, meeting the first crystalline domain at an angle. There appears to be some growth of one crystalline domain into the other one, creating a type of intermediate region, or boundary. The important feature of note here is that the morphology seen in this sample (the clear difference in phases) is as a result of the 60 °C fraction that has been removed from this material. The phases still appear connected, but they have clear boundaries between them.

There are three very distinct domain morphologies visible in Figure 4.33, sample “Less80C B”. The majority of the top half of the image consists of the polypropylene matrix, with slightly darker regions also visible. It is difficult to see any sort of discernable lamellar morphology, and no thick lamellae with any growth direction are observed within this matrix. This suggests that it could possibly be a α phase crystalline domain.

The bottom part of the image consists of resin that filled a “void”, present in the sample. This is pointed out because there are two different domains in this image. The lighter one of the two domains is next to the matrix and the darker domain (on its other side) next to the resin.

It appears that the matrix grows into the dark domain in the middle. Thicker, needle-like crystal structures are visible all along the boundary of the matrix and this darker domain. It also appears that this domain is what connects the matrix to the outer domain next to the resin. This very dark domain seems to be the rubbery material of the polymer, and an agglomeration of dark particles is visible within this domain.

Chen et al.¹¹ carried out a study on IPPC particle morphology and found that the EPR phase tends to be on the outer surface of the PP particles, with PE inclusions. Bearing this in mind, one could say that this domain close the resin could be the amorphous rubbery material and that the agglomerates of particles in this domain are PE inclusions.

The domain in the middle could possibly be copolymer material that seems to connect the matrix with the EPR phase.⁹ Once again, it is important to note that removal of the 80 °C fraction causes these boundary regions between the

separated phases to be clear and distinct, making the morphological differences clearly visible.

The TEM image of the sample where both the 60 °C and 80 °C fractions were removed (Figure 4.34) shows a clear and distinct boundary present between two major domains. The lighter, upper half of the image appears to be the matrix of the polymer and is connected to a large, darker domain.

Close observation of the boundary between these two domains reveals that there is a type of intermediate crystalline structure present. On the left hand side of the boundary it appears that the matrix is growing into the darker domain, with a growth direction towards the right of the image, but on the right hand side of the boundary it appears that the matrix of the polymer is also growing into the darker domain, but towards the left of the image. This crystalline region has the characteristics of the α phase of iPP.

Further away from the boundary, however, it appears that there is a definite growth direction of the lamellae in the matrix, towards the right side of the image. These lamellae also appear to be very thin and difficult to see close to the boundary of these two domains.

From the above discussion, it would appear that the observed α phase crystalline domain at the boundary region between the two largest observed phases is only visible due to the removal of both the 60 °C and 80 °C copolymer fractions, and we see a morphology that is quite different to the case when they were removed individually.

Figure 4.35, sample “Less90C” shows there are two main phase-separated domains: the most crystalline domain in the middle and the darker domain on the outer edge. Very thick lamellae appear to be present, with a thickness in the region of 30 nm. These lamellae are randomly oriented and, due to their thickness, might be β phase crystalline lamellae.

There is no clearly defined boundary between the two domains. This suggests that there is less phase separation present, than observed when either of, or both, the 60 °C and 80 °C fractions are removed. In other words, fractions 60 °C and 80 °C, when present, encourage more homogenous and finer phase

separations, indicating that they have a block copolymer nature, of isotactic PP linked to EPR.

Figure 4.36 (Less110C sample) shows no discernable crystalline order, but it does show some crystalline lamellae to be present. They are not very clear, but appear to be long and thick, some in the region of 10 nm to 20 nm. This is to be expected when more crystalline material such as the (100 °C fraction) is removed.

Figure 4.37 (Less110C sample) shows large phase-separated domains and there appear to be crystalline lamellae present, parallel to one another and a growth direction towards the bottom of the image.

A very interesting observation was also made in sample “Less110C A” (Figure 4.38 (a) and (b)). A type of core-shell particle is clearly visible within the rubber domain of the sample. This was also visible in the “Less80C B” sample, but it was not as clear. It would appear that upon removal of the 110 °C fraction from the polymer (which comprises most of the crystalline material), the ratio of rubbery to crystalline content in the polymer increases to the extent that phase inversion occurs, making these core-shell particles more apparent.

Chen et al.¹² studied these core-shell particles, and revealed their structure to be the following. The core of the particle consists mainly of PE, with some PP crystals also present, and seem to be encapsulated by EPR. They also speculated that the outer shell of the particle is partially made up of PE and PP crystals due to the short PE-PP block copolymers that are present.¹³

In this study it was also observed that these core-shell particles tend to agglomerate together, forming a larger multi core-shell particle, and the diameter of these particles range from 10 nm to 130 nm (see Appendix E, Figure E12).

Large phase-separated domains are visible in Figure 4.39, indicating that very long crystalline lamellae are definitely present, arranged parallel to one another, with a growth direction visible from the top to the bottom of the image, and the darker domains appear to be parallel to this crystalline domain.

The contrast of the image is however not as good as the other sample images. A possible reason could be that upon removal of the 120 °C fraction, there is some reduction in crystalline perfection, causing the crystalline domains to become stained to a larger extent than normal, and hence the contrast difference between the crystalline and amorphous domains becomes less defined. This is in good agreement with the DSC results (Section 4.3.3) that showed a broad melt peak, with a bimodal shape, indicating various amounts of different crystalline domains, and less perfect than that of the reference sample.

4.3.9 FOURIER TRANSFORM INFRARED SPECTROSCOPY

The results of the PAS FTIR analyses are given in Tables 4.9 and 4.10 and Figures 4.40 and 4.41.

Table 4.9: PAS-FTIR peak ratios of PP, series A, relative to the PP content

Sample ID	Ratios (PP)	
	Crystalline iPP to total ^a	Amorphous/crystalline ^b
E-REF A	0.50	1.02
Less80C A	0.57	0.97
Less90C A	0.93	0.96
Less100C A	0.94	1.00
Less110C A	0.58	1.00
Less110C A	0.62	1.02
Less120C A	0.75	0.99
Less120C A	0.72	0.97

a: Calculated from absorption at 998 and 2920 cm⁻¹

b: Calculated from absorption at 972 and 998 cm⁻¹

Table 4.10: PAS-FTIR peak ratios of PP, series B, relative to the PP content

Sample ID	Ratios (PP)	
	Crystalline iPP to total ^a	Amorphous/crystalline ^b
E-REF B	0.52	0.98
Less25C B	0.59	0.78
Less60C B	0.35	0.89
Less80C B	0.58	0.98
Less60&80C B	0.44	0.91

a: Calculated from absorption at 998 and 2920 cm^{-1}

b: Calculated from absorption at 972 and 998 cm^{-1}

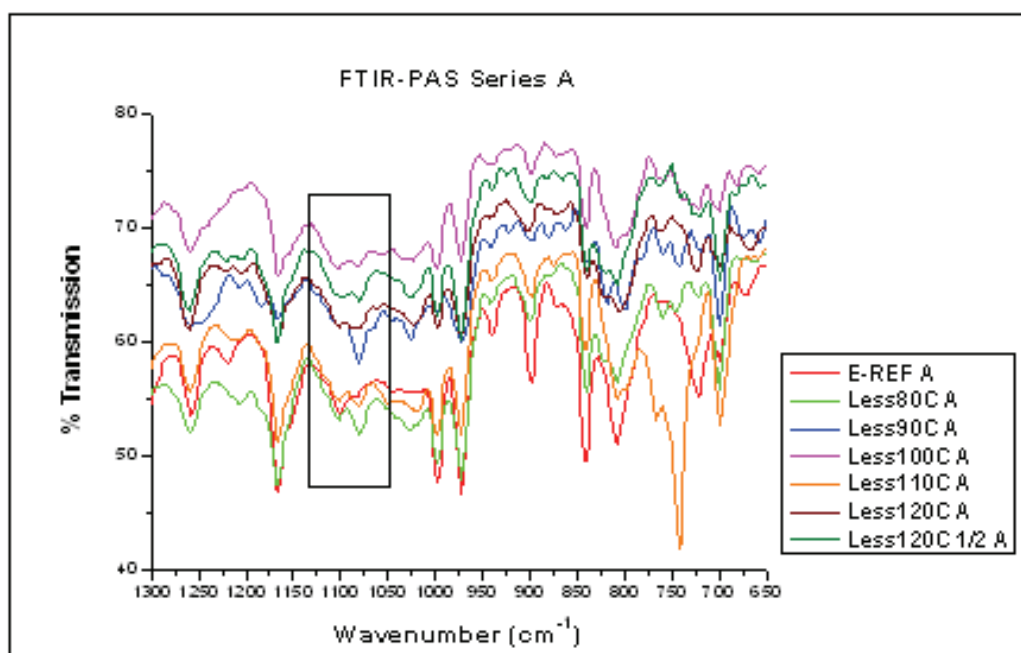


Figure 4.40: PAS-FTIR spectrum for sample series A (block indicates the 1100 cm^{-1} range).

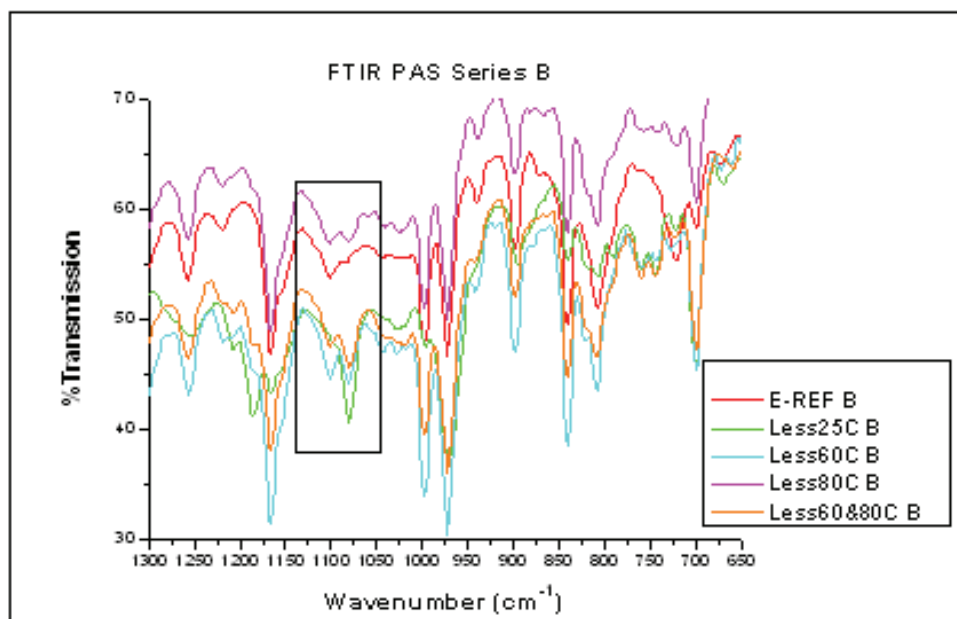


Figure 4.41: PAS-FTIR spectrum for sample series B (block indicates the 1100 cm⁻¹ range).

According to Hongjun et al.¹³ the vibrational frequencies of the infrared spectrum of PP copolymers are as follows. The peak visible at 2920 cm⁻¹ is due to the vibrational frequency of the C-H group. The peaks visible at 840 cm⁻¹ and 998 cm⁻¹ are due to PP crystalline material, with an amorphous PP peak at 972 cm⁻¹, while the peak due to amorphous PE is at 700 cm⁻¹ and crystalline PE at 722 cm⁻¹.

It was decided to determine relative infrared vibrational frequency ratios of PP material within each sample, as a quick and simple method to determine what happens to the polymer sample with regards to the content of amorphous material. To this end the areas under the relevant peaks were calculated from each spectrum. These results are presented in Tables 4.9 and 4.10.

The results show that as soon as the fractions at 25 °C, 80 °C, 90 °C and 100 °C are removed from the polymer material the relative amount of PP crystalline material to that of the whole polymer increases. This is expected, as these fractions are typically less crystalline than the 110 °C and 120 °C fractions.

Upon looking at the ratios of crystalline PP material present in the Less60C B sample, however, the apparent decrease in crystalline PP content compared to

the whole sample is difficult to explain. It appears as if the use of FTIR to quantify composition of the samples is not clear-cut.

Similarly, when we compare the ratio of crystalline to amorphous material present within each sample, the values appear to be fairly similar throughout, although there are some variations. The only real change we see is when the 25 °C fraction is removed, and to a lesser extent the 60 °C fraction.

The appearance of two bands in the 1100 cm^{-1} region of the IR spectra is really interesting. These bands (at 1100 cm^{-1} and 1080 cm^{-1}) change in intensity as the composition of recombined material changes.

According to Geng et al.¹⁴ it would appear that these bands (or band) is due to the hexagonal crystal form of the PP in the polymer, and is greatly influenced by the conformational environment of the polymer chains, with the intensity of bands in this region increasing with increased crystallinity. The band at 1100 cm^{-1} is reported to be due to the presence of 6 or more propylene units in a chain helix, but less than 12 units. When more than 12 units are in the helix, the band appears at 998 cm^{-1} .

We do, however, observe not one band here, but two bands which, revealed the following: All the samples show two IR adsorption bands, one more intense than the other. The exceptions were the “E-REF” sample, which showed only the one band at 1100 cm^{-1} , and the “Less25C B” sample, which showed only one band at 1080 cm^{-1} .

From this it was concluded that, since the TEM and SEM results showed no discernable phase separation for the E-REF samples A and B and Less25C B, but did show phase separation for the other samples, the presence of two bands in this 1100 cm^{-1} IR band region is due to phase separation in the polymer.

Another observation made is that the intensity of the bands in the “Less25C B” sample is a lot higher than the intensity of the reference sample’s bands. This could imply that increased intensity of these bands could be linked to increased crystallinity, since the DSC results showed an increase in crystallinity for the “Less25C B” sample compared to the “E-REF A & B” samples.

The “Less60C B” sample also showed a higher intensity for both the bands in the IR spectrum, and similarly had a higher crystallinity than the “E-REF” samples. The reverse is true, however, for some of the other samples such as the “Less80C B”, where more intense bands than recorded for the reference sample, corresponding with a slightly lower overall crystallinity.

As these bands are apparently due to the presence of short helical PP segments,^{15,16} the question arises as to why there are two bands, and why the relative intensities of these two bands change when different fractions of the material are removed. Time-resolved FTIR studies on PP has revealed that the band at 841 cm^{-1} , which is due to at least 12 or more propylene units in a helical chain, is still present when the polymer is molten.¹² This indicates that some form of order may still exist in the amorphous state. It can be postulated that the presence of these two bands is due to short PP helices in different environments. These environments might be crystalline and amorphous, or crystalline and ordered amorphous or even different crystalline environments.

The fact that these bands are only present in these samples that show, by TEM observation, significant phase separation could mean that these bands could be used to indicate phase separation, or even batch-to-batch variations in commercially produced materials.

One final observation made from the appearance of two bands in this region, when comparing samples “Less60C B” and “Less80C B”. The “Less60C B” sample shows that these two bands in the 1100 cm^{-1} IR region almost have the same intensity and shape, while for the “Less80C B” sample these bands have different intensities, the band at 1100 cm^{-1} showing a higher intensity. TEM and SEM results showed that these two samples exhibit phase separation, and the observed phase separation for the “Less60C B” sample is larger than for the “Less80C B” sample. This would indicate that the closer these bands appear in terms of relative intensities to one another in the same sample, the larger the phase separation that is present. This is supported by the FTIR, SEM and TEM results for the “Less60C B” and “Less120C B”, samples showing these two bands to be more or less the same in their intensities.

Further more, SEM and TEM analyses revealed larger phase separation, larger for these two samples than the others.

It must be remembered here that these samples were all subjected to isothermal crystallization before analyses.

4.3.10 WIDE ANGLE X-RAY DIFFRACTION SPECTROSCOPY

TEM results indicated that there might be a variety of crystalline modifications present within the samples, specifically the recombined samples from which the copolymer fractions were removed (Less60C, Less80C and Less90C). TEM also revealed large phase separated domains present within these samples. These results, led to the decision to carry out wide angle X-ray diffraction (WAXD) analyses on the samples, to further investigate the crystalline phases present.

WAXD is a well-developed technique, relatively little sample preparation is needed and the analysis time is very short. Good spectra can be obtained in a matter of minutes. WAXD would reveal if there are α , β , or γ isotactic PP crystalline phases present within each sample.

The WAXD results are shown in Figure 4.42:

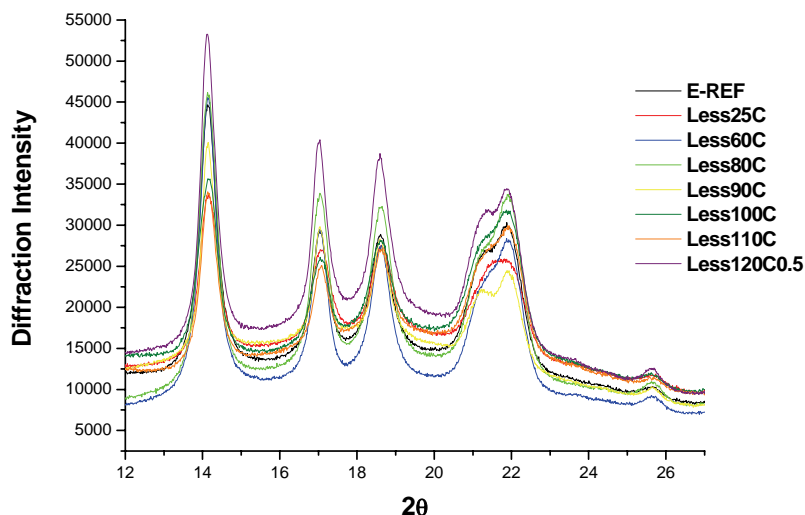


Figure 4.42: WAXD spectra of sample series A and B.

There are no diffraction peaks due to β or γ phase present in any of the samples. Only the crystalline modifications of the monoclinic α phase at 2θ values of 14° (110), 16.8° (040), 18.6° (130), 21.9° (131/ 041) and 25.6° (061) are present, which is in good agreement with the literature.^{16, 17}

As the spectra were obtained using different sample masses, it was not possible to obtain quantitative information from the spectra in order to compare the different recombined samples. It was possible, however, to investigate relative differences in the samples based on the distribution of the peaks.

It was decided to use the diffraction peak of the (131/041) crystal modifications at 21.9° to determine a relative difference between the samples, since these peaks appear to show some bimodal character that changes depending on the sample observed, specifically the recombined samples (Less60C, Less80C and Less90C).

This diffraction peak at 21.9° for each sample was smoothed, normalized and deconvoluted into two representative peaks, of which the average R^2 values across the samples was 0.999. This means that the deconvoluted peaks are a very good representation of the original peak.

The next step involved calculating representative areas of each of the deconvoluted peaks, and determining a ratio for each sample between the area of peak 1 and peak 2 (see Figure 4.43) in order to compare these ratios between the samples so that a relative difference among them may be observed.

An example of the deconvolution is shown in Figure 4.43. The other, similar figures are given in the appendix.

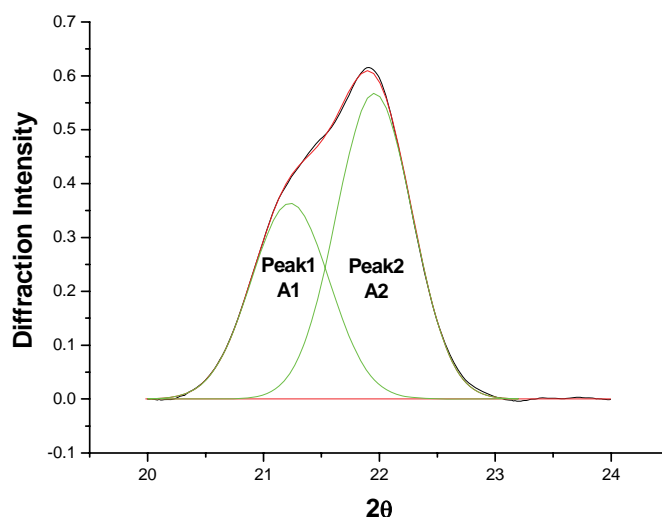


Figure 4.43: WAXD spectrum of the “Less60C” sample: deconvolution of the diffraction peak at 21.9 °.

Table 4.11 shows the calculated ratios for each sample.

Table 4.11: Area ratios of the deconvoluted WAXD peaks at 21.9 °

Sample ID	A1	A2	Ratio A1/A2
E-REF	0.31	0.40	0.76
Less25C	0.25	0.32	0.80
Less60C	0.31	0.47	0.66
Less80C	0.27	0.49	0.55
Less90C	0.22	0.31	0.69
Less100C	0.25	0.40	0.64
Less110C	0.28	0.35	0.80
Less120C ¹ / ₂	0.27	0.38	0.70

These results showed significant differences in the ratios between the samples, specifically the (Less60C, Less80C and Less90C) samples. This was to be expected, since these recombined samples exclude the copolymer fractions. Other analytical techniques also gave results that indicate that removal of the copolymer fractions have a significant effect.

It is unclear from the literature as to what exactly can cause the bimodal effect observed for 21.9° diffraction peak, i.e. the crystal modifications (131/041). FTIR analysis done on these samples revealed the presence of small crystallizable chain sequences of 6 to 12 propylene units present in those recombined samples where the copolymer fractions were removed. It is possible therefore, that the presence of these sequences has an effect on the extent of the crystalline modifications (131/041). In addition, the absence of the copolymer fractions could, by the way the copolymer influences the amorphous/crystalline phase separation, also influence the crystalline modification under discussion. Both TEM and WAXD analyses of the annealed samples offer strong evidence that the modification of the crystalline morphology is caused by the absence of certain partially crystalline fractions.

4.4 SUMMARY

Overall, it was found that removing fractions and recombining material led to significant changes in morphology (as observed by SEM and TEM), thermal properties (DSC) and crystallinity (WAXD). The IPPC materials are designed to be impact resistant materials that retain their temperature resistance and strength properties of the parent iPP, so removal of the EPR phase and the highly crystalline phase of the polymer are academically interesting, but of little practical significance. It is therefore the effect of the removal of the copolymer fractions (constitutes 30% of the overall polymer material) that is of the most interest from a practical standpoint. It is quite clear that the effect of removing those fractions that were isolated by TREF at 60 °C, 80 °C and 90 °C could have practical implications. These copolymer fractions clearly influence the phase-separation behaviour of the material significantly. If we look at the microhardness measurements we see that removal of the 60 °C and 80 °C fractions lead to hardness values that are slightly higher or comparable with the reference material (refer to Figure 4.14). Removing the 90 °C fraction appears to lower the hardness with respect to the reference material (Figure 4.13). If we look at the DMA data we see that removing these fractions shifts the $\tan \delta$ maximum to a lower temperature and broadens the transition (Figure 4.18). This relates to a better impact strength at room temperature. It therefore appears that we could improve the hardness/impact

balance of this particular copolymer by subtle alterations to those molecular species present in the copolymer that elute in the 60 °C to 80 °C range during TREF separation.

Results of TEM studies on the isothermally crystallized samples were quite revealing. A staining regimen was developed that allowed us to see distinct phase differences on the samples analyzed. Removal of the copolymer fractions could be seen to have significant effects on the morphology of the samples, and clear phase boundaries could be seen in the absence of these fractions.

Results of FTIR studies were in conclusive, regarding the ability to clearly and easily see changes in the morphology (and therefore properties) reflected in changes to the absorption bands normally associated with amorphous and crystalline ethylene and propylene sequences, although changes in crystallinity could be observed. The appearance of bands at 1100 and 1080 cm^{-1} was interesting, particularly as there were two bands in the samples that showed (by TEM analysis) clear phase separation. These bands could be significant in detecting differences in phase separation of different batches of the same polymer. (It must be borne in mind, however, that these bands were only visible in samples that had undergone isothermal crystallization.)

WAXD revealed no evidence of any crystalline form other than the α phase to be present, but the WAXD data did suggest that there is a correlation between the bimodal nature of the 2θ peak at 21.9 ° and the double peak observed in FTIR spectra at 1100-1080 cm^{-1} .

4.5 REFERENCES

1. Tan, H., Li, L., Chen, Z., Song, Y., Zheng, Q., *Polymer*, 46, 2005, p 3522.
2. Grant, D. M., Paul, E. G., *Journal of American Chemical Society*, 86, 1964, p 2984.
3. Pretorius, M.S., *Characterization of molecular properties of propylene impact copolymers*, MSc thesis, University of Stellenbosch, Stellenbosch, 2007.

4. Paul, E. G., Grant, D. M., *Journal of the American Chemical Society*, 85, 1963, p 1701.
5. Joubert, D., Sasol Polymers, private communication.
6. Chen, J. H., Zhong, J. C., Cai, Y. H.; Su, W. B., Yang, Y. B., *Polymer*, 48, 2007, p 2946.
7. Busico, V., Cipullo, R., Monaco G., Vacatello M., *Macromolecules*, 30, 1997, p 6251.
8. Shebani, A. N., The correlation of the molecular structure of polyolefins with environmental stress cracking resistance, MSc thesis, University of Stellenbosch, Stellenbosch, 2006.
9. Li, J. X., Cheung, W. L., *Journal of Applied Polymer Science*, 72, 1999, p 1529.
10. Tortella, N., Beatty, C. L., *Polymer Engineering and Science*, 2008, p 1476.
11. Chen, Y., Chen, Y., Chen, W., Yang, D., *European Polymer Journal*, 43, 2007, p 2999.
12. Chen, Y., Chen, Y., Chen, W., Yang, D., *Journal of Applied Polymer Science*, 108, 2008, p 2379.
13. Hongjun, C., Xiaolie, L., Xiangxu, C., Dezhu, M., Jianmin, W., Hongsheng, T., *Journal of Applied Polymer Science*, 71, 1999, p 103.
14. Geng, Y., Wang, G., Cong, Y., Bai, L., Li, L., Yang, C., *Macromolecules*, 42, 2009, p 4751.
15. Nielsen, J. R., Hathaway, C. E., *Journal of Molecular Spectroscopy*, 10, 1963, p 366.
16. Nishino, T., Matsumoto, T., Nakamae, K., *Polymer Engineering and Science*, 40, 2000, p 336.
17. Shangguan, Y., Zhao, L., Tao, L., Zheng, Q., *Journal of Polymer Science: Part B: Polymer Physics*, 45, 2007, p 1704.

CHAPTER 5 CONCLUSIONS AND RECOMMENDATIONS FOR FUTURE WORK

5.1 CONCLUSIONS

The impact copolymer (CMR 648, Sasol Polymers) selected for this study was successfully fractionated according to crystallizability. Selected fractions were removed, and the remainder of the material recombined. Fractions and recombined materials were fully characterized and the properties of the recombined material studied.

TREF analysis showed that the soluble, amorphous fraction of polymer comprised 20% of the overall content of the polymer. Roughly 30% of the polymer consists of partially crystalline copolymer, while the remaining 50% is more crystalline isotactic polypropylene.

Salient facts about the fractions

- The fractions that had the most significant effect on phase separation and resultant properties such as hardness and impact resistance (in practical terms) were those that were eluted at 60 °C, 80 °C and 90 °C during the TREF fractionation.
- The ethylene content of these fractions (determined by ¹³C NMR) was 30.4, 35.2 and 2.8 mole % respectively.
- All three of these fractions had quite wide molecular weight distributions.
- The 60 °C and 80 °C fractions had limited crystallinity, and it is proposed that they are made up of ethylene-rich and propylene-rich copolymer sequences.
- The 90°C fraction exhibited the highest molecular weight and polydispersity of the fractions, and had the highest crystallinity.

Salient facts about the recombined materials

- There were significant changes in the properties of the recombined materials Less60C, Less80C and Less90C, compared to the reference sample (E-REF).
- The overall crystallinity of these samples increased from the E-REF sample to the Less60C sample, but was significantly decreased for the Less80C and Less90C samples.
- Microhardness determination showed that the Less60C and Less80C samples had hardness values greater than or equal to that of the E-REF sample. The Less90C sample had a hardness value that was significantly lower than that of the reference material.
- DMA analysis showed a single, narrow T_g region for the E-REF sample, but upon removal of the 60 °C fraction of material, sample Less60C as well as the other recombined samples, indicated the appearance of a series of broad, multiple T_g regions, which indicated the presence of increased chain mobility and large scale phase separation.
- Removal of the 60 °C and 80 °C fractions shifts the $\tan \delta$ (T_g) maximum (determined by DMA) to a lower temperature and broadened the transition. This can be related to a better impact strength at room temperature. It would therefore appear that the hardness/impact balance of this particular polymer could be improved by subtle alterations to those molecular species present in the copolymer, eluting at 60 °C to 80 °C during fractionation by TREF.
- SEM analysis revealed large differences in the surface morphology of the recombined samples. A crevice-like morphology was seen for all the recombined samples. The presence of rubber-like particle morphology on the surface of these samples was also seen, but it was less pronounced for the Less60C and Less80C samples. Core-shell particle morphology was also visible on the surface of these recombined samples, specifically for the Less60C, Less80C and Less90C samples.

- A useful TEM technique was developed and used to show clear morphological differences between the recombined samples. Clear phase separation between the amorphous and crystalline domains could be seen, specifically for the Less60C, Less80C and Less90C samples. The Less110C sample also revealed interesting core-shell particle morphology. A difference in crystalline phases, specifically the crystalline structure and growth direction, was also seen for these samples.
- FTIR analysis of the isothermally crystallized, recombined samples, revealed specific bands in the 1100 – 1080 cm⁻¹ range. These bands varied in intensity from sample to sample and appear to be related to the extent of the phase separation present.

5.2 RECOMMENDATIONS FOR FUTURE WORK

The study could be expanded to incorporate other impact copolymers. The findings regarding the FTIR analyses should be further investigated. In addition, fine-tuning the removal or addition of the copolymer fractions will add to the model that we are busy establishing with regard to the relationship between chemical composition distribution, morphology and properties.

The study should be scaled up to the extent where enough material can be obtained to prepare samples for impact tests on the recombined materials. This will allow us to test our hypothesis regarding the hardness/impact balance of these materials.

APPENDIX A: ^{13}C Nuclear magnetic resonance spectra of the removed fractions at various temperatures of the IPPC (CMR 648)

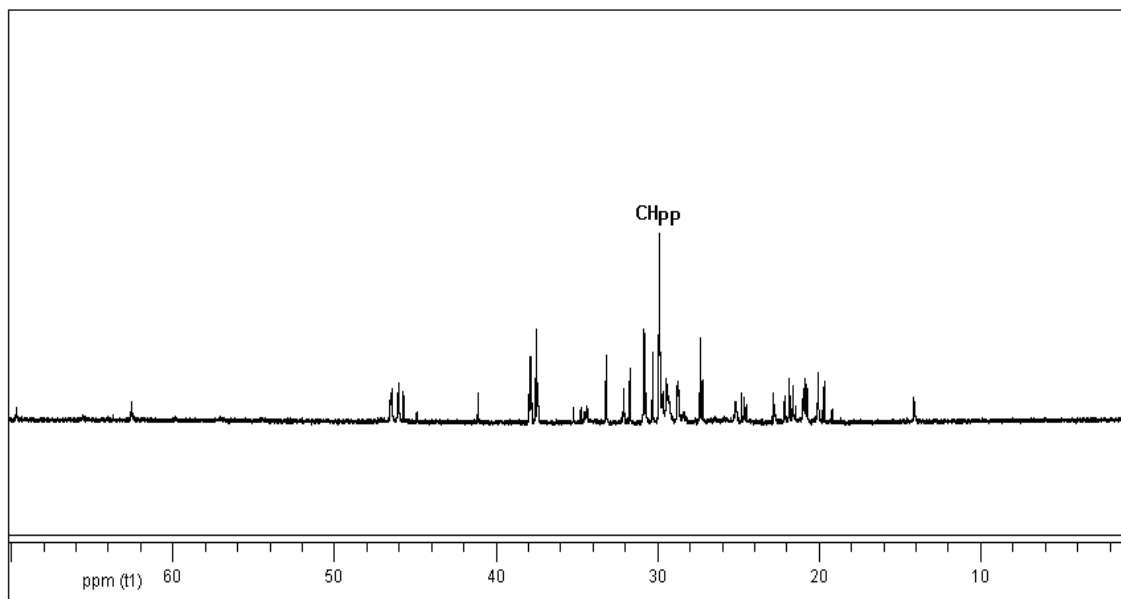


Figure A1: ^{13}C NMR spectrum of the removed fraction at 25 °C.

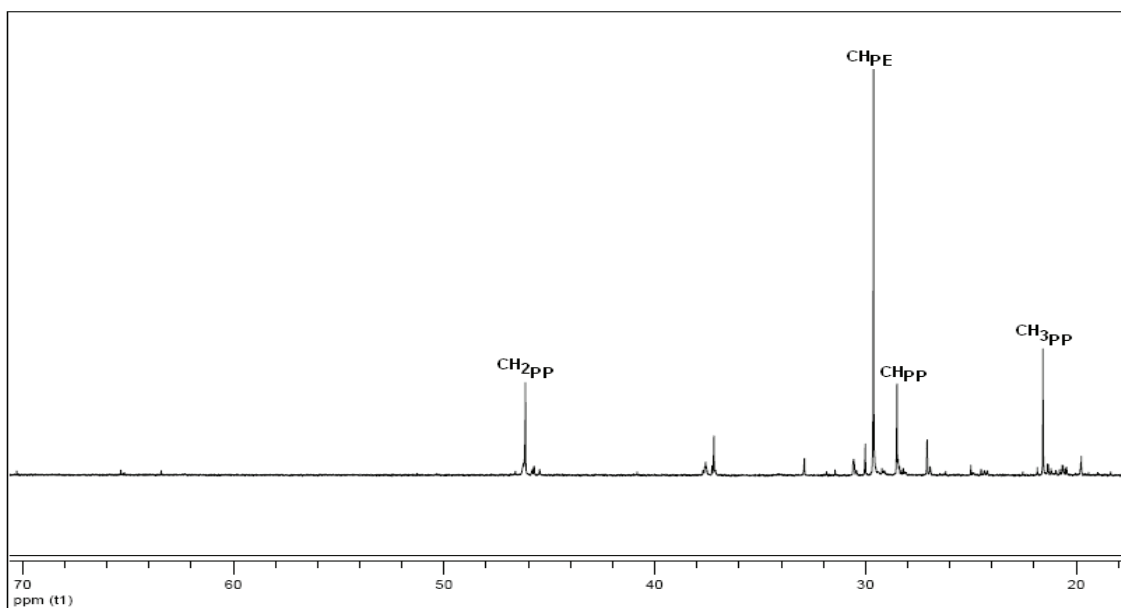


Figure A2: ^{13}C NMR spectrum of the removed fraction at 80 °C.

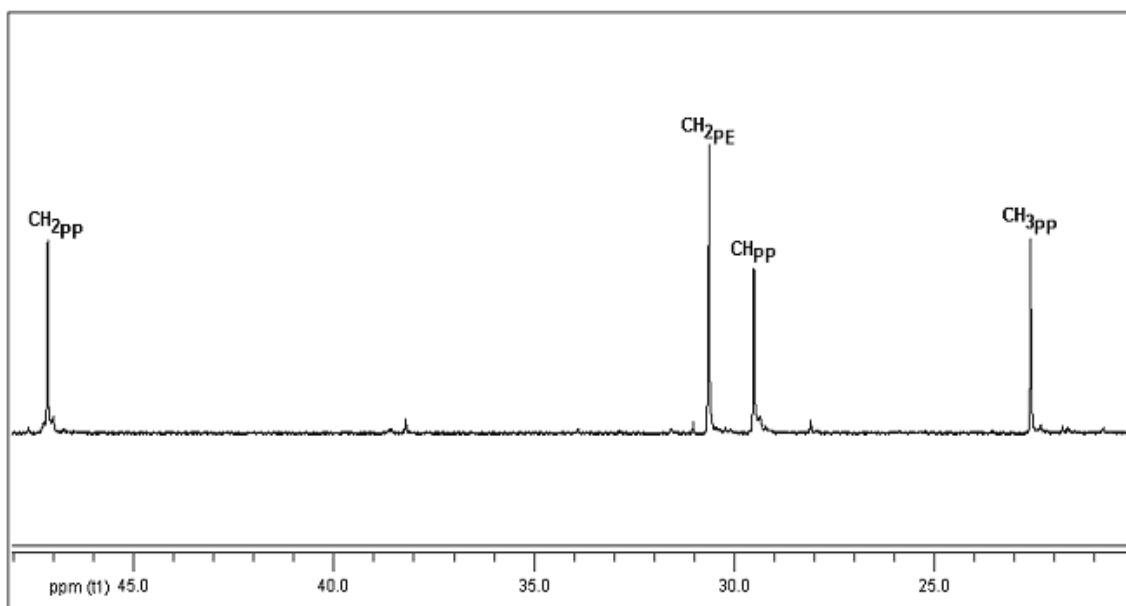


Figure A3: ^{13}C NMR spectrum of the removed fraction at 90 °C.

APPENDIX B: Differential scanning caloriometry thermograms of the recombined samples of the IPPC (CMR 648)

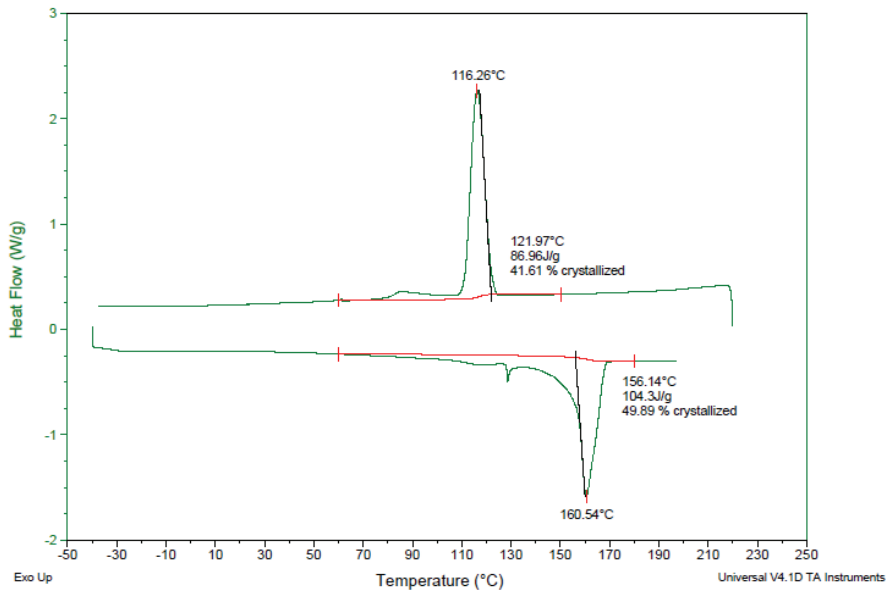


Figure B1: DSC thermograms of sample "E-REF A".

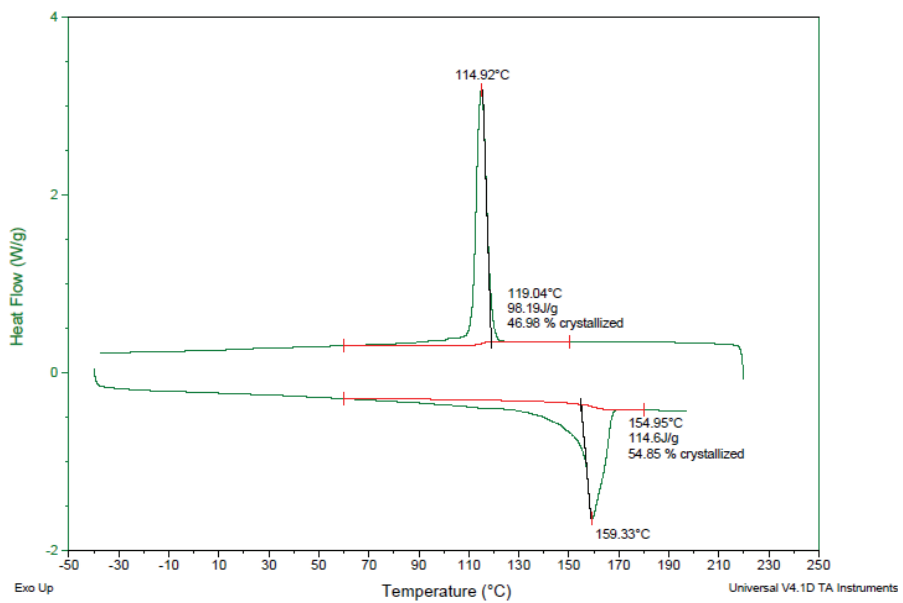


Figure B2: DSC thermograms of sample "Less25C".

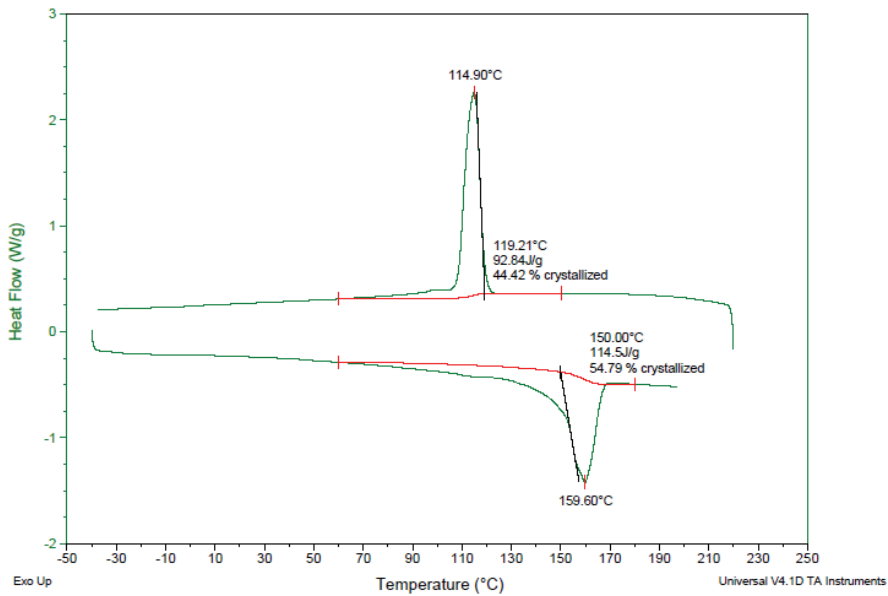


Figure B3: DSC thermograms of sample "Less60C B".

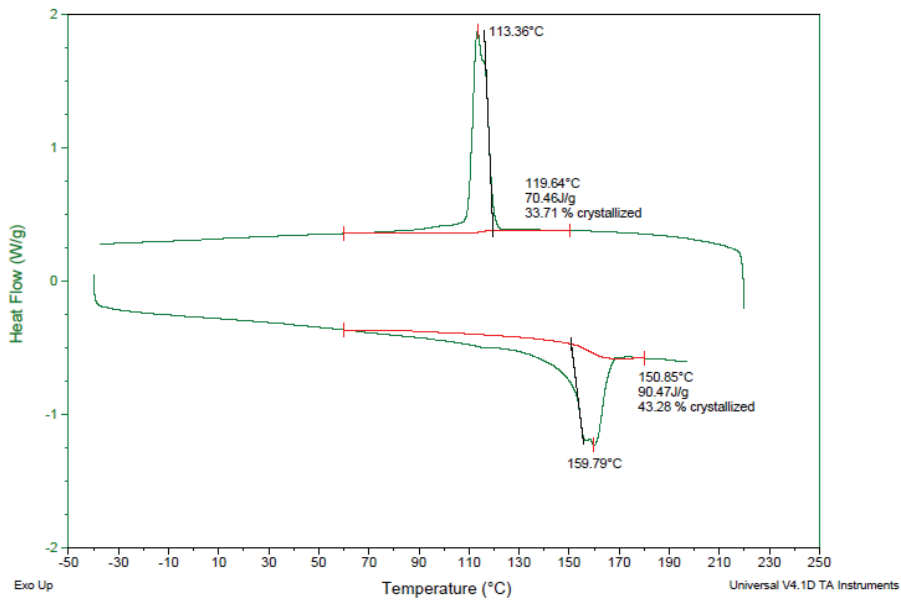


Figure B4: DSC thermograms of sample "Less80C A".

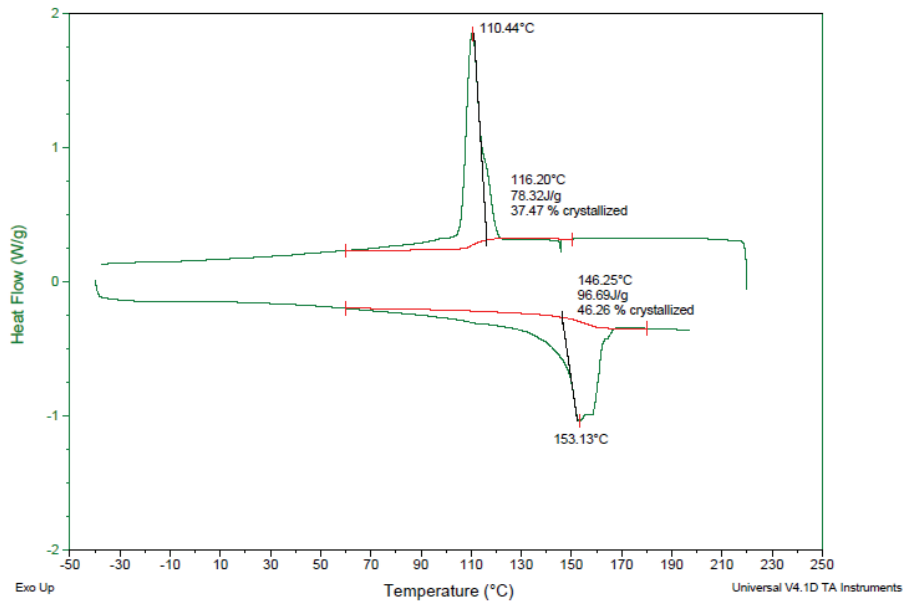


Figure B5: DSC thermograms of sample "Less80C B".

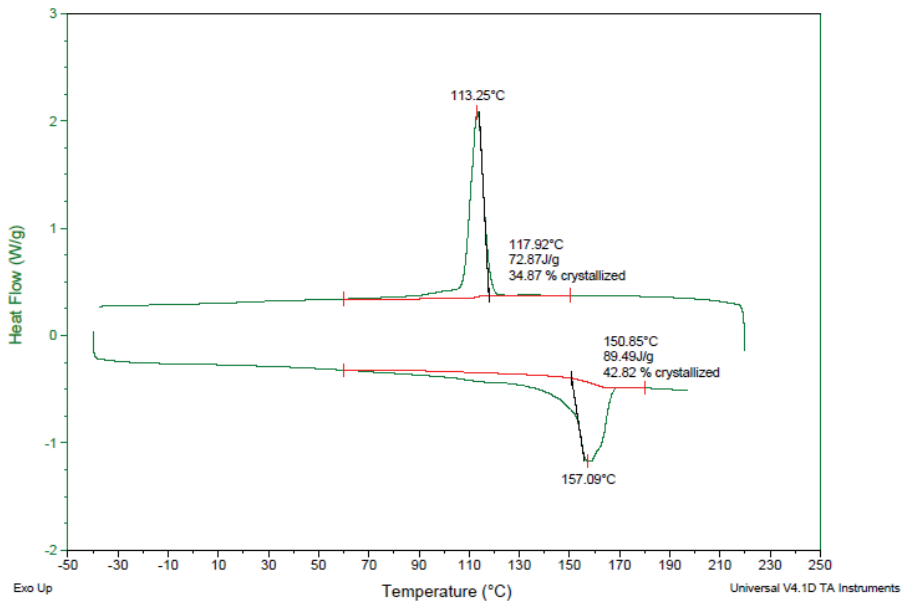


Figure B6: DSC thermograms of sample "Less60&80C B".

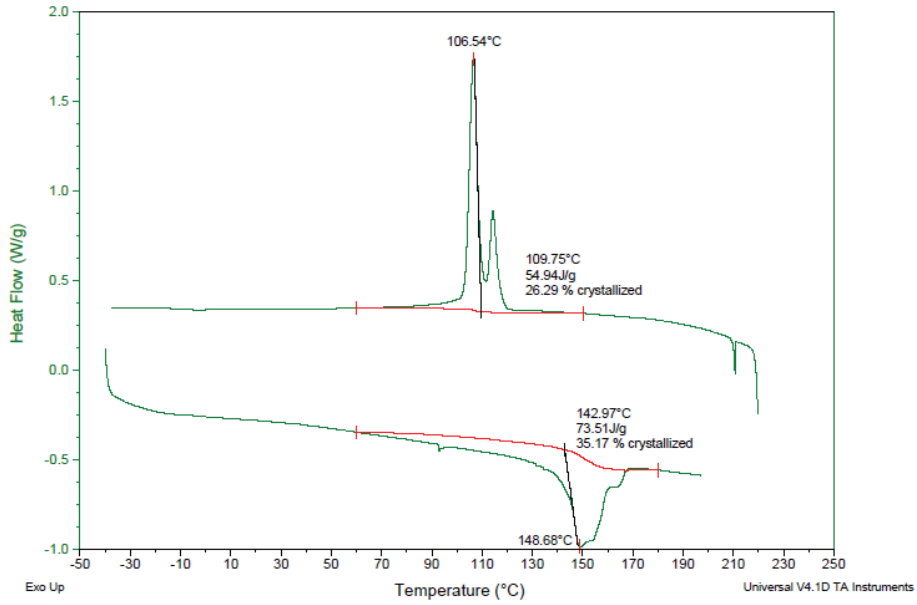


Figure B7: DSC thermograms of sample "Less90C A".

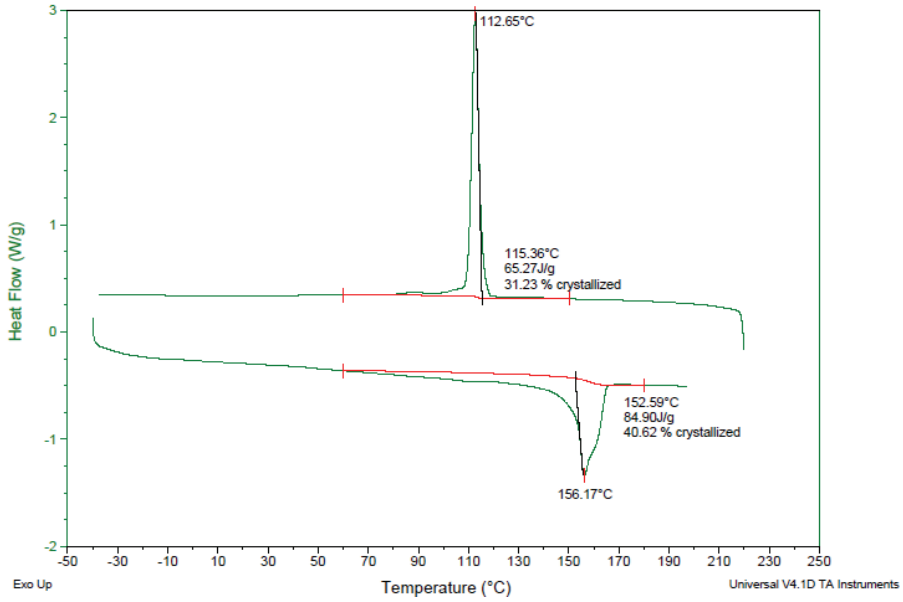


Figure B8: DSC thermograms of sample "Less100C A".

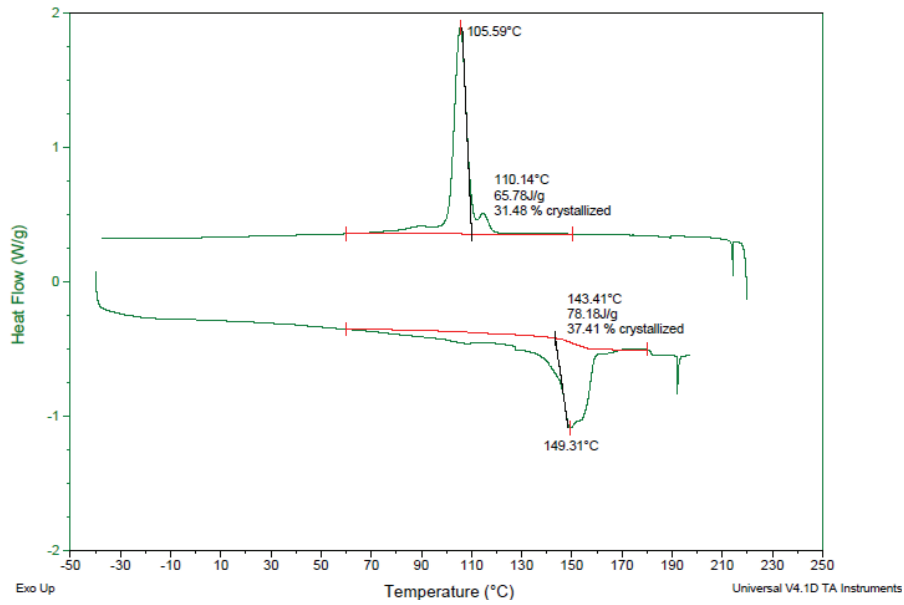


Figure B9: DSC thermograms of sample "Less110C A".

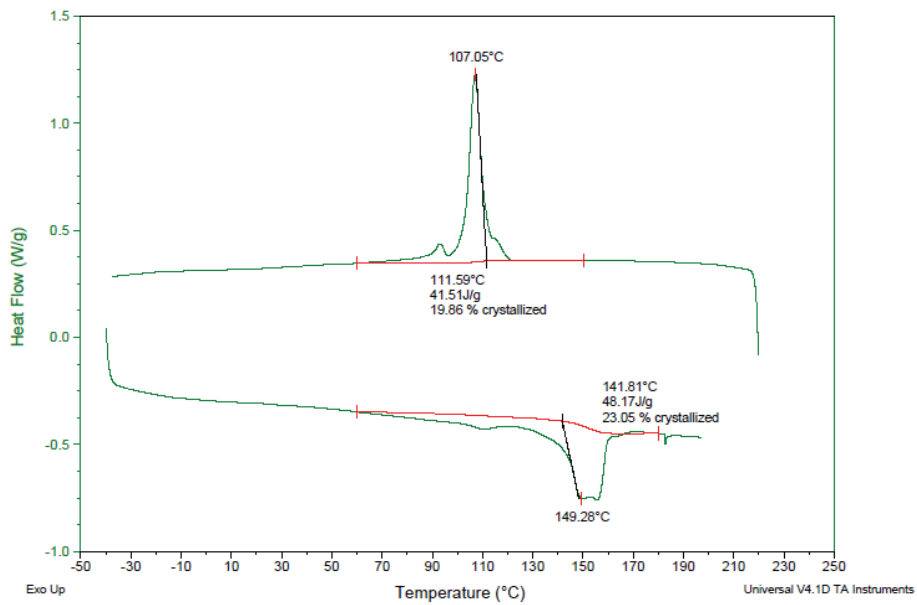


Figure B10: DSC thermograms of sample "Less120C A".

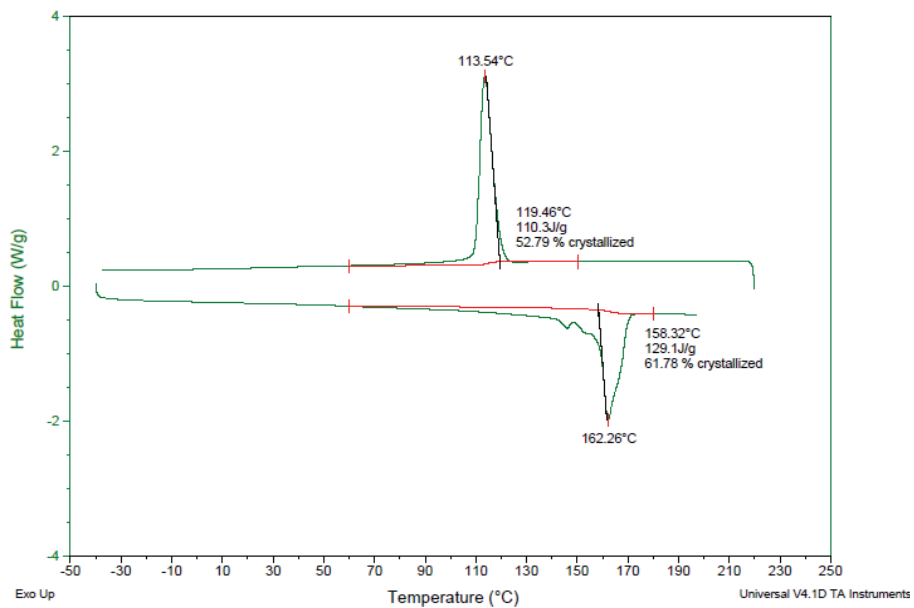


Figure B11: DSC thermograms of sample “Less120C ½ A”, 50% by weight of the 120 °C fraction has been removed before recombination of the sample.

APPENDIX C: Differential scanning caloriometry thermograms of the removed fractions at various temperatures of the IPPC (CMR 648)

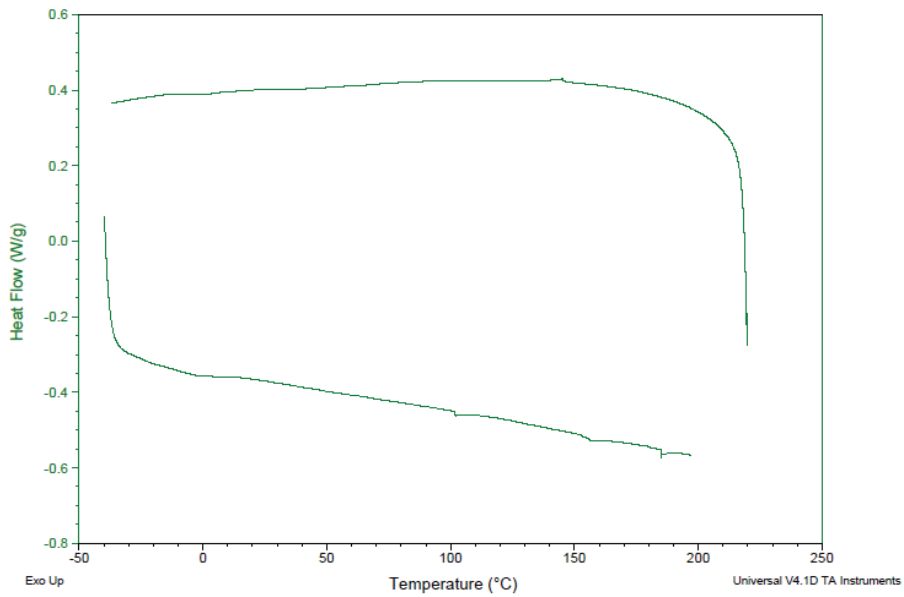


Figure C1: DSC thermograms of the removed fraction at 25 °C.

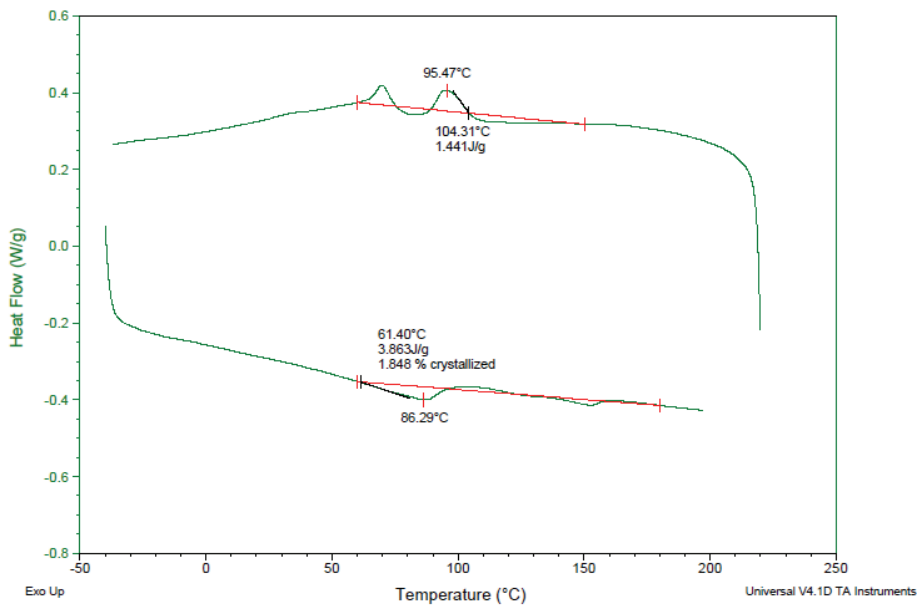


Figure C2: DSC thermograms of the removed fraction at 60 °C.

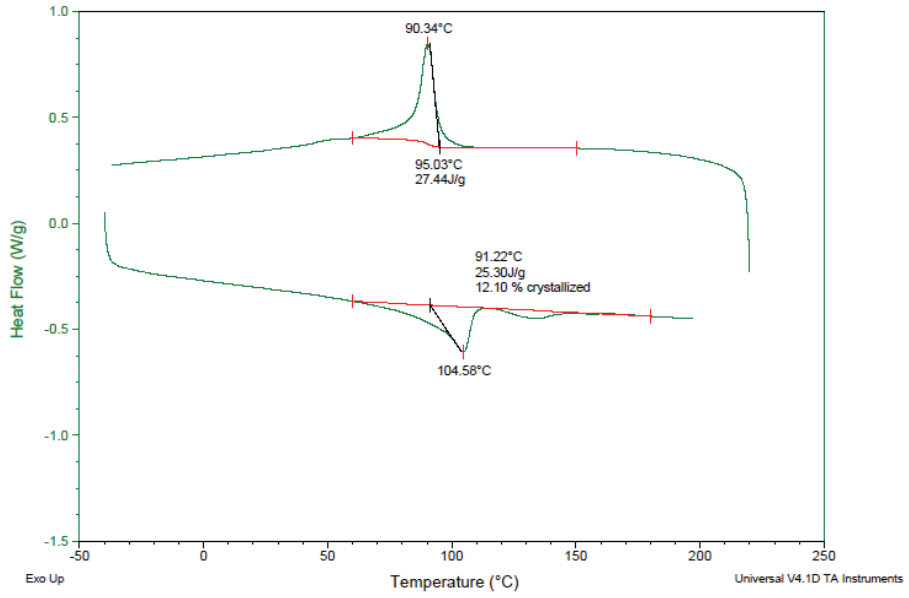


Figure C3: DSC thermograms of the removed fraction at 80 °C.

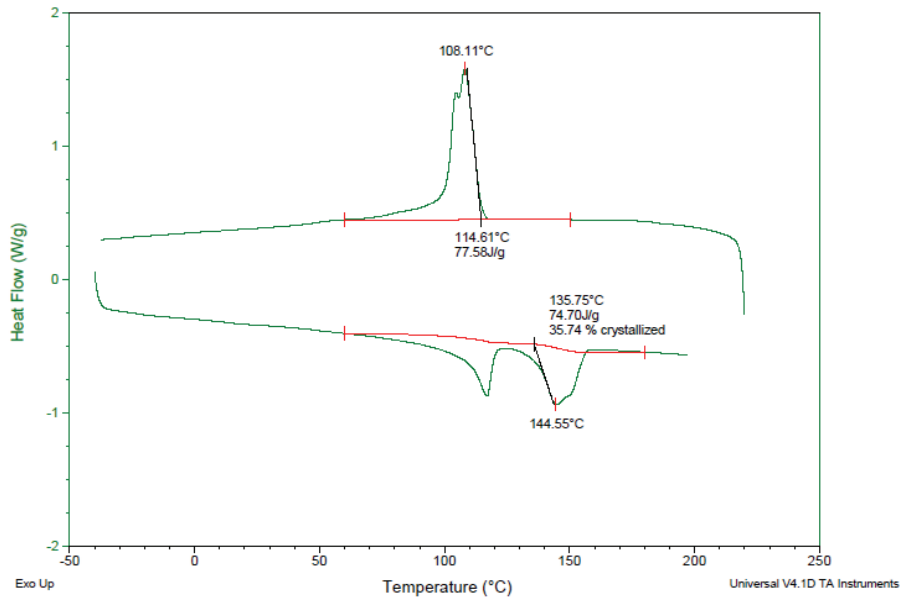


Figure C4: DSC thermograms of the removed fraction at 90 °C.

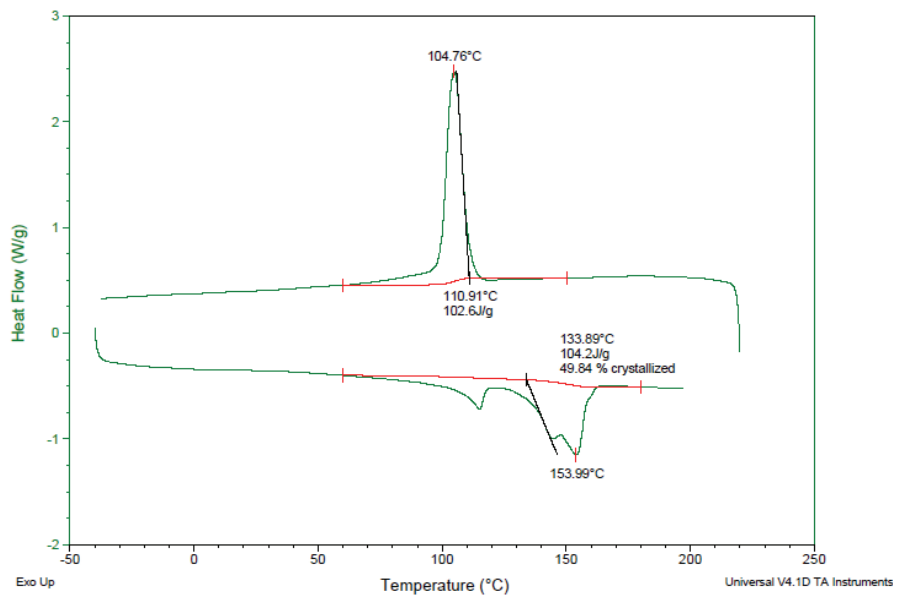


Figure C5: DSC thermograms of the removed fraction at 100 °C.

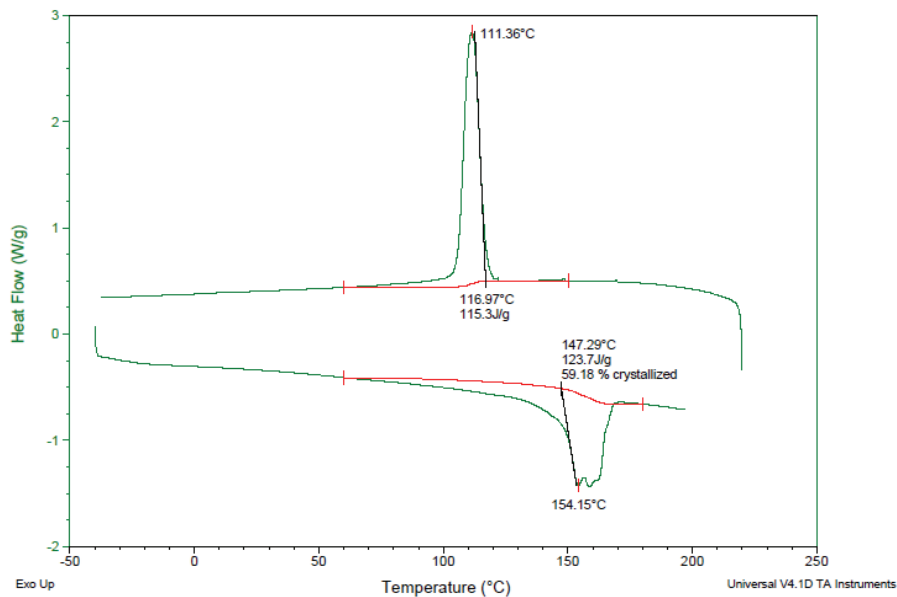


Figure C6: DSC thermograms of the removed fraction at 110 °C.

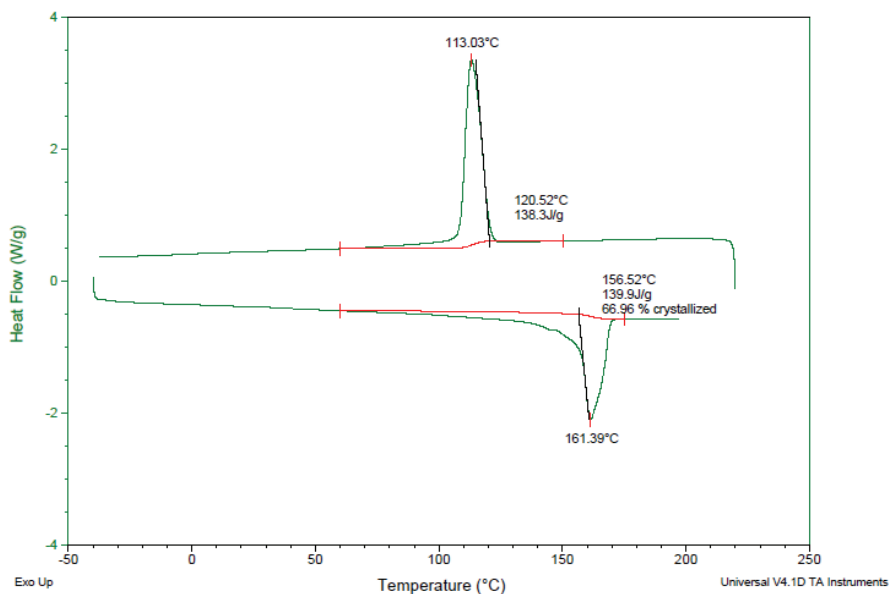


Figure C7: DSC thermograms of the removed fraction at 120 °C.

Fraction Sample ID	Crystallization peak temperature (°C)	Melting peak temperature (°C)	Crystallinity (%)
25C	-	-	-
60C	95.47	86.29	1.85
80C	90.34	104.58	12.10
90C	108.11	144.55	35.74
100C	104.76	153.99	49.84
110C	111.36	154.15	59.18
120C	113.03	161.39	66.96

Table C1: DSC results of the removed fractions at the various temperatures.

APPENDIX D

Dynamic mechanical analysis graphs of the recombined samples of the IPPC (CMR 648)

TAN DELTA

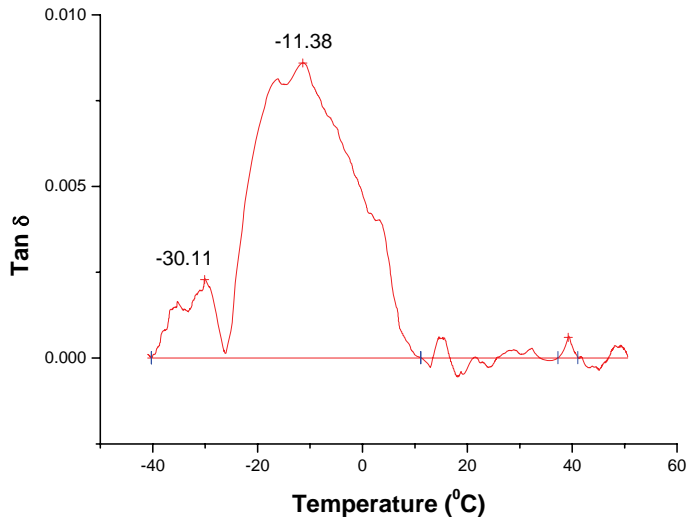


Figure D1: Dynamic mechanical analysis, $\tan \delta$, sample "Less60C B".

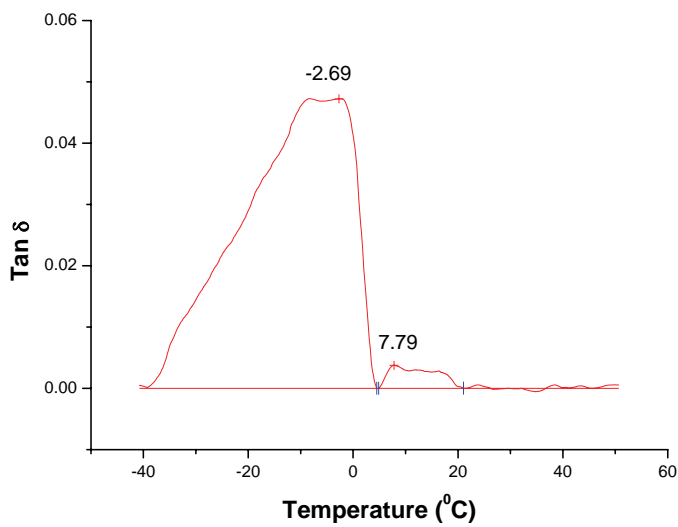


Figure D2: Dynamic mechanical analysis, $\tan \delta$, sample "Less80C B".

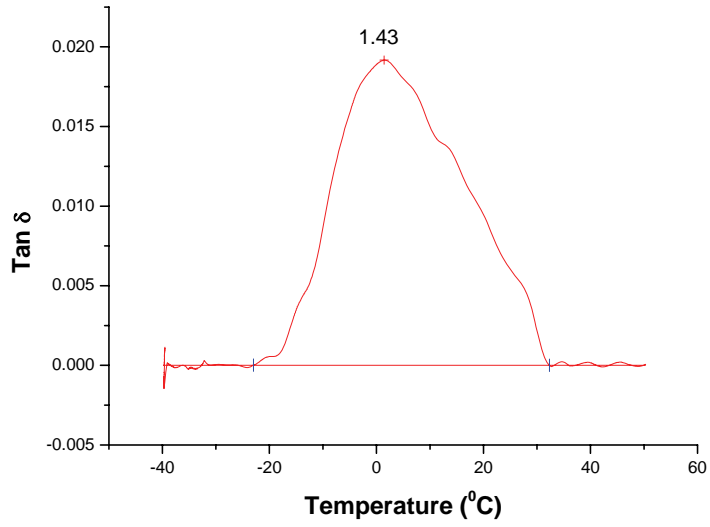


Figure D3: Dynamic mechanical analysis, tan δ , sample "Less90C A".

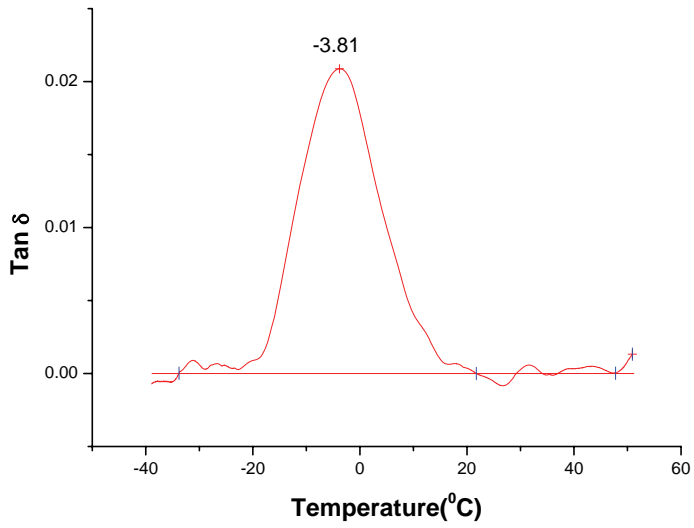


Figure D4: Dynamic mechanical analysis, tan δ , sample "Less100C A".

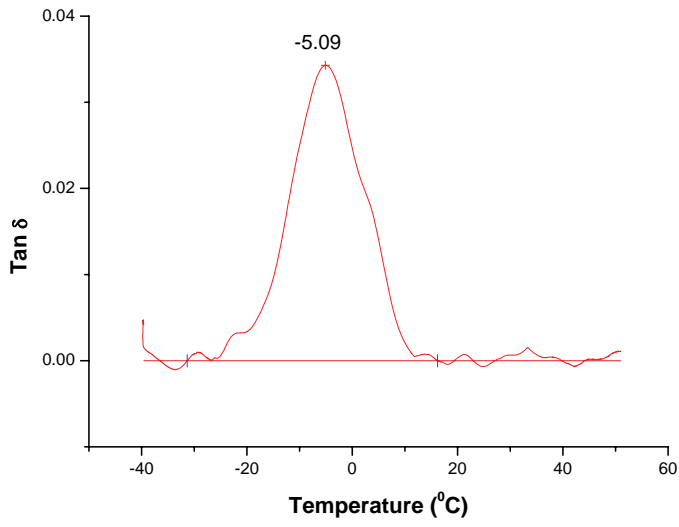


Figure D5: Dynamic mechanical analysis, tan δ , sample "Less110C A".

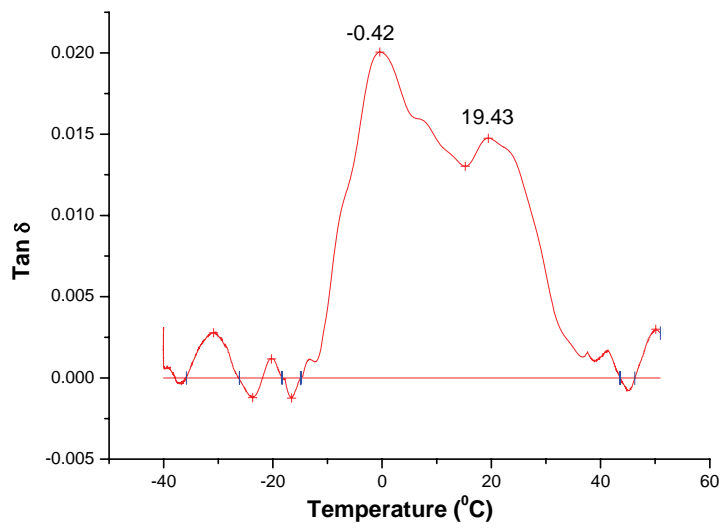


Figure D6: Dynamic mechanical analysis, tan δ , sample "Less120C A".

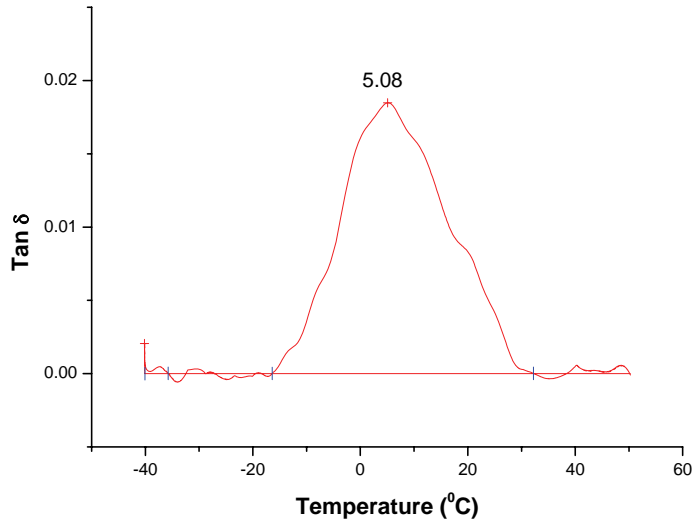


Figure D7: Dynamic mechanical analysis, $\tan \delta$, sample "Less120C 1/2 A".

LOSS MODULUS

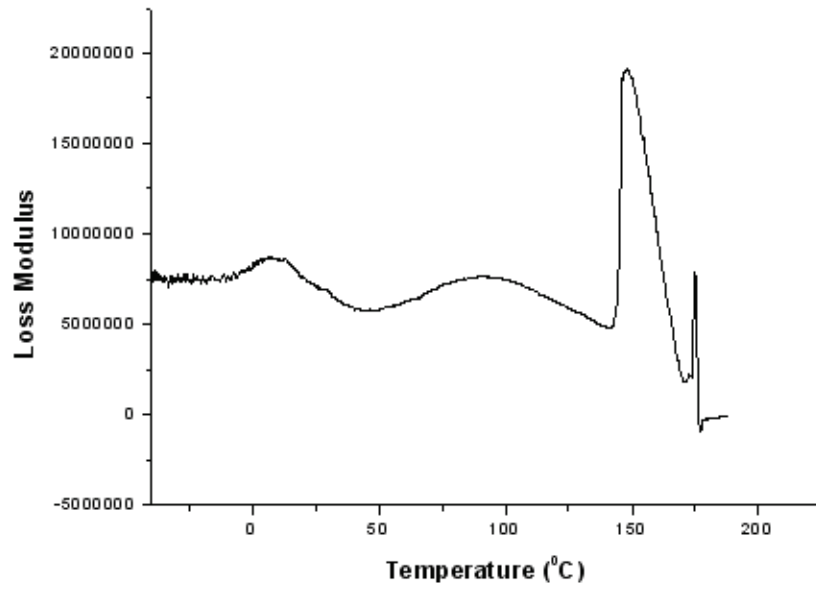


Figure D8: Dynamic mechanical analysis, loss modulus, sample "E-REF".

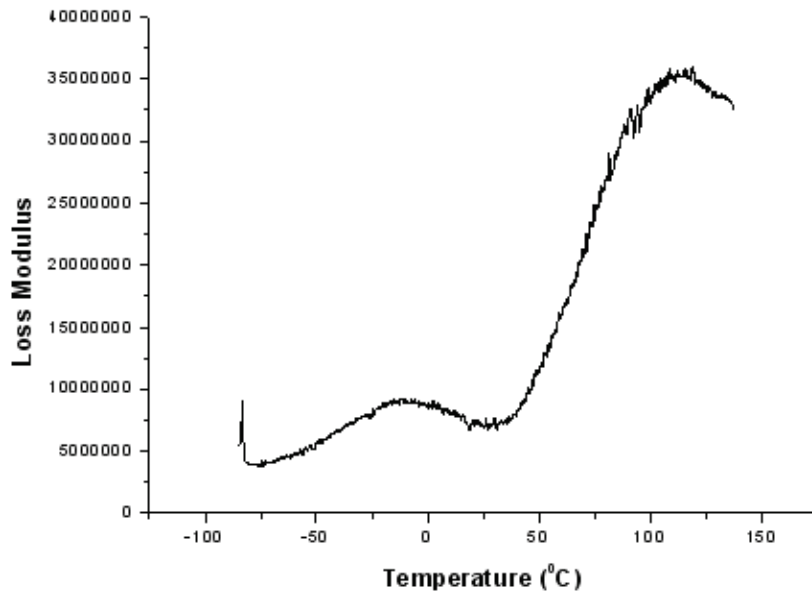


Figure D9: Dynamic mechanical analysis, loss modulus, sample "Less60C B".

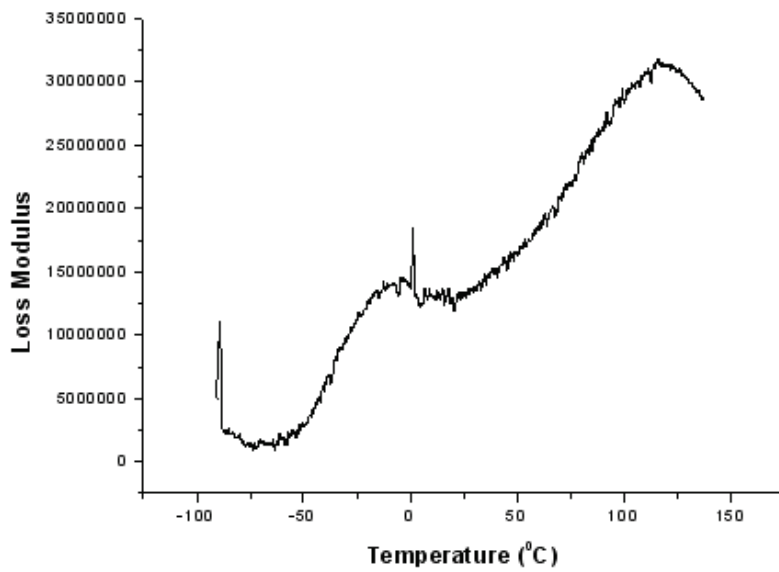


Figure D10: Dynamic mechanical analysis, loss modulus, sample "Less80C A".

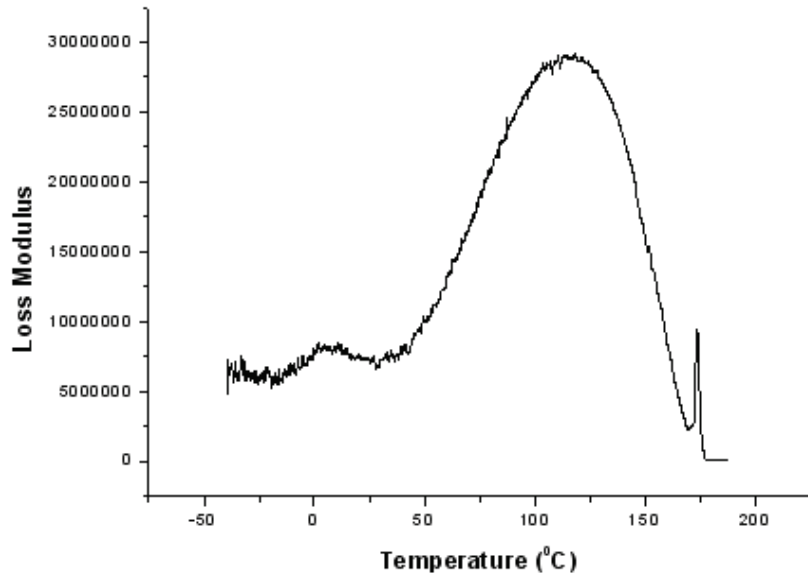


Figure D11: Dynamic mechanical analysis, loss modulus, sample “Less80C B”.

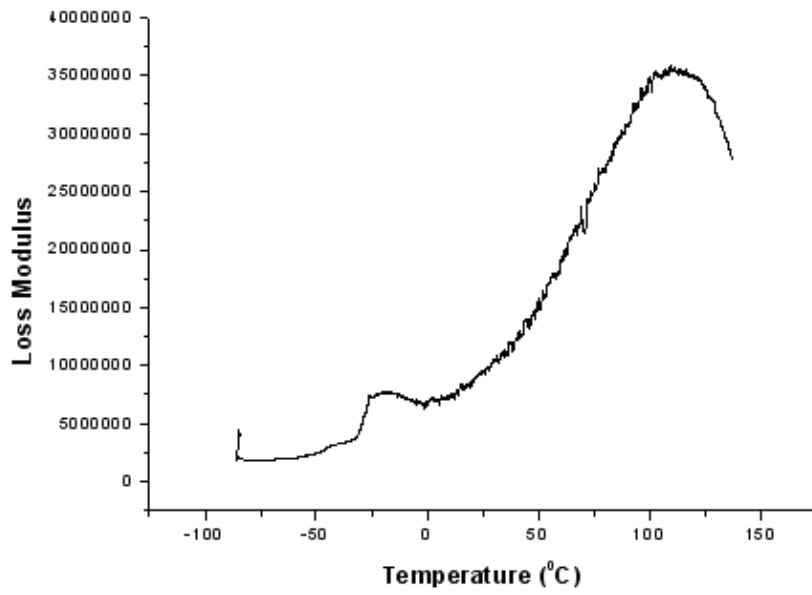


Figure D12: Dynamic mechanical analysis, loss modulus, sample “Less60&80C B”.

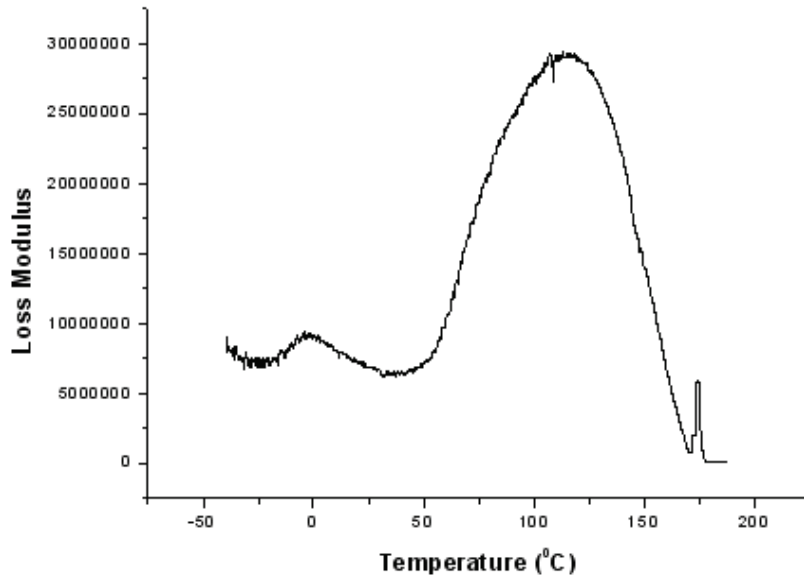


Figure D13: Dynamic mechanical analysis, loss modulus, sample "Less90C A".

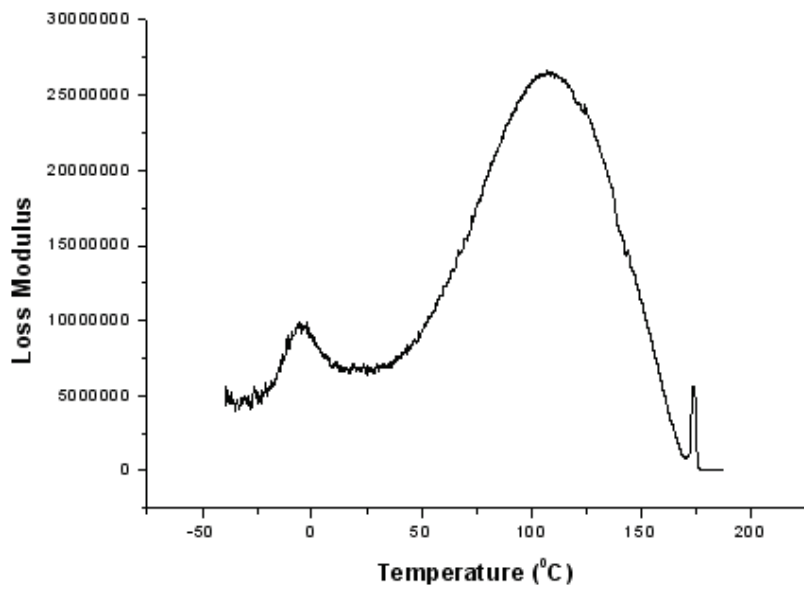


Figure D14: Dynamic mechanical analysis, loss modulus, sample "Less100C A".

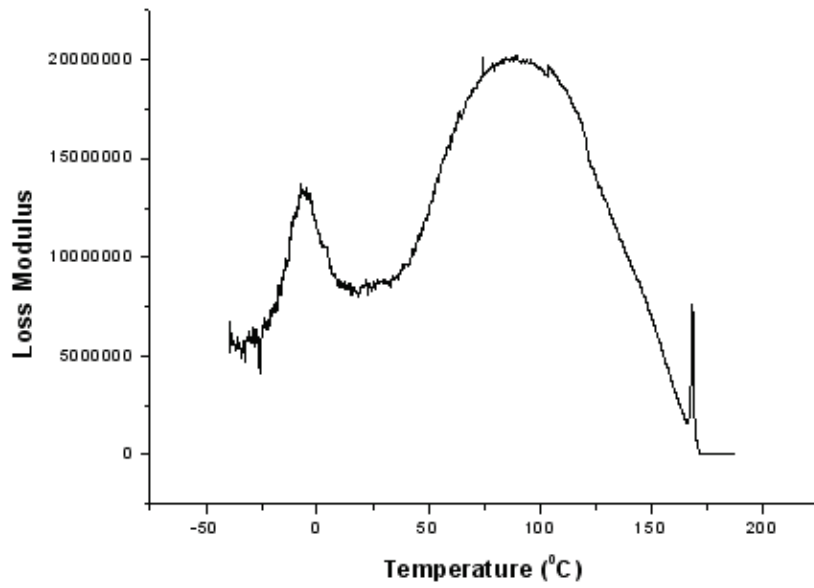


Figure D15: Dynamic mechanical analysis, loss modulus, sample "Less110C A".

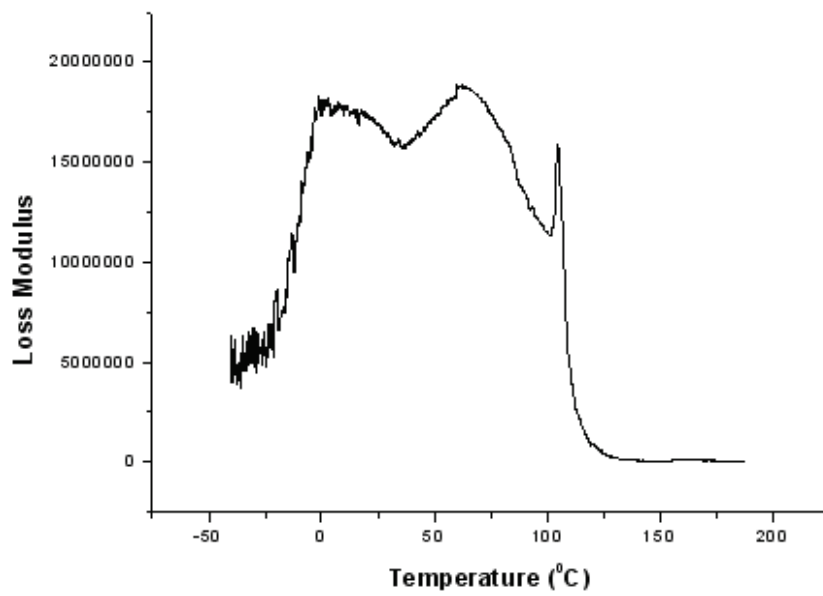


Figure D16: Dynamic mechanical analysis, loss modulus, sample "Less120C A".

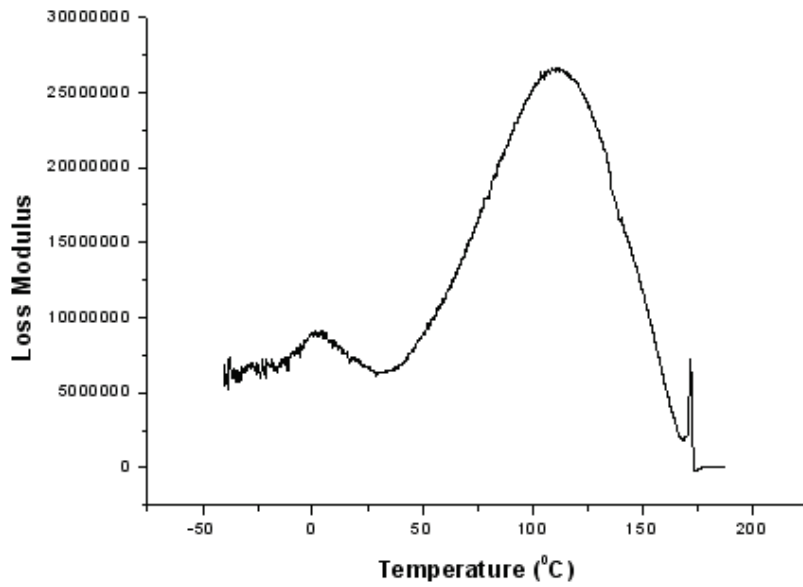


Figure D17: Dynamic mechanical analysis, loss modulus, sample “Less120C 1/2 A”.

STORAGE MODULUS

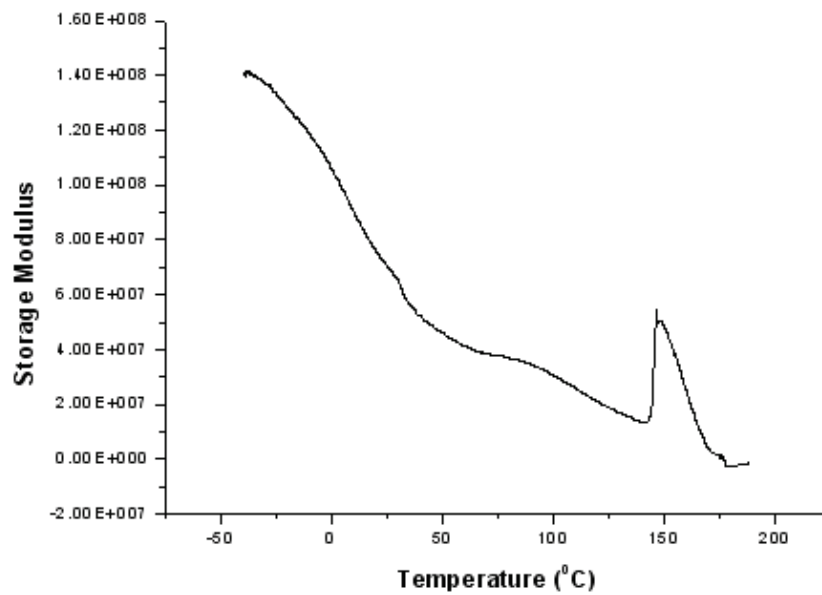


Figure D18: Dynamic mechanical analysis, storage modulus, sample “E-REF A”.

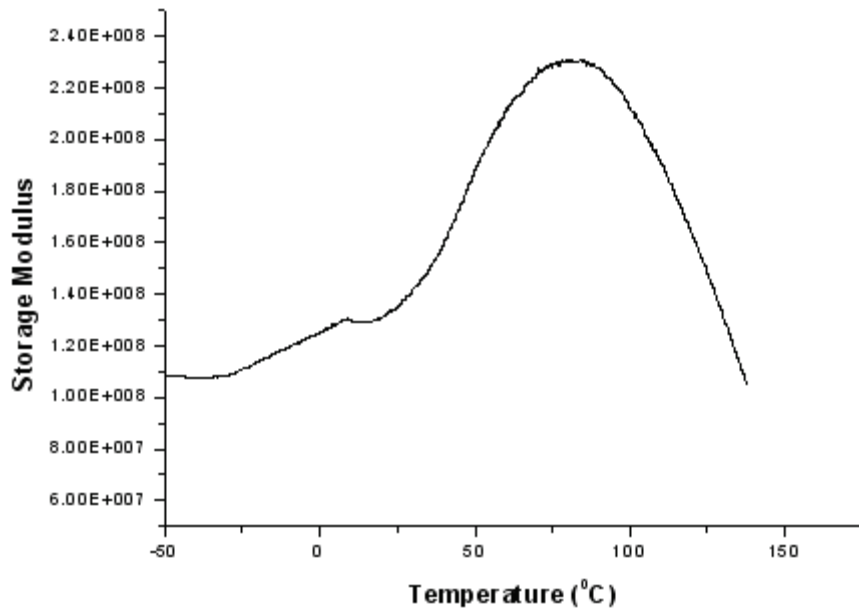


Figure D19: Dynamic mechanical analysis, storage modulus, sample “Less60C B”.

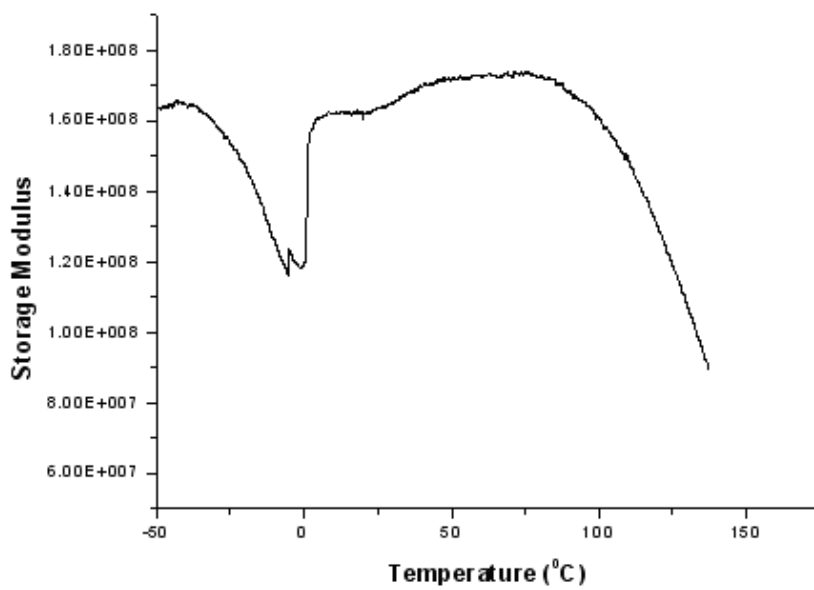


Figure D20: Dynamic mechanical analysis, storage modulus, sample “Less80C A”.

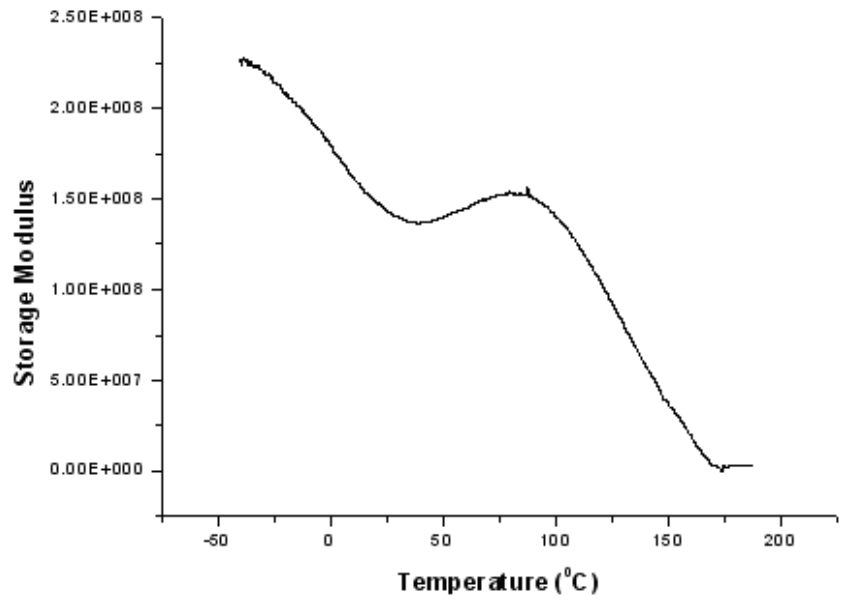


Figure D21: Dynamic mechanical analysis, storage modulus, sample “Less80C B”.

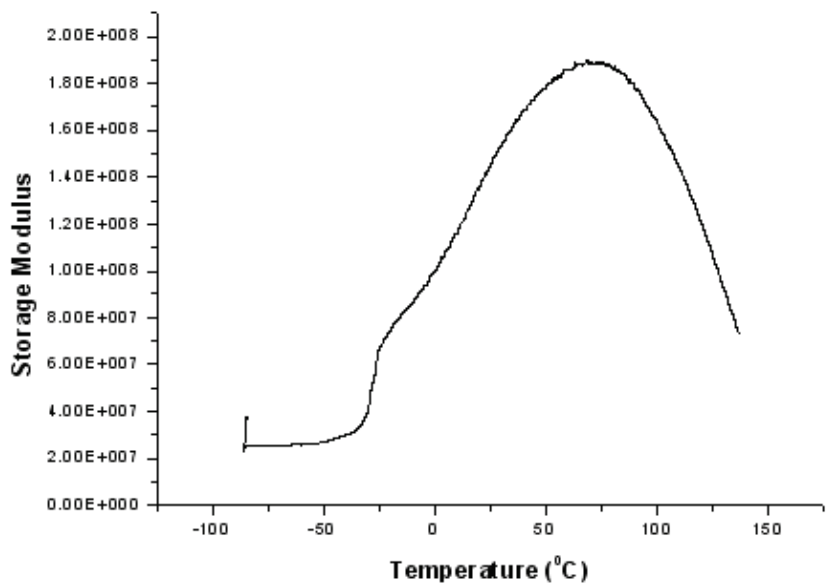


Figure D22: Dynamic mechanical analysis, storage modulus, sample “Less60&80C B”.

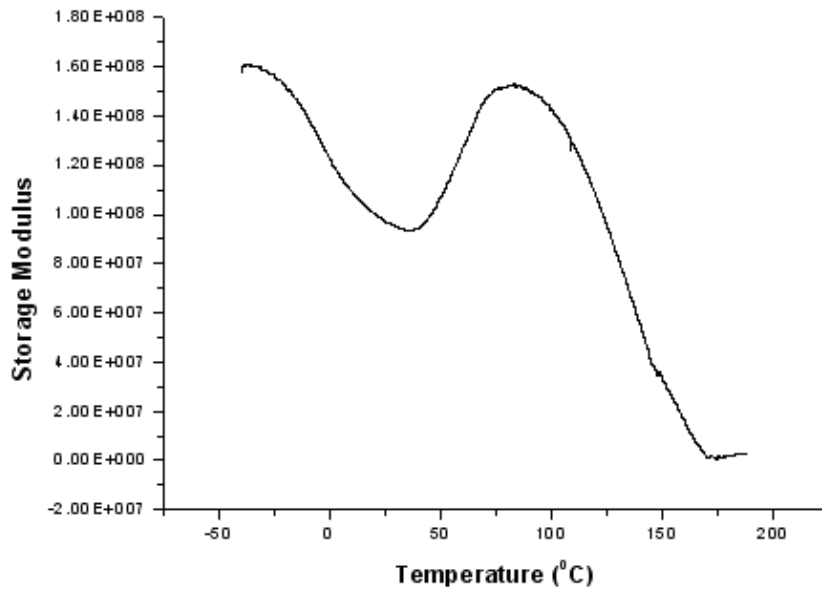


Figure D23: Dynamic mechanical analysis, storage modulus, sample “Less90C A”.

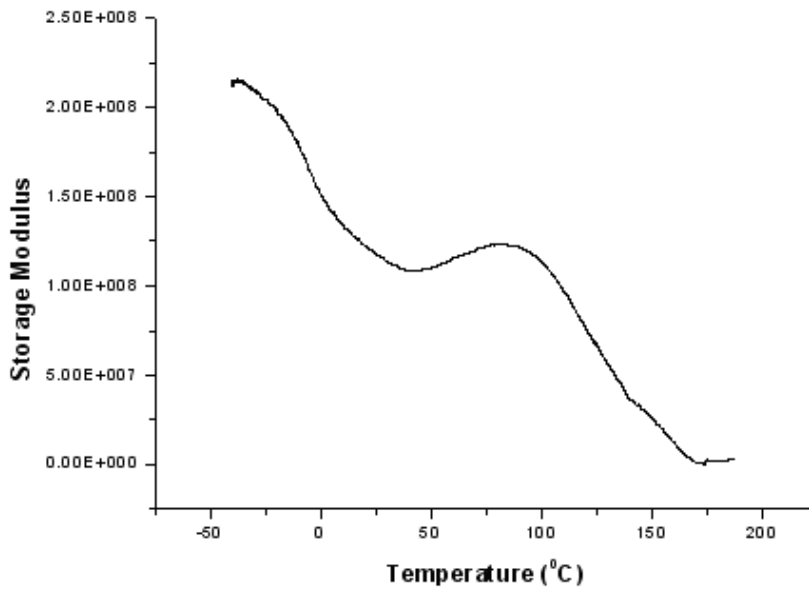


Figure D24: Dynamic mechanical analysis, storage modulus, sample “Less100C A”.

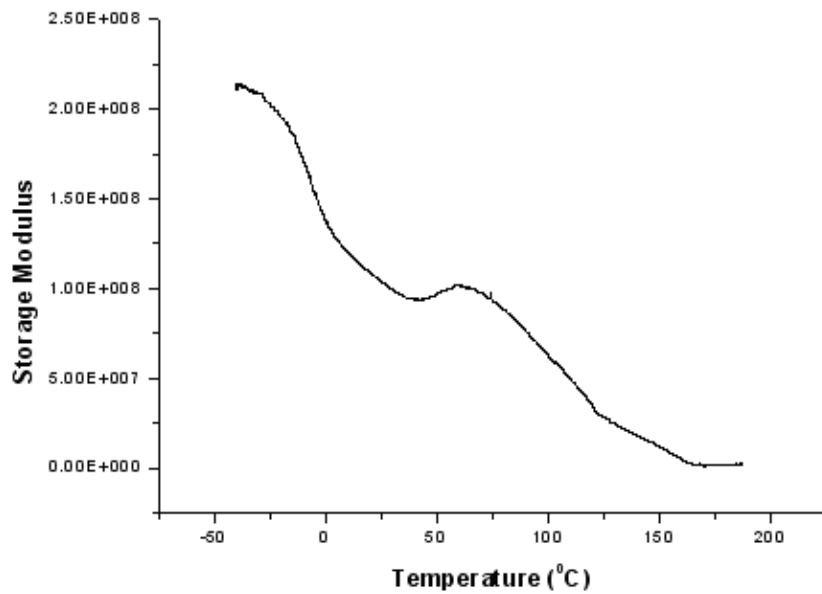


Figure D25: Dynamic mechanical analysis, storage modulus, sample “Less110C A”.

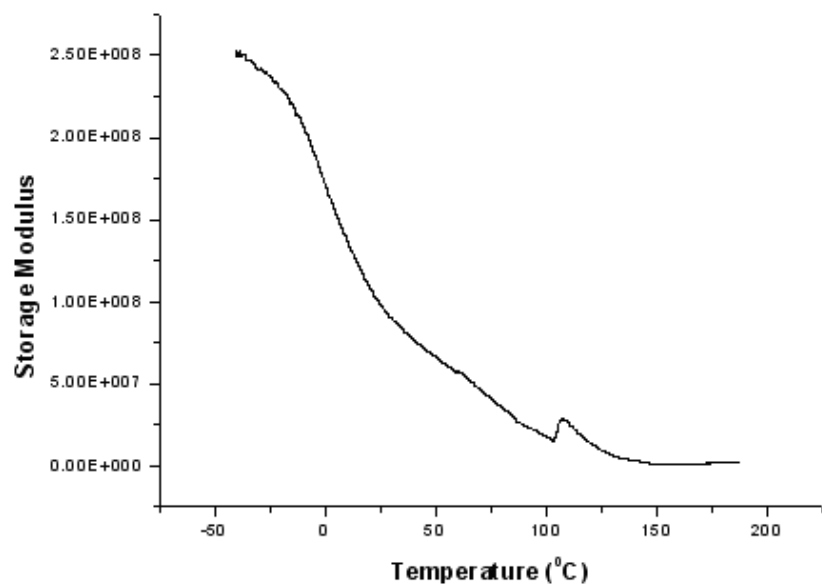


Figure D26: Dynamic mechanical analysis, storage modulus, sample “Less120C A”.

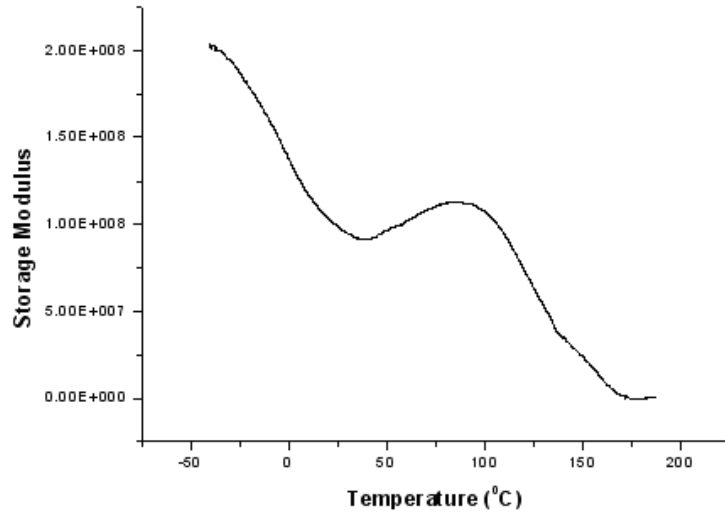


Figure D27: Dynamic mechanical analysis, storage modulus, sample “Less120C 1/2 A”.

APPENDIX E: Transmission electron microscopy images of the recombined samples of the IPPC (CMR 648)

Images taken at 50 nm

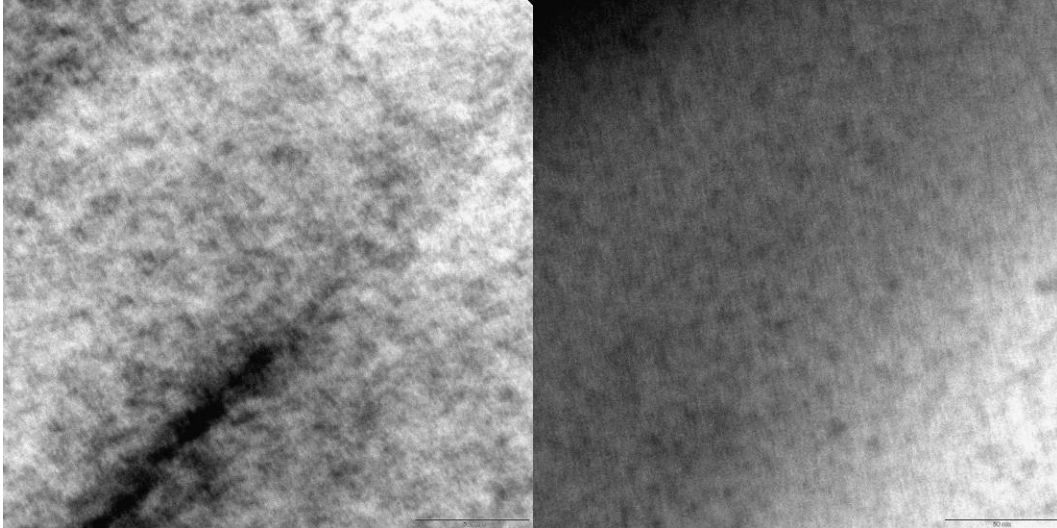


Figure E1: TEM images of sample "E-REF B".

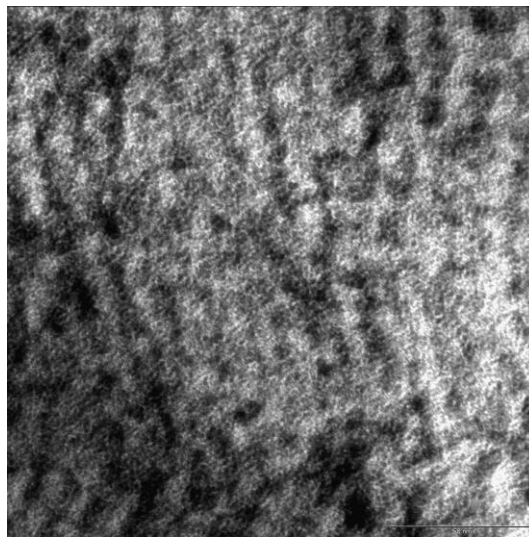


Figure E2: TEM image of sample "Less60C B".

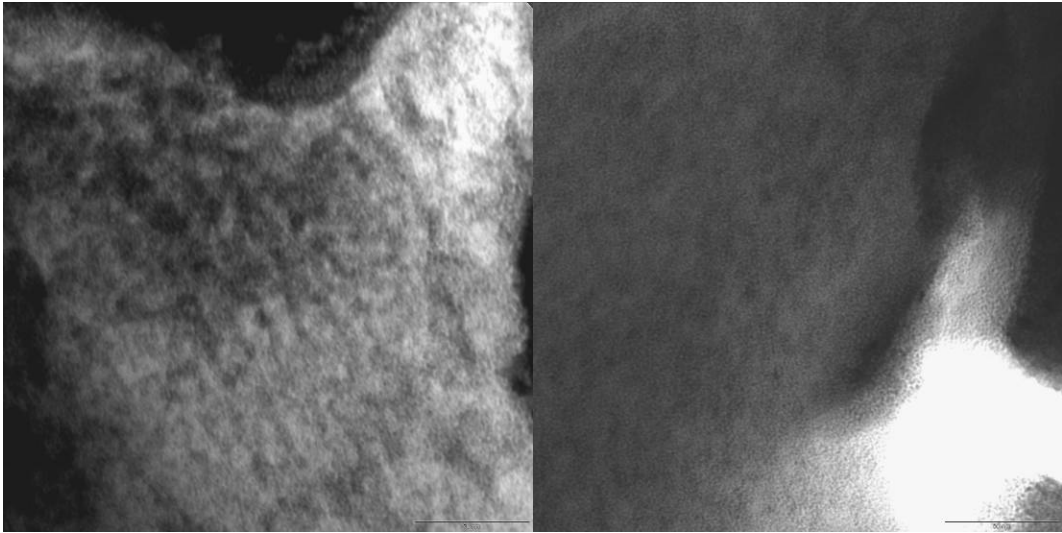


Figure E3: TEM images of sample “Less80C B”.

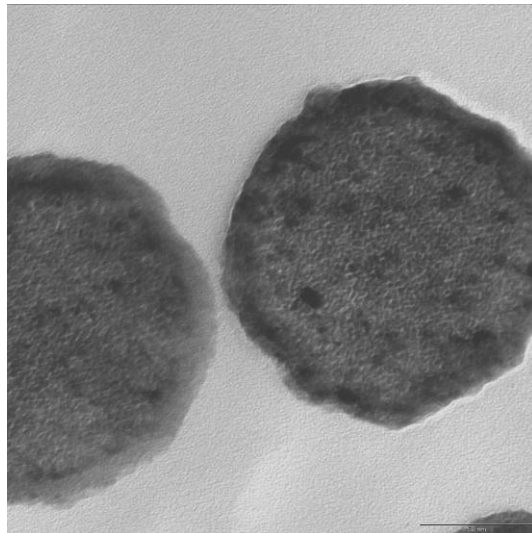


Figure E4: TEM image of sample “Less110C A”.

Images taken at 100 nm

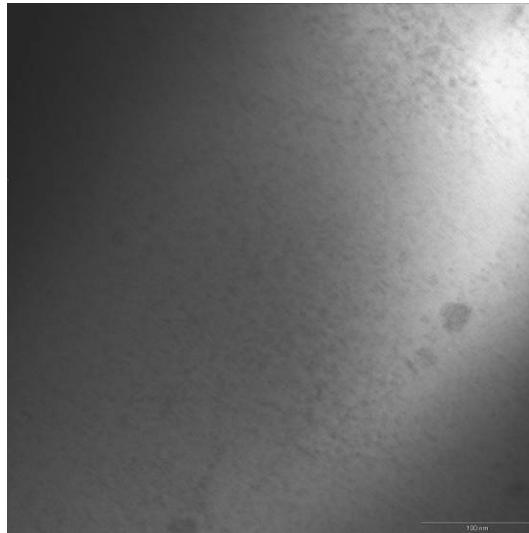


Figure E5: TEM image of sample “E-REF B”.

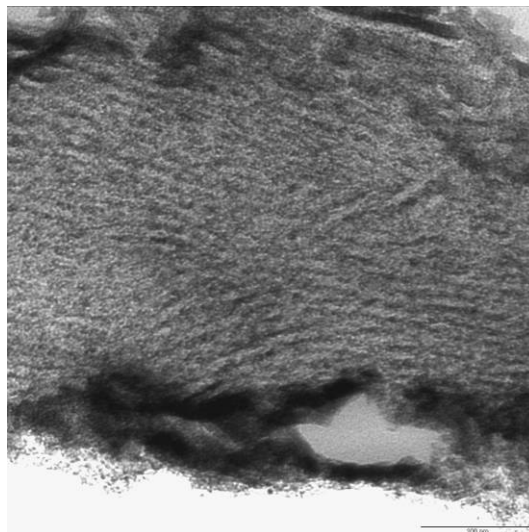


Figure E6: TEM image of sample “Less60C B”.

Images taken at 200 nm

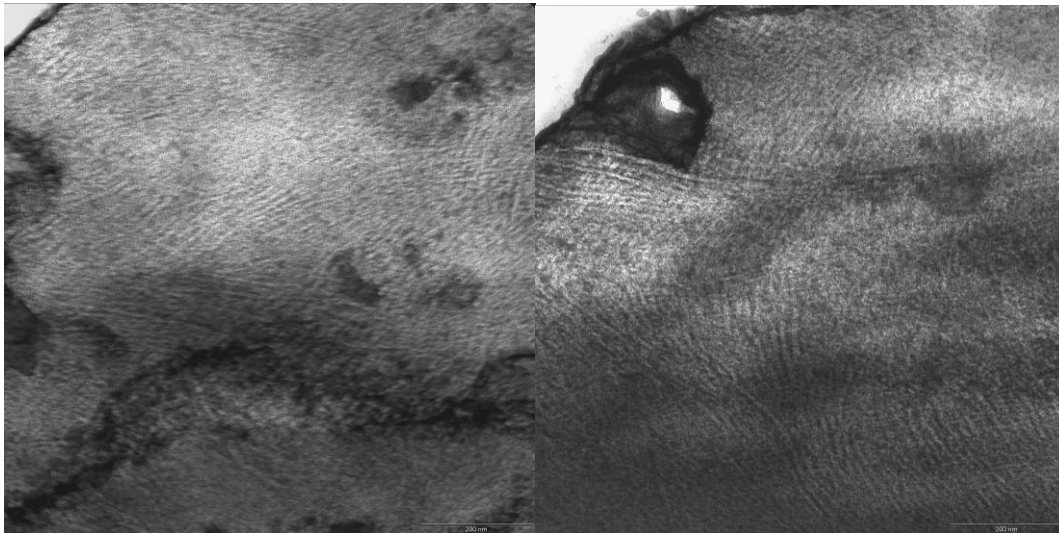


Figure E7: TEM images of sample "Less60C B".

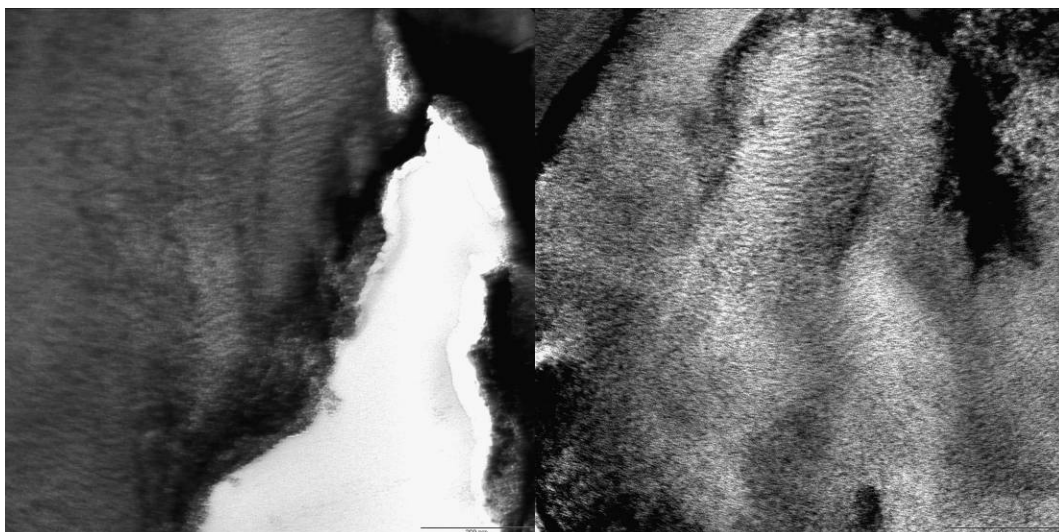


Figure E8: TEM images of sample "Less90C A".

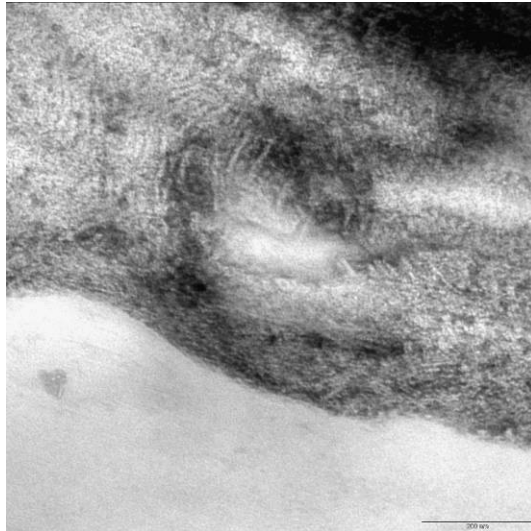


Figure E9: TEM images of sample “Less110C A”.

Images taken at 500 nm

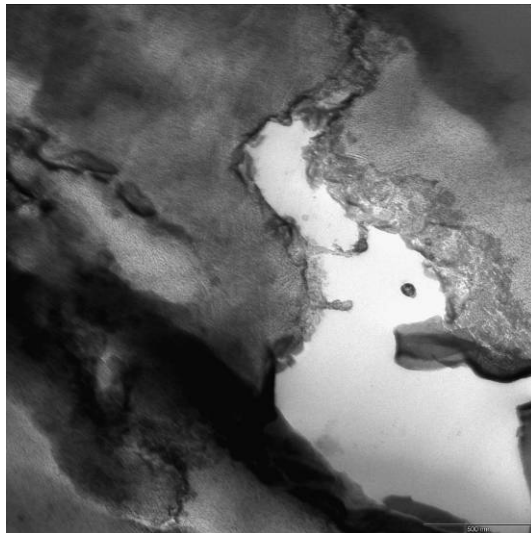


Figure E10: TEM image of sample “Less60C B”.

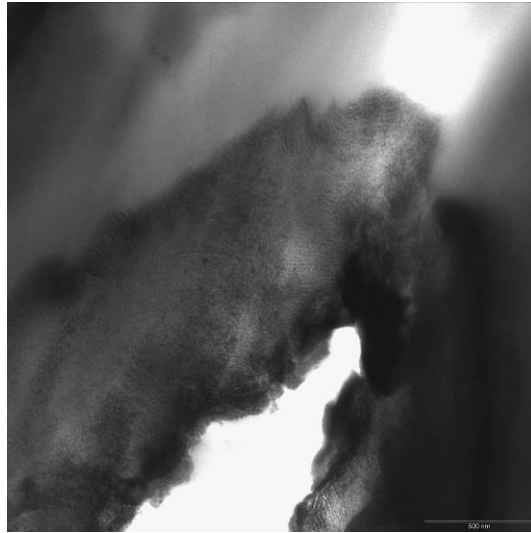


Figure E11: TEM image of sample “Less90C A”.

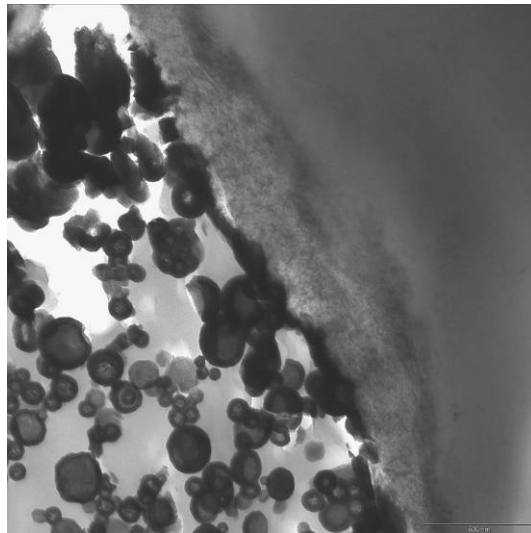


Figure E12: TEM image of sample “Less110C A”.

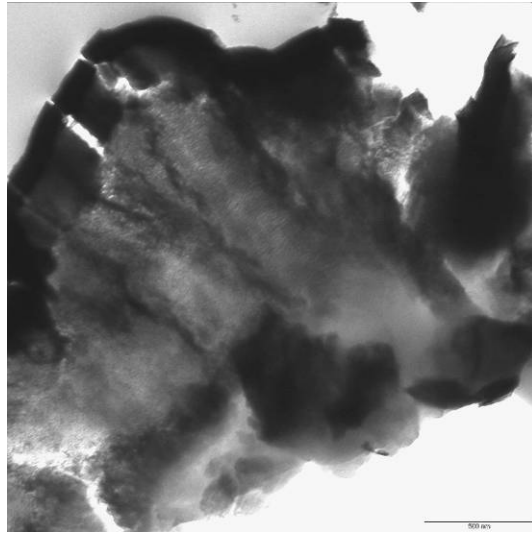


Figure E13: TEM image of sample “Less120C A”.

APPENDIX F

Wide angle X-ray diffraction scattering spectra of the recombined samples of the IPPC (CMR 648)

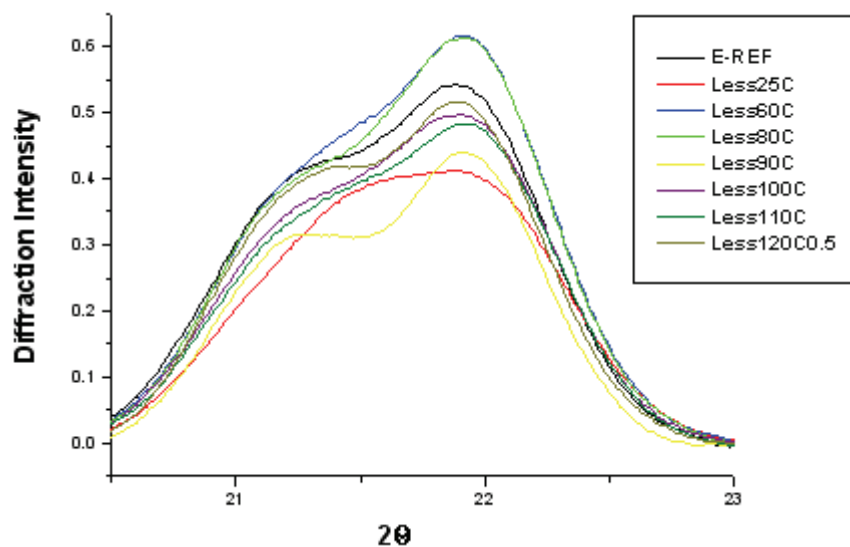


Figure F1: WAXD spectra of the diffraction peak at 21.9 ° of each of the recombined samples of experiment A.

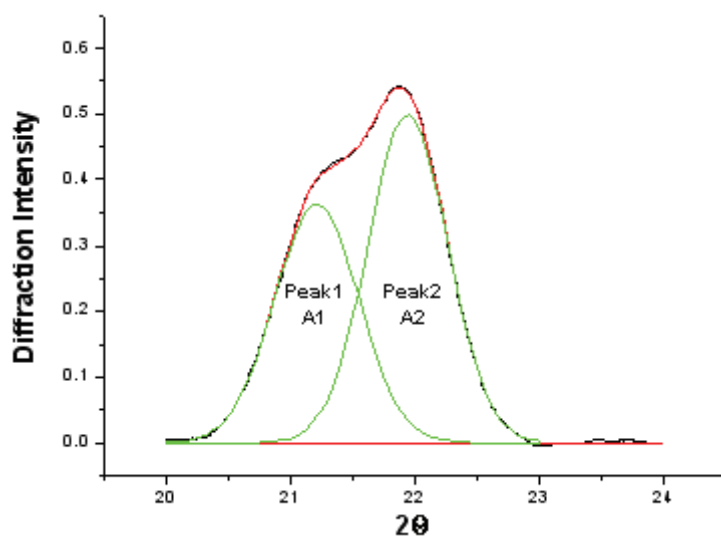


Figure F2: WAXD of the “E-REF A” sample, deconvolution of the diffraction peak at 21.9 °.

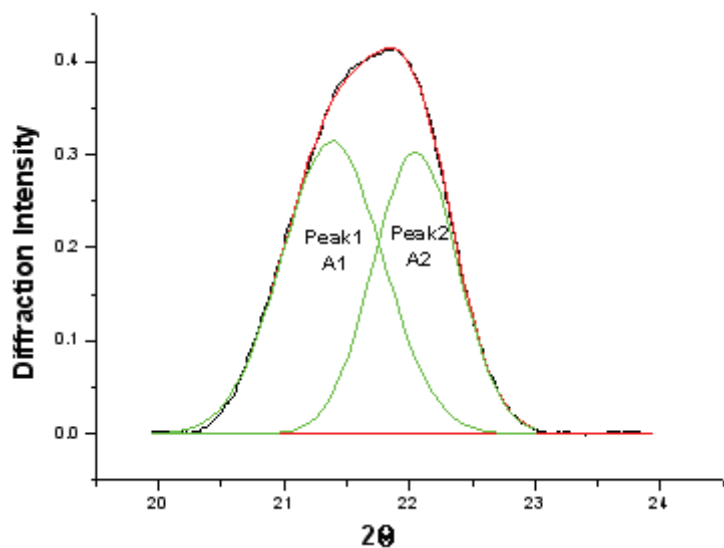


Figure F3: WAXD of the "Less25C A" sample, deconvolution of the diffraction peak at 21.9 °.

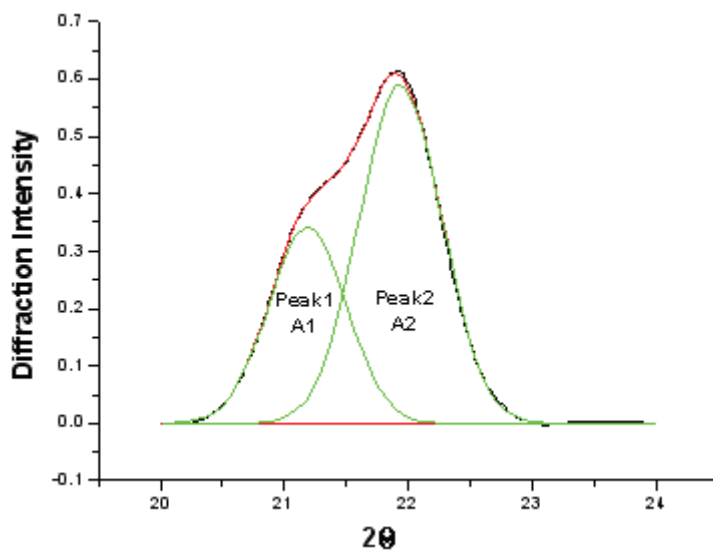


Figure F4: WAXD of the "Less80C A" sample, deconvolution of the diffraction peak at 21.9 °.

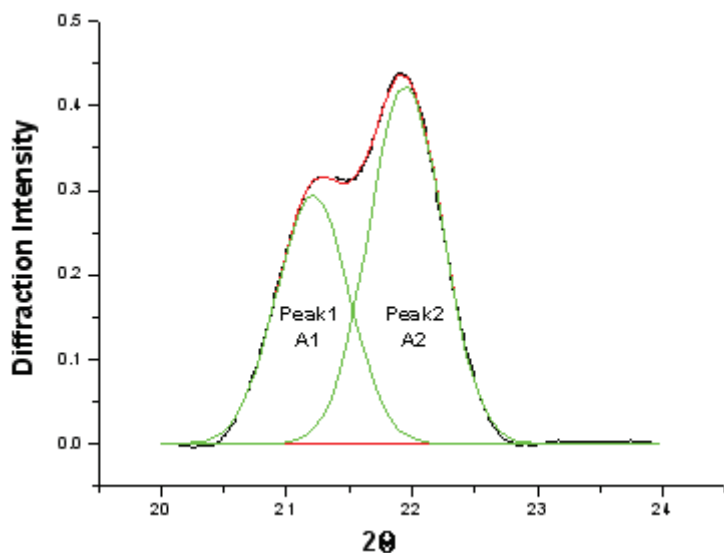


Figure F5: WAXD of the "Less90C A" sample, deconvolution of the diffraction peak at 21.9 °.

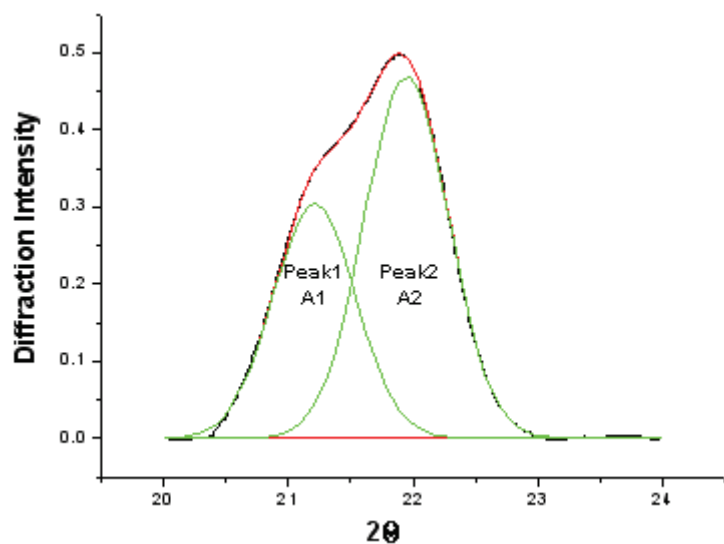


Figure F6: WAXD of the "Less100C A" sample, deconvolution of the diffraction peak at 21.9 °.

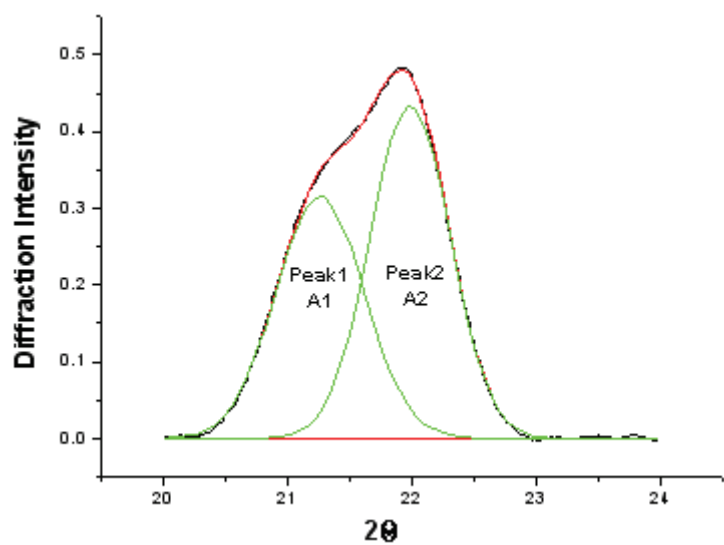


Figure F7: WAXD of the “Less110C A” sample, deconvolution of the diffraction peak at 21.9 °.

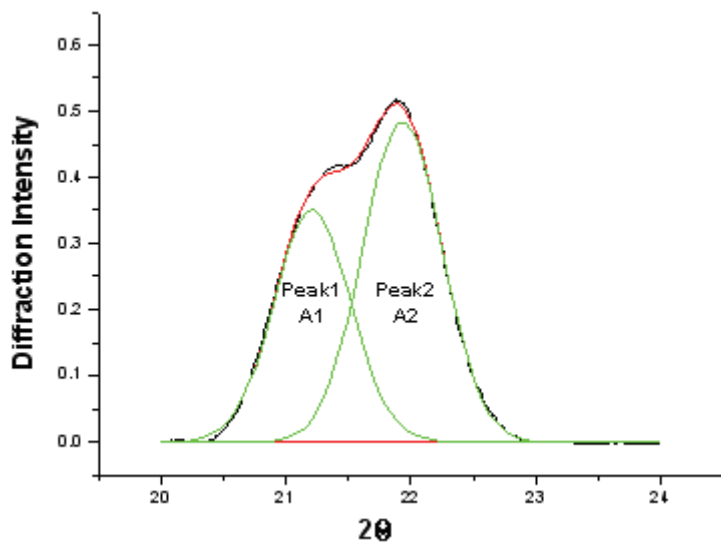


Figure F8: WAXD of the “Less120C 1/2 A” sample, deconvolution of the diffraction peak at 21.9 °.
